東海大学大学院　令和 3 年度博士論文

Aircraft Flight Control Using a Coefficient Diagram Method: Modeling, Controller Design and Simulation Analysis with a Case Study of Fixed-wing Aircraft

（係数図法を用いた航空機の飛行制御：モデリング，制御器設計およびシミュレーション解析：固定翼機のケーススタディ）

指導　　山本　佳男　教授

東海大学大学院総合理工学研究科
総合理工学専攻

エカチャイ･アーサー
Ekachai Asa

Abstract

This thesis aims to develop the aircraft flight control system and propose two effective aircraft flight control systems. The first system is the “Aircraft flight control by CDM-designed Servo State-feedback system” or ACDM-SS. ACDM-SS is the servo state-feedback system for simultaneously controlling the aircraft's longitudinal and lateral-directional dynamics motion. The Coefficient Diagram Method or CDM is used to design the servo state-feedback gains of ACDM-SS. CDM is an algebraic approach to provide a controller design method. The control system designed by CDM exhibits a good balance of stability, response and robustness. The second system is the “Aircraft flight control by CDM-designed Model Reference Adaptive System” or ACDM-RAS. ACDM-RAS is the Model Reference Adaptive System which employs a design concept based on the Lyapunov function theory. ACDM-RAS uses the ACDM-SS as the reference model. The ACDM-RAS is expected to improve the performance of ACDM-SS and decrease uncertainty which may arise from imperfect modeling, approximate inversion, or sudden changes in the system parameters. The performance comparison of ACDM-RAS and ACDM-SS is conducted by means of flight simulation under various flight conditions. The simulation results show that ACDM-RAS can handle the varying flight maneuvers, stabilize aircraft in flight, and improve the performance of ACDM-SS. The proposed systems, both ACDM-RAS and ACDM-SS have straightforward structures, and their design processes also are not complicated with no need of deep mathematical knowledge.

Acknowledgments

First of all, I would like to express my sincere gratitude to my thesis advisor, Professor Yoshio Yamamoto, for his invaluable help and constant encouragement throughout my doctoral education.

I would also like to express my gratitude extended to two professors from KMITL who are essential to my education. The first person is Professor Jongkol Ngamwiwit. Her teaching and advice do not benefit only my research but also benefit my life. The second person is Professor Taworn Benjanarasuth, who always supported me since I was a student at KMITL.

I want to show my gratitude to my dissertation committee: Professor Koichi Koganezawa (Department of Mechanical Engineering), Professor Atsushi Okuyama (Department of Precision Engineering), Professor Yoshinobu Inada (Department of Aeronautics and Astronautics) for generously offering their time, support, guidance, and goodwill throughout my thesis examination.

I gratefully acknowledge the scholarship from Civil Aviation Training Center CATC, Thailand. This scholarship allows me to achieve my Ph.D., and I will use my experience to be most beneficial back to CATC. I also would like to thank all staff at CATC who have worked hard instead of me throughout my studies.

To conclude, I cannot forget to thank my sister and her children and friends for all the unconditional support and encouragement. Thanks also to my wife, Dr. Areerat Sensod, for all her help and patience for me. Finally, I would like to thank my parents, Mr. Pinit and Mrs. Kaeyoon Asa, who always believe in me and give everything in their life for my success.

Ekachai Asa

Table of Contents

List of Tables

List of Figures

List of Symbols

g	=	gravity acceleration, ft/sec^2
h	=	altitude, ft
L', M', N'	=	dimensional derivative of moment
p	=	roll angular rate, rad/sec
q	=	pitch angular rate, rad/sec
r	=	yaw angular rate, rad/sec
t_s	=	settling time, sec
u	=	velocity, ft/sec
V_{P_1}	=	true airspeed, ft/sec
X', Y', Z'	=	dimensional derivative of force
α	=	angle of attack, rad
β	=	sideslip angle, rad
δ	=	deflection of control surfaces, rad
ϕ	=	roll angle, rad
γ_i	=	stability index
γ_i^*	=	stability limit
θ	=	pitch angle, rad
Θ_1	=	steady state pitch angle, rad
τ	=	equivalent time constant, sec
ψ	=	yaw angle, rad

Subscripts

A	=	aileron
E	=	elevator
LatDir, LD	=	relative to the lateral-directional dynamics
Long, L	=	relative to the longitudinal dynamics
rL	=	reduce matrix of the longitudinal dynamics
rLD	=	reduce matrix of the lateral-directional dynamics
R	=	rudder
T	=	thrust

Chapter 1

Introduction

The aviation industry is one of the many primary industries without which our everyday life will not be as easy as what it is now due to aircraft utility. There is continuous growth in demands of using the aircraft. These demands are from various activities, such as transportation, search-and-rescues, exploration and so on. Because of an extremely high economic impact of the aviation industry, a market competition also tends to be very high in this industry. Once a customer decides to purchase any type of aircraft, it does not mean that the aircraft has only its market value but also yields to the maintenance costs followed from operating that aircraft, which brings additional economic benefits for the manufacturers. Therefore, both aircraft manufacturers and aircraft parts manufacturers strive to improve the efficiency of the aircraft and meet the requirements of customers to gain a vast market share. So, it is inevitable that there are high trade competitions and enormous investments in the aviation industry. Due to the reason already mentioned, there has been a rapid change in this industry from the past century. Every part related to the aviation industry has been affected and stimulated to respond to this rapid change. Itis indisputable to say that an essential part of the industry, then is the aircraft itself.

From the reason stated above, the aircraft technologies, the structure design, the material used, and the aircraft systems such as a flight control system, an electrical power system, instrument systems, an air navigation system, a communication system are all being under the research and development. Especially in the flight control system, whose rapid evolution occurred in many past decades, the form of system has evolved from the mechanical system to the hydro-mechanical system and then advanced to the automatic

control system to replace the manual flight control system. These development goals are multifaceted, such as increasing the efficiency of aviation, reducing production costs, increasing safety, improving operating comfort, and all in response to the industry.

1.1 Aviation and Flight Control Evolution

Humans are curious about nature's flight system and aspire to fly like other flying creatures such as birds. These ideas gave rise to a long history of aviation [1] – [5]. From those days, the day humans want to fly, many flying vehicles exist in the present. These flying vehicles can be classified into various types based on the mode of classification. For example, flying vehicles can be classified into “lighter than air vehicles” and “heavier-than-air vehicles” according to lift methods. Airship and Kite balloons are examples of “lighter than air vehicles”. While gliders, fixed-wing aircraft, and rotorcraft are examples of “heavier-than-air vehicles”. However, these different flying vehicles have one thing in common: their flight dynamics can be described by a specific set of equations of motion. Generally, these equations contain six degrees of freedom: three translational modes and three rotational modes and can be called the six degrees of freedom (6 DOF) equations of motion of a rigid vehicle or flight dynamics model. The flight dynamics model can predict a vehicle's trajectory and orientation during the flight. When flight dynamics knowledge is integrated with other technology such as the evolution of flight control actuator, computer network, communication technology and control technology, these amount to establishing an automatic flight control system [6] – [8]. From the many advantages of this system, such as increased flight quality and safety measures, the automatic flight control system has become an essential part of modern aircraft. More specialized studies have been conducted according to the increasing importance of the automatic flight control system [9] – [11]. Designing the automatic flight control system is related to other fields, in addition to the

aircraft flight dynamics, such as Aerodynamics, Rigid-body dynamics, and System theory. Even though more studies or research are devoted to the automatic flight control system, designing of an automatic flight control system is still an arduous task and sometimes needed advanced mathematical knowledge besides aviation knowledge alone.

On the other views about the automatic flight control system, it is not a standalone system although it is one of the essential systems in modern aircraft. This system also needs to coordinate in operation with other aircraft systems to complete the flight's mission, such as communications, navigation, and traffic collision avoidance systems. Therefore, if an automatic flight control system effectively controls the flight or stabilizes the aircraft in flight, it will be easy to apply to other aircraft systems. In addition, if the structure of the flight control system becomes simple, uncomplicated, and has few restrictions, it will be easy to adjust the system for compatibility with other systems or requirements. Moreover, it is especially beneficial if the processes used to design a system have clear design criteria. It is easy to understand and can predict system performance in advance. Contribution of these advantages becomes remarkable in reduction of the design or analysis time of the system when being used in conjunction with other systems or when problems arise with others systems or the flight control system itself. It brings a good benefit in modern aircraft design, which has complex relations among the various systems.

1.2 Previous Works in the Aircraft Flight Dynamics

The aircraft flight dynamics control has a long history. Since the rise of aircraft flight dynamics knowledge and control technology, there have been a vast amount of research efforts devoted to the aircraft flight control system related to aircraft dynamics motion for many different types of flying vehicles. Generally, the aircraft flight dynamics motion can be separated into two major parts. There are aircraft longitudinal dynamics

motion and lateral-directional motion. As far as the motion of aircraft is concerned, there are many pieces of research examples about aircraft flight control systems specific to both longitudinal dynamics motion and lateral directional motion.

The examples in terms of longitudinal dynamics motion are as follows. The adaptive controller of F. Gavilan, R. V., and J. Á. A. [12] for controlling the longitudinal flight dynamics of an aircraft is designed by using the adaptive backstepping method. Engine physical limits are incorporated into the design to obtain a novel hybrid adaptation law that guarantees closed-loop system stability. Simulation results show good performance to follow given airspeed and flight-path angle references by actuating elevator deflections and aircraft engine thrust.

In the paper of A. Maqsood and T. H. Go [13], the analysis technique using linear dynamics and the multiple scale method in conjunction with bifurcation theory is used to analyze the longitudinal dynamics of a small agile unmanned aerial vehicle or UAV. This UAV is equipped with the aerodynamic vectoring feature under general envelope trim conditions between hover and cruise flight conditions. The research successfully describes the peculiar dynamics behavior of this UAV, which is mainly attributed to the class of small UAVs flying at a high angle of attack, and the aerodynamic vectoring feature enhances its occurrence.

The problem of fault-tolerant control for a class of uncertain nonlinear systems in the presence of actuator faults for aircraft longitudinal dynamics motion is discussed in the work of Q. Shen, B. J. and V. C. [14]. Adaptive fuzzy observers are designed by using a backstepping approach to provide a bank of residuals for fault detection and isolation. In their simulation results, the estimation algorithms and fault-tolerant control scheme have better dynamic performances in the presence of actuator faults.

The nonlinear controller based on the total energy control system to control the aircraft altitude and airspeed is proposed in the research of M. E. Argyle and R. W. Beard [15]. The control is achieved by manipulating the aircraft's total energy and distribution rates to account for the dynamic coupling. Furthermore, the simulation results show that the nonlinear controller performs better than the total energy control system standard PI-type controller.

J. Yan, J. B. H., R. E. H. and D. S. B. [16] used transfer function techniques to analyze the response of an aircraft to an elevator step deflection. Furthermore, it showed that the aircraft's initial response to an elevator step command is characterized by the instantaneous acceleration center of rotation or IACR.

The works from A. M. Wickenheiser, E. G. and M. W. [17] and [18] demonstrate a new bioinspired flight capability: perching through a morphing aircraft concept. Besides the traditional aircraft control surfaces, the proposed morphing aircraft consists of variable wing incidence, tail boom angle, and tail incidence. The transient and steady-state behavior of this aircraft changing flight condition and vehicle reconfiguration is discussed.

In paper of Y. Ameho and E. Prempain [19] used three Linear Parametrically Varying synthesis algorithms to design the controller to improve the ADMIRE fighter aircraft longitudinal dynamics handling qualities. Two algorithms were proved successful in longitudinal dynamics handling. In contrast, the latter can provide beneficial information about the parameter space to achieve good design by avoiding ill-suited parameter combinations. Modern techniques are used to estimate wind from a flight vehicle usually has an estimation error. This error comes from sensor measurements and mathematical models of the aircraft's dynamics.

H. G. McClelland and C. A. Woolsey [20] presents a methodology to isolate the modeling error for common simplified forms of the dynamic flight model during straight-and-level longitudinal flight, and the proposed is demonstrated via an example study in which both open-loop and closed-loop flight simulations.

In the paper of V. H. Nguyen and T. T. Tran [21], a hybrid robust control design method is proposed for a third-order Single-Input Single-Output (SISO) lower-triangular model of nonlinear dynamic systems in the presence of disturbances. The proposed control method was proved a well-tracking command with asymptotic stability, provides robustness in the presence of uncertainties and eliminates a chattering phenomenon.

The researches relate to lateral-directional dynamics motion are shown as follows. The later-directional dynamics control of UAV by using the backstepping technique is presented in the paper of S. Swarnkar and M. Kothari [22]. The adaptive design is used to learn and control unknown dynamics for the whole flight regime.

The reinforcement-learning lateral-directional flight controller to prevent or recover aircraft from losing control in flight has been discussed by I. K. Ashraf and E.-J. Van Kampen [23]. The controller is designed based on value function-based single network adaptive critic (J-SNAC), the one of Adaptive Critic Designs (ACD) algorithm. Simulation with F16 aircraft was done to evaluate for tracking two different heading command signals, robustness against sensor noises, and partial failure of the ailerons.

P. C. Shrivastava and R. F. Stengel [24] details the conditions for stability boundaries of linear systems containing control saturation on unstable lateral-directional dynamics. This work examines the effects of control saturation on unstable lateral-directional dynamics through the fourth-order models with the flight control logic based

on minimum control energy linear-quadratic-regulatory theory and found that the stability boundaries can be described by unstable limit cycles surrounding stable equilibrium points.

T. H. Go [25] details the analysis of the lateral-directional aircraft dynamics under the cubic variation of the lateral moment to sideslip. The results obtained confirm the findings in the author's previous works that the weak static moment nonlinearity does not lead to wing rock, and the static moment nonlinearity can cause wing rock. Moreover, the results also give the knowledge, which is very useful in aircraft design to avoid wing rock or the wing rock alleviation strategy of an existing aircraft.

N. Abramov, M. G., M. D. and A. K. [26] showed the comparative analysis of two forms of aerodynamic representation in terms of their impact on the lateral-directional stability characteristics. The results show that the unsteady aerodynamic model exhibits good results than the conventional aerodynamic derivative model both for flight dynamics analysis and control design at high angles of attack and provide an accurate prediction of stability characteristics and be applied for control design beyond stall conditions.

In R. Livneh [27], the literal approximation method for improving approximation of the lateral-directional dynamics of rigid aircraft is presented. Compared to the traditional method, the proposed method shows a more meaningful improvement in accuracy than the traditional approximation.

S. A. Snell, W. L. G. Jr. and D. F. E. [28] analyzes the lateral-directional dynamics of a supermaneuverable aircraft and the control laws which reduce the levels of lateral acceleration and sideslip encountered during aggressive rolling maneuvers at high angles of attack. The paper's conclusion states that a significant reduction in lateral acceleration measured at the pilot's station is only attainable by compromising the roll-rate performance.

The cancellation control laws which reduce the high levels of lateral acceleration encountered during aggressive rolling maneuvers executed at a high angle of attack are designed in A. Snell [29]. The proposed control laws can reduce the high level of lateral acceleration as expected but must be exchanged with slower roll response, poor Dutch-roll damping, or a combination of the two.

The investigation of recovery of the lateral-directional stability of commercial aircraft when its vertical stabilizer is damaged is presented in L. Zhaoxing, F. J., G. X., L. J., W. S. and W. Y. [30]. The recovery is made through a unique differential thrust-based adaptive controller designed based on the Lyapunov stability.

A linear-adaptive controller for lateral-directional dynamics control of F-14 aircraft is presented in C. Tournes and B. Landrum [31]. The controller design is based on the combination of the disturbance-observers and Subspace-Stabilization Theory. The disturbance-observers method is used to estimate and cancel out the combined effects of nonlinear, uncertain, and off-nominal terms in real-time. At the same time, Subspace-Stabilization Theory is used to steer the system "error-state" to a certain subspace S representing the desired servo-tracking error behavior while controlling the subsequent motion of the error-state the subspace S to the origin. Simulation results are compared with previous results obtained using gain scheduling and H-infinite and exhibit good performance. These previous researches present the technique specific to only one type of dynamics motion by assuming some conditions to the other dynamics motion or regardless. The other proposed researches also can be classified by consideration of the used controller techniques. For example, the Proportional–Integral–Derivative controller or PID controller is a well-known controller used for flight control systems. There are using the conventional PID controller to design the flight control system directly or cooperates with other controller form as the hybrid controller or use the PID controller as the baseline.

X. Xiao, J. J. Z. and Q. Z. [32] presents the PID controller for flight stability of the UAV. In order to improve flight stability, this research designed the reconfigurable control law strategy based on the consideration of several typical actuator failures. The simulation results show that the controller applied to the unmanned tiltrotor aircraft has good performance.

The attitude control of the four-rotor aircraft is improved in T. Hongpeng and Weibo [33]. The differential leading PID algorithm is assigned to stabilize the attitude angle of the quadrotor. The proposed algorithm is compared with the conventional PID control algorithm and exhibits good performance in attitude stabilizing at high-frequency interference and frequent lifting environment.

The PI algorithm and quaternion method combination is used to improve the integral separation PID control algorithm, detailed in H. Y. Tian and L. Li [34]. The simulation by using MATLAB shows that the improved integral separation PID exhibits a good performance than the conventional PID controller and the integral separation controller.

B. Porter, A. M. and T. M. [35] presents the design of digital model-following flight-mode control systems for the F-16 aircraft. The controller is designed based on the previous results for fast non-interacting digital signal following systems incorporating fast-sampling error-actuated digital PID controllers.

An attempt to improve the attitude control and flight stability of a quadrotor aircraft is introduced in Y. Yu and J. Chen [36]. The controller design method is based on the visual servo feedback concept. The target image features information is extracted by the Scale-Invariant Feature Transform (SIFT) algorism and used as an input signal of the PID flight control system.

A new method for roll reversal phenomenon control and eliminating is introduced in M. Mirzaei [37]. The proposed controller is designed by using the sliding mode control based on an online identifier that estimates the control input direction. The results show that the system has a good performance and robustness.

Y. Ochi, H. K. and M. W. [38] propose the derivation of the linear dynamic model of a powered paraglider from a nonlinear dynamic model. This linear model can be described by the payload states of the paraglider, which facilitates dynamical analysis and controller design. Based on this linear model, a PID controller shows good control performance and desirable stability.

P. Kumar, S. N. and J. R. [39] introduces the bat algorithm and differential evolution for tuning the controller parameters using the robust stability criteria for the multi-objective optimization to design the fractional-order PID (FOPID) and integer-order PID controllers are discussed. From conclusion shows the bat algorithm gives better results in terms of the time domain performances, but differential evolution gives better robustness to the control system.

In A. Z. Azfar and D. Hazry [40], a new method in sensor fusion and inclination angle estimation is applied to the PID controller for stabilizing the quadrotor, while D. Luo, W. X., S. W. and Y. M. [41] present the PID controller for the UAV formation flight distributed formation control and the switching strategy for completing the three kinds of conventional formation. The simulation results also show the effectiveness of the proposed controller.

Other techniques used to design the flight control system also have the neural network [42] – [44] and the fuzzy logic [45] – [47].

1.3 Thesis Motivation

1.3.1 Problem statement

Although many pieces of research activities achieved their individual purposes to some extent, automatic flight control is still a challenge, and there are still exciting aspects yet able to develop. The essential points of interest in this thesis are identified as follows:

- **The aircraft mathematical models:** The automatic control system designing usually starts with the mathematical model of the plant of interest, and this mathematical model must represent the system's dynamics behavior or the relationship between the inputs and the interested variables or the outputs of the system. Knowing the system's dynamics is essential for a control system designer to analyze the system before and after designing. Therefore, the model's accuracy directly influences the system performance or the system design. Generally, the mathematical model can be divided by following the system type: nonlinear or linear. Determining the nonlinear system's mathematical model is always tricky for beginners and skilled ones encountering the more complex system. That may cause many problems in the control system design processes. Finding a proper control design method to obtain the nonlinear system's mathematical model usually requires deep mathematical knowledge in design and analysis, and sometimes determining aerodynamic characteristics based on the concept of aerodynamic derivatives are difficult or impossible. On the other hand, determining the linear system's mathematical model is far more straightforward than the nonlinear system. The derivation of the linear model is usually obtained by approximating the nonlinear system at flight conditions of interest. Therefore, the linear model may not be accurate in describing all dynamics behavior of the actual system. Generally,

the actual plants are inherently nonlinear systems, and an aircraft is also a nonlinear system without an exception. Choice of mathematical model type to represent aircraft affects many points in control system design, such as the choice of the control design method and the system's performance analysis. Therefore, selecting the mathematical model, which can accurately describe the system's behavior and benefit the design processes, is of vital importance.

- **The controller and design method:** As already stated, many types of controllers or design methods have been proposed for the aircraft's automatic flight control system. However, choosing the most effective controller for the plant depends on several factors. For example, in the conventional PID controller, the implementation of this controller type is done by adjusting the value of PID's gains (K_p, K_i, and K_d) to get the best response of the system. The selection of these gain values causes variation in the observed response against the desired response. Trial-and-error may be used to determine these gains. Another example is a controller based on neural networks. The proper network structure is one crucial part of this controller type. However, there is no specific rule for determining the network structure. The appropriate structure can be achieved through the designer's experience and trial and error. In the fuzzy logic-based controller, setting exact fuzzy rules and membership functions is a difficult task. Validation and Verification of a fuzzy knowledge-based system needs extensive testing with hardware. Although each controller can achieve its control objective, there are some limitations in design, such as requiring a deep understanding of the behavior of the system, the system designer must have more experience regarding the system, or design's processes still requires trial and error which might not find the optimum point. Besides the controller type, the controller design process or

controller design method is another interesting factor. The design method has straightforward processes or the tuning decision, which is interesting and maybe more beneficial for design and analysis processes.

1.3.2 The expected aircraft flight control system

Upon reviewing the previous works about aircraft flight dynamics control, it was noticed that there are many points are yet to be improved. According to the author's idea, the expected aircraft flight control system should be characterized as follows.

1) The system should have a simple structure or model, which makes it easy to design, analyze, and customize the system before and after the design. A servo state-feedback system [48] is the most suitable answer for this purpose. The first reason is that the servo state-feedback system can be started with the linear mathematical model, which dramatically reduces the complex task when working with the nonlinear model. The second reason is that the linear model structure is also straightforward and makes further modification easy. There are many applications based on the servo state-feedback system, such as the inverted pendulum system [49], the two-wheeled balancing robot [50], and the magnetic levitation system [51].
2) The controller design method for this expected system should have the concept as same in the model. The design processes should be straightforward and easy to modify if required. Therefore, the Coefficient Diagram Method, also known as CDM, is chosen to design this servo state-feedback system. CDM has straightforward design processes, clear tuning criteria, and CDM also has a specific diagram, which is helpful in design processes. CDM has provided successful controller designs for various

practical control problems over the past decade, and a great amount of research efforts have been done on CDM [52] – [71]. Besides the widespread use of CDM in various fields, various controllers are also designed based on CDM in the field of aeronautics [72] – [76]. Inaccuracies or uncertainties which may arise due to the linear model approximation when the designed controller is applied to nonlinear plant need to be addressed. For that purpose, the concept of a model-reference adaptive system is implemented to the servo state-feedback designed based on CDM.

1.4 Contribution and Outline of Thesis

The automatic aircraft flight control system is proposed in this thesis. The proposed system is called Aircraft flight control by CDM-designed Model-Reference Adaptive System or, in short, ACDM-RAS. ACDM-RAS is the model-reference adaptive control system, and the reference model, which is used in ACDM-RAS, is the servo state-feedback system designed by Coefficient Diagram Method. This servo state-feedback system will be called ACDM-SS. ACDM-SS comprises two servo state-feedback systems: the aircraft longitudinal and lateral-directional dynamics controllers, and ACDM-SS can simultaneously control both aircraft dynamics motions. Using the Coefficient Diagram Method or CDM to design ACDM-SS from the linear models can reduce design complications, and use of the adaptive system is intended to compensate inaccuracies or uncertainties, which may be caused by model approximation. The proposed ACDM-RAS is able to handle the varying flight maneuvers and stabilize aircraft in flight. In addition, the ACDM-RAS can improve the performance of ACDM-SS by compensating any restrictions of ACDM-SS. The structure of ACDM-RAS is also quite straightforward. The

design processes and system analysis are not complicated with no need of mathematically involved method.

The outline of this thesis is as follows: In Chapter 2, the derivation of the aircraft flight dynamics model is presented. Coefficient Diagram Method or CDM, the control system design theory, is described in Chapter 3. At the same time, the design processes of the servo state-feedback system using CDM and the model-reference adaptive system are explained in Chapter 4. Simulation studies and results for the different control strategies proposed are presented in Chapter 5. Finally, the conclusion and suggestions for further work are given in Chapter 6.

Chapter 2

Aircraft Flight Dynamics and Model

2.1 Overview

In this chapter, the aircraft flight dynamics mathematical models [81] – [87] used in Chapters 4 and 5 for designing the controller and flight simulation are described. Generally, these aircraft flight dynamics models are typically nonlinear; however, the purpose of this thesis is to develop the aircraft flight control system. This system is the Model-Reference Adaptive System or MRAS where the reference model used is designed by CDM. Therefore, these aircraft dynamics models need to be converted to a linear system suitable for the CDM controller design method. When the aircraft dynamics models are converted to the linear model, these models can be divided into two essential parts: the aircraft longitudinal dynamics model and lateral-directional dynamics model. These two models are adjusted to have the desired control parameters and are further used in the controller design in the later chapter.

2.2 Coordinate Systems

2.2.1 Inertial and vehicle-fixed coordinate system

The coordinate system or coordinate frame must be firstly defined before the aircraft flight dynamics models are derived. The frame introduced first is called an inertial frame. This frame is undergoing neither rectilinear acceleration nor rotation. An example of a genuinely inertial frame S is a frame whose origin is fixed at the Earth's center and referring to specific stars. However, frame S is more complex and not suitable for the

desired aircraft modeling. In the aircraft flight dynamics model's derivation, the earth frame is assumed to be an inertial frame. This earth frame is a Cartesian coordinate system. The frame's origin is fixed to a point on the earth's surface with axes oriented true north, east, and downward to the center of the earth, frame E, as shown in Figure 2.1.

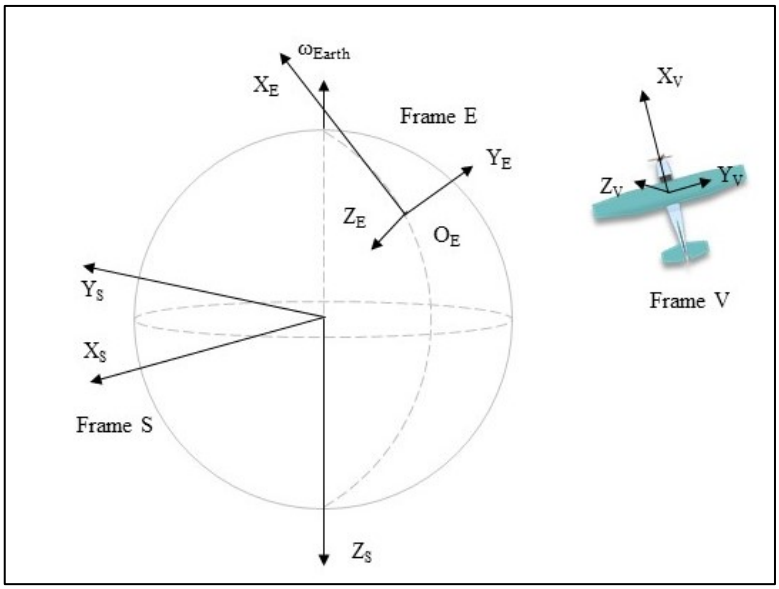

Figure 2.1. Inertial frame and vehicle-fixed frame.

The second frame is vehicle-fixed, which is rigidly attached to the vehicle and therefore moves with a vehicle. The frame's origin is placed at the aircraft's center of gravity. The positive x-axis lies along the aircraft's symmetrical axis in the forward direction, and the positive y-axis is perpendicular to the symmetrical axis of the aircraft in the right direction. The positive z-axis is perpendicular to the x-y plane, making the right-hand orientation. This frame V is also shown in Figure 2.1.

2.2.2 Euler angle

The Euler angles ϕ, θ, and ψ are defined as vehicle bank angle, vehicle pitch angle, and vehicle heading angle, respectively. These angles are used to express the vehicle-fixed frame's orientation to the earth frame, as shown in Figure 2.2.

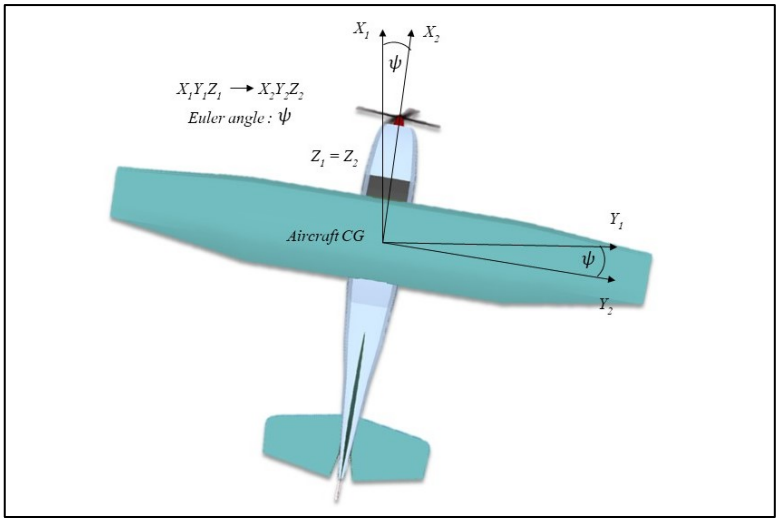

(a) Heading angle

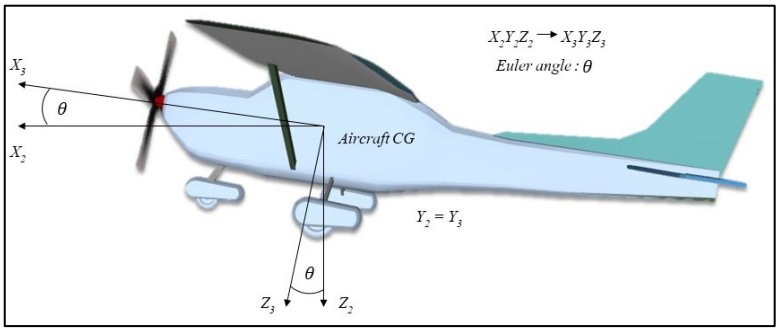

(b) Pitch angle

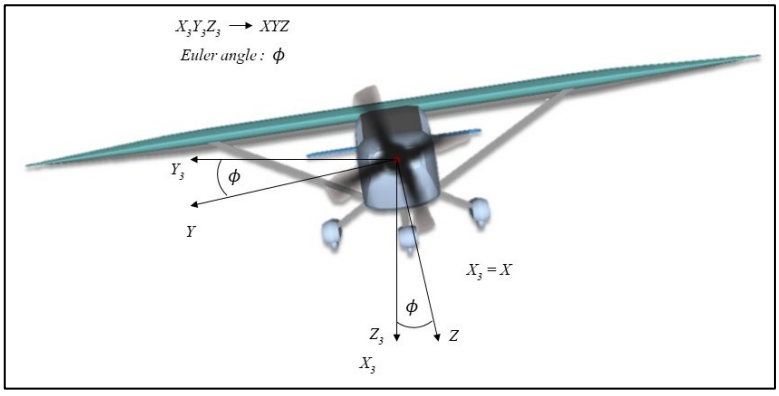

(c) Bank angle

Figure 2.2. Euler angles.

The transformation of the earth frame to the vehicle-fixed frame can be done using the Direction Cosine Matrix or DCM. The DCM can be expressed in term of Euler angles as shown in Eq. (2.1).

$$\mathbf{T}_{E-V}(\phi,\theta,\psi)=\begin{bmatrix}\cos\theta\cos\psi & \cos\theta\sin\psi & -\sin\theta\\ \sin\phi\sin\theta\cos\psi-\cos\phi\sin\psi & \sin\phi\sin\theta\sin\psi+\cos\phi\cos\psi & \sin\phi\cos\theta\\ \cos\phi\sin\theta\cos\psi+\sin\phi\sin\psi & \cos\phi\sin\theta\sin\psi-\sin\phi\cos\psi & \cos\phi\cos\theta\end{bmatrix} \quad (2.1)$$

2.2.3 Vector notation

The components of the necessary vectors in the vehicle-fixed frame are defined as in Eq. (2.2). These vectors will derive the six scalar equations of motion, covering the aircraft dynamics, and will be derived in the next section.

Vehicle velocity vector $\mathbf{V}_V$, Position of mass element relative to vehicle center of mass $\mathbf{p}$, gravity vector $\mathbf{g}$, and Angular velocity of Frame V with respect to Frame E $\boldsymbol{\omega}_{V,E}$ are defined as Eq. (2.2 a).

$$\begin{aligned}\left.\frac{d\mathbf{p}_V}{dt}\right|_E &\triangleq \mathbf{V}_V = U\mathbf{i}_V + V\mathbf{j}_V + W\mathbf{k}_V\\ \mathbf{p} &= x\mathbf{i}_V + y\mathbf{j}_V + z\mathbf{k}_V\\ \mathbf{g} &= g_x\mathbf{i}_V + g_y\mathbf{j}_V + g_z\mathbf{k}_V\\ \boldsymbol{\omega}_{V,E} &= P\mathbf{i}_V + Q\mathbf{j}_V + R\mathbf{k}_V\end{aligned} \quad (2.2\text{ a})$$

Aerodynamic and Thrust Force vectors are designed as Eq. (2.2 b).

$$\begin{aligned}\mathbf{F}_{Aero} &= F_{A_X}\mathbf{i}_V + F_{A_Y}\mathbf{j}_V + F_{A_Z}\mathbf{k}_V\\ \mathbf{F}_{Thrust} &= F_{T_X}\mathbf{i}_V + F_{T_Y}\mathbf{j}_V + F_{T_Z}\mathbf{k}_V\end{aligned} \quad (2.2\text{ b})$$

Aerodynamic and Thrust Moment vectors are designed as Eq. (2.2 c).

$$\begin{aligned}\mathbf{M}_{Aero} &= L_A\mathbf{i}_V + M_A\mathbf{j}_V + N_A\mathbf{k}_V\\ \mathbf{M}_{Thrust} &= L_T\mathbf{i}_V + M_T\mathbf{j}_V + N_T\mathbf{k}_V\end{aligned} \quad (2.2\text{ c})$$

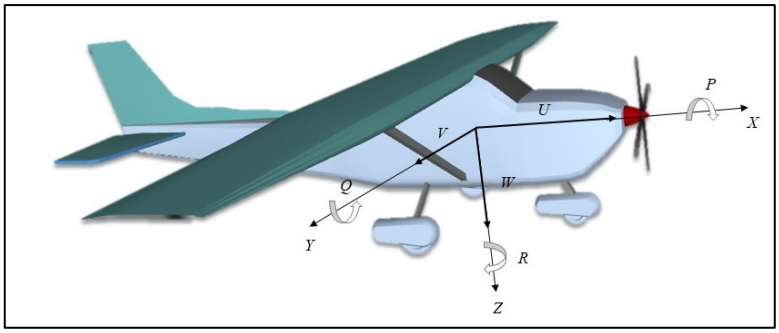

(a) Components of $\mathbf{V}_V$ and $\boldsymbol{\omega}_{V,E}$

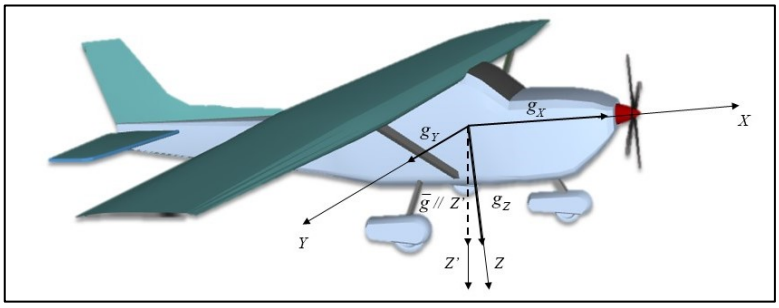

(b) Components of $\mathbf{g}$

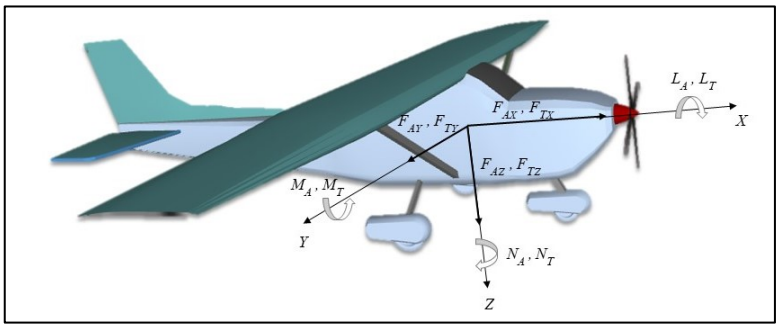

(c) Components of Force and Moment

Figure 2.3. Vector components.

2.3 Aircraft Flight Dynamics

2.3.1 Aircraft translational and rotational motion

From a vehicle, as shown in Figure 2.4, it is considered that the aircraft's mass $dm = \rho_V dV$ is acted by the forces consisting of gravitation plus external forces. By using

Newton's second law and equilibrium internal forces, the translational and relational momentum of the mass *dm* are expressed as

$$\int_{Vol} \left. \frac{d}{dt} \right|_E \left(\rho_V \left. \frac{d\mathbf{p}'}{dt} \right|_E dV \right) = \int_{Vol} \rho_V \mathbf{g} dV + \int_{Surface} d\mathbf{f}_{ext} \tag{2.3}$$

$$\int_{Vol} \left. \frac{d}{dt} \right|_E \left(\mathbf{p}' \times \rho_V \left. \frac{d\mathbf{p}'}{dt} \right|_E dV \right) = \int_{Vol} \mathbf{p}' \times \rho_V \mathbf{g} dV + \int_{Surface} \mathbf{p}' \times d\mathbf{f}_{ext} \tag{2.4}$$

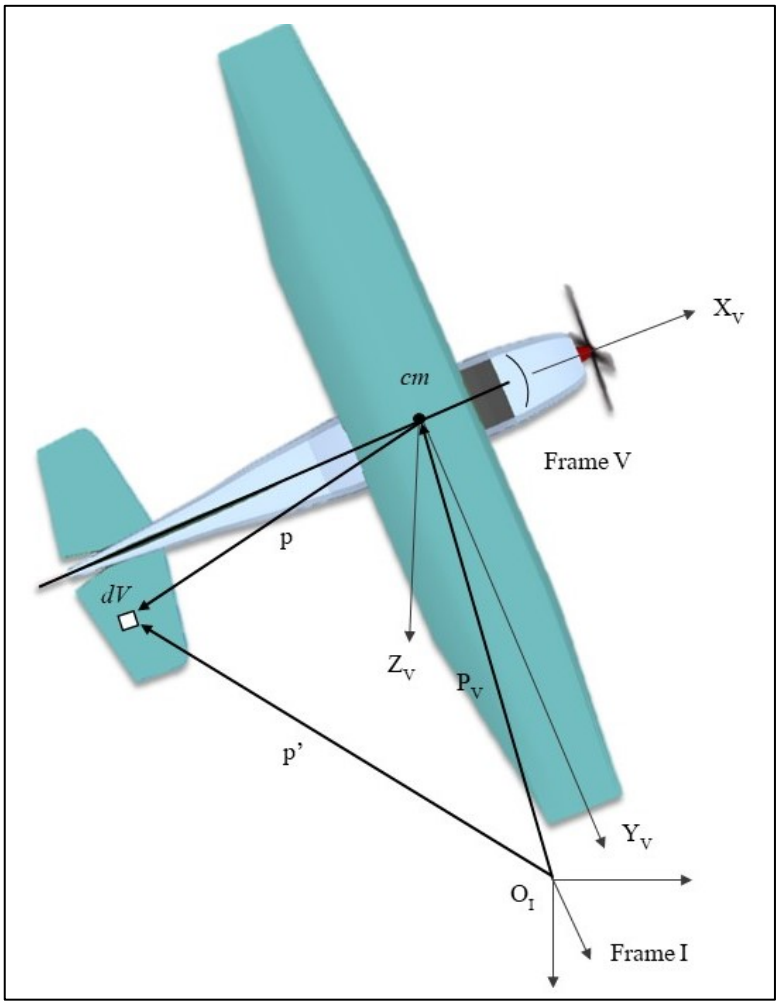

Figure 2.4. Position vectors.

However, these equations are expressed in terms of particles' position to the earth frame, which is not a suitable form for the derivation of aircraft dynamics. With the vehicle-

fixed frame and the assumption that the aircraft is a rigid body, the aircraft's mass and mass distribution are treated constant; thus Eq. (2.3) and (2.4) can be rewritten as below.

$$\left.\frac{d}{dt}\right|_E \left(m \left.\frac{d\mathbf{p}_V}{dt}\right|_E \right) \triangleq m \left.\frac{d\mathbf{V}_V}{dt}\right|_E = \int_{Vol} \rho_V \mathbf{g} dV + \int_{Surface} d\mathbf{f}_{ext} \tag{2.5}$$

$$\int_{Vol} \mathbf{p} \times \left(\rho_V \left(\left(\left. \frac{d\boldsymbol{\omega}_{V,I}}{dt} \right|_E \times \mathbf{p} \right) + \boldsymbol{\omega}_{V,I} \times \left(\boldsymbol{\omega}_{V,I} \times \mathbf{p} \right) \right) dV \right) = \int_{Surface} \mathbf{p} \times d\mathbf{f}_{ext} \tag{2.6}$$

For the right side of Eq. (2.5) and (2.6), the gravity force is assumed constant. Let the external forces and moments act on the vehicle arises due to aerodynamic and thrust effects. The equations of motion for a rigid vehicle with a constant density distribution governing the translational and rotational motion of aircraft can be expressed as

$$\left.\frac{d}{dt}\right|_E \left(m \left.\frac{d\mathbf{p}_V}{dt}\right|_E \right) = m \left.\frac{d\mathbf{V}_V}{dt}\right|_E = m\mathbf{g} + \mathbf{F}_{Aero} + \mathbf{F}_{Thrust} \tag{2.7}$$

$$\int_{Vol} \mathbf{p} \times \left(\rho_V \left(\left(\left. \frac{d\boldsymbol{\omega}_{V,I}}{dt} \right|_E \times \mathbf{p} \right) + \boldsymbol{\omega}_{V,I} \times \left(\boldsymbol{\omega}_{V,I} \times \mathbf{p} \right) \right) dV \right) = \mathbf{M}_{Aero} + \mathbf{M}_{Thrust} \tag{2.8}$$

2.3.2 Scalar equations of motion

There are a set of equations of motion that can be used to describe the aircraft flight dynamics, and this set of equations can be obtained by using Eq. (2.7) and (2.8). These equations comprise three translational equations of motion and three rotational equations of motion. They are suitable and sufficiently accurate to model the dynamics of conventional aircraft. Before the derivation of these equations of motion, it is necessary to introduce one vector translation. Consider a generic vector **A** that initially defines with respect to the earth frame. If vector **A** needs to be expressed with respect to the vehicle-

fixed frame, the vehicle-fixed frame's angular velocity $\omega_{V,E}$ with respect to the earth frame must be introduced. Thus, the expression of the vector **A** can be expressed as

$$\left.\frac{d\mathbf{A}}{dt}\right|_E = \left.\frac{d\mathbf{A}}{dt}\right|_V + \omega_{V,E} \times \mathbf{A} \tag{2.9}$$

Substituting Eq. (2.2) into Eq. (2.7) and (2.8) with the relationship given in Eq. (2.9), the three scalar equations for translational motion are expressed as

$$\begin{aligned} m\left(\dot{U} + QW - VR\right) &= -mg\sin\theta + F_{A_X} + F_{T_X} \\ m\left(\dot{V} + RU - PW\right) &= mg\cos\theta\sin\phi + F_{A_Y} + F_{T_Y} \\ m\left(\dot{W} + PV - QU\right) &= mg\cos\theta\cos\phi + F_{A_Z} + F_{T_Z} \end{aligned} \tag{2.10}$$

and the three scalar equations for rotational equations are expressed as

$$\begin{aligned} &I_{xx}\dot{P} - I_{xz}\left(\dot{R} + PQ\right) - I_{yz}\left(Q^2 - R^2\right) - I_{xy}\left(\dot{Q} - RP\right) + \left(I_{zz} - I_{yy}\right)RQ = L_A + L_T \\ &I_{yy}\dot{Q} + \left(I_{xx} - I_{zz}\right)PR - I_{xy}\left(\dot{P} + QR\right) - I_{yz}\left(\dot{R} - PQ\right) + I_{xz}\left(P^2 - R^2\right) = M_A + M_T \\ &I_{zz}\dot{R} - I_{xz}\left(\dot{P} - QR\right) - I_{xy}\left(P^2 - Q^2\right) - I_{yz}\left(\dot{Q} + RP\right) + \left(I_{yy} - I_{xx}\right)PQ = N_A + N_T \end{aligned} \tag{2.11}$$

where $\mathbf{I}_{\bullet}$ are the moments and products of inertia.

There are another set of equations that need to be addressed; the kinematic equations. These equations represent the kinematic relationship between the angular and translational rates and can be expressed as

$$
\begin{aligned}
P &= \dot{\phi} - \dot{\psi}\sin\theta \\
Q &= \dot{\theta}\cos\phi + \dot{\psi}\cos\theta\sin\phi \\
R &= \dot{\psi}\cos\theta\cos\phi - \dot{\theta}\sin\phi
\end{aligned}
\tag{2.12}
$$

Inverting Eq. (2.12) yields the following angular kinematic form,

$$
\begin{aligned}
\dot{\phi} &= P + Q\sin\phi\tan\theta + R\cos\phi\tan\theta \\
\dot{\theta} &= Q\cos\phi - R\sin\phi \\
\dot{\psi} &= \left(Q\sin\phi + R\cos\phi\right)\sec\theta
\end{aligned}
\tag{2.13}
$$

Summarizing Eq. (2.10) through (2.13), the nine nonlinear equations of motion governing the rigid dynamics of the aircraft have been developed. In the next section, the small perturbation theory will be applied to these equations for aircraft dynamics modeling.

2.3.3 The study of nonlinear aircraft dynamics

In this section, the small perturbation theory is applied to Eq. (2.10) to (2.13) for analyzing the aircraft dynamics behavior in the neighborhood of a reference condition. The small perturbation theory can be summarized into five steps as below.

1) Derive the nonlinear equations governing the aircraft dynamics, and this step has been done in the previous section.
2) Express all degrees of freedom in the equations from step 1 regarding a reference condition plus deviations from this reference condition.
3) Extract two sets of equations from the results obtained in the step 2 into the reference set and perturbation set.
4) Use the reference set for studying the reference conditions of interest.

5) Use the Perturbation set and the reference conditions selected in the step 4, for analyzing the aircraft's perturbation dynamics.

Following the second step of the small perturbation, all the variables expressed in terms of the reference, and perturbation quantities are listed in Table 2.1.

Table 2.1. The reference and perturbation quantities.

$U = U_{rs} + u$	$V = V_{rs} + v$	$W = W_{rs} + w$
$P = P_{rs} + p$	$Q = Q_{rs} + q$	$R = R_{rs} + r$
$\theta = \Theta_{rs} + \theta$	$\phi = \Phi_{rs} + \phi$	$\psi = \Psi_{rs} + \psi$
$F_{A_X} = F_{A_{X_{rs}}} + f_{A_X}$	$F_{A_Y} = F_{A_{Y_{rs}}} + f_{A_Y}$	$F_{A_Z} = F_{A_{Z_{rs}}} + f_{A_Z}$
$F_{T_X} = F_{T_{X_{rs}}} + f_{T_X}$	$F_{T_Y} = F_{T_{Y_{rs}}} + f_{T_Y}$	$F_{T_Z} = F_{T_{Z_{rs}}} + f_{T_Z}$
$L_A = L_{A_{rs}} + l_A$	$M_A = M_{A_{rs}} + m_A$	$N_A = N_{A_{rs}} + n_A$
$L_T = L_{T_{rs}} + l_T$	$M_T = M_{T_{rs}} + m_T$	$N_T = N_{T_{rs}} + n_T$

The variable subscripts with *rs* mean the reference variables, and the lower-case italics variables mean the perturbation variables. Under the small perturbation assumption and variables in Table 2.1, Eq. (2.10) to (2.13) can be extracted into the reference and perturbation equations as shown below.

The translational equations in the reference set are

$$\begin{aligned} m\left(\dot{U}_{rs} + Q_{rs}W_{rs} - V_{rs}R_{rs}\right) &= -mg\sin\Theta_{rs} + F_{A_{X\_rs}} + F_{T_{X\_rs}} \\ m\left(\dot{V}_{rs} + R_{rs}U_{rs} - P_{rs}W_{rs}\right) &= mg\cos\Theta_{rs}\sin\Phi_{rs} + F_{A_{Y\_rs}} + F_{T_{Y\_rs}} \\ m\left(\dot{W}_{rs} + P_{rs}V_{rs} - Q_{rs}U_{rs}\right) &= mg\cos\Theta_{rs}\cos\Phi_{rs} + F_{A_{Z\_rs}} + F_{T_{Z\_rs}} \end{aligned} \tag{2.14}$$

The translational equations in the perturbation set are

$$
\begin{aligned}
m\left(\dot{u}+\left(Q_{rs}w-W_{rs}q\right)-\left(V_{rs}r+R_{rs}v\right)\right) &= -mg\cos\Theta_{rs}\theta+f_{A_X}+f_{T_X}\\
m\left(\dot{v}+\left(R_{rs}u+U_{rs}r\right)-\left(P_{rs}w+W_{rs}p\right)\right) &= mg\left(\cos\Theta_{rs}\cos\Phi_{rs}\phi-\sin\Theta_{rs}\sin\Phi_{rs}\theta\right)+f_{A_Y}+f_{T_Y}\\
m\left(\dot{w}+\left(P_{rs}v+V_{rs}p\right)-\left(Q_{rs}u+U_{rs}q\right)\right) &= -mg\left(\cos\Theta_{rs}\sin\Phi_{rs}\phi+\sin\Theta_{rs}\cos\Phi_{rs}\theta\right)+f_{A_Z}+f_{T_Z}
\end{aligned}
\tag{2.15}
$$

The rotational equations in the reference set are

$$
\begin{aligned}
I_{xx}\dot{P}_{rs}-I_{xz}\left(\dot{R}_{rs}+P_{rs}Q_{rs}\right)+\left(I_{zz}-I_{yy}\right)Q_{rs}R_{rs} &= L_{A_{rs}}+L_{T_{rs}}\\
I_{yy}\dot{Q}_{rs}+\left(I_{xx}-I_{zz}\right)P_{rs}R_{rs}+I_{xz}\left(P_{rs}{}^{2}-R_{rs}{}^{2}\right) &= M_{A_{rs}}+M_{T_{rs}}\\
I_{zz}\dot{R}_{rs}-I_{xz}\left(\dot{P}_{rs}-Q_{rs}R_{rs}\right)+\left(I_{yy}-I_{xx}\right)P_{rs}Q_{rs} &= N_{A_{rs}}+N_{T_{rs}}
\end{aligned}
\tag{2.16}
$$

The rotational equations in the perturbation set are

$$
\begin{aligned}
I_{xx}\dot{p}-I_{xz}\left(\dot{r}+\left(Q_{rs}p+P_{rs}q\right)\right)+\left(I_{zz}-I_{yy}\right)\left(R_{rs}q+Q_{rs}r\right) &= l_A+l_T\\
I_{yy}\dot{q}+\left(I_{xx}-I_{zz}\right)\left(R_{rs}p+P_{rs}r\right)+2I_{xz}\left(P_{rs}p-R_{rs}r\right) &= m_A+m_T\\
I_{zz}\dot{r}-I_{xz}\left(\dot{p}-\left(R_{rs}q+Q_{rs}r\right)\right)+\left(I_{yy}-I_{xx}\right)\left(Q_{rs}p+P_{rs}q\right) &= n_A+n_T
\end{aligned}
\tag{2.17}
$$

The kinematics equations in the reference set are

$$
\begin{aligned}
P_{rs} &= \dot{\Phi}_{rs}-\dot{\Psi}_{rs}\sin\Theta_{rs}\\
Q_{rs} &= \dot{\Theta}_{rs}\cos\Phi_{rs}+\dot{\Psi}_{rs}\sin\Phi_{rs}\cos\Theta_{rs}\\
R_{rs} &= -\dot{\Theta}_{rs}\sin\Phi_{rs}+\dot{\Psi}_{rs}\cos\Phi_{rs}\cos\Theta_{rs}
\end{aligned}
\tag{2.18}
$$

The kinematics equations in the perturbation set are

$$
\begin{aligned}
p &= \dot{\phi} - \dot{\Psi}_{rs} \sin\Theta_{rs}\theta - \sin\Theta_{rs}\dot{\psi} \\
q &= \cos\Phi_{rs}\dot{\theta} - \dot{\Theta}_{rs}\sin\Phi_{rs}\phi + \dot{\Psi}_{rs}\left(\cos\Phi_{rs}\cos\Theta_{rs}\phi - \sin\Phi_{rs}\sin\Theta_{rs}\theta\right) + \sin\Phi_{rs}\cos\Theta_{rs}\dot{\psi} \\
r &= \cos\Phi_{rs}\cos\Theta_{rs}\dot{\psi} - \dot{\Theta}_{rs}\cos\Phi_{rs}\phi - \sin\Phi_{rs}\dot{\theta} - \dot{\Psi}_{rs}\left(\sin\Phi_{rs}\cos\Theta_{rs}\phi + \cos\Phi_{rs}\sin\Theta_{rs}\theta\right)
\end{aligned}
\tag{2.19}
$$

The angular kinematics equations in the reference set are

$$
\begin{aligned}
\dot{\Phi}_{rs} &= P_{rs} + Q_{rs}\sin\Phi_{rs}\tan\Theta_{rs} + R_{rs}\cos\Phi_{rs}\tan\Theta_{rs} \\
\dot{\Theta}_{rs} &= Q_{rs}\cos\Phi_{rs} - R_{rs}\sin\Phi_{rs} \\
\dot{\Psi}_{rs} &= \left(Q_{rs}\sin\Phi_{rs} + R_{rs}\cos\Phi_{rs}\right)\sec\Theta_{rs}
\end{aligned}
\tag{2.20}
$$

The angular kinematics equations in the perturbation set are

$$
\begin{aligned}
\dot{\phi} &= p + \tan\Theta_{rs}\left(\sin\Phi_{rs}q + \cos\Phi_{rs}r + \left(Q_{rs}\cos\Phi_{rs} - R_{rs}\sin\Phi_{rs}\right)\phi\right) \\
&\quad + \left(Q_{rs}\sin\Phi_{rs} + R_{rs}\cos\Phi_{rs} + \left(\dot{\Phi}_{rs} - P_{rs}\right)\tan\Theta_{rs}\right)\theta \\
\dot{\theta} &= \cos\Phi_{rs}q - \sin\Phi_{rs}r - \left(Q_{rs}\sin\Phi_{rs} + R_{rs}\cos\Phi_{rs}\right)\phi \\
\dot{\psi} &= \dot{\Psi}_{rs}\tan\Theta_{rs}\theta + \left(\sin\Phi_{rs}q + \cos\Phi_{rs}r - \left(R_{rs}\sin\Phi_{rs} - Q_{rs}\cos\Phi_{rs}\right)\phi\right)/\cos\Theta_{rs}
\end{aligned}
\tag{2.21}
$$

2.4 Aircraft Dynamics Linear Model

2.4.1 Linear equations of motion

The cores of aircraft dynamics linear models come from the set of perturbation equations. Consider Eq. (2.15) under the flat-earth condition, and aircraft has a constant mass. Therefore, by dividing Eq. (2.15) with the mass m, the differential equations of *u*, *v*, and *w* can be expressed as

$$
\begin{aligned}
\dot{u} &= \left(V_{rs}r + R_{rs}v\right) - \left(Q_{rs}w - W_{rs}q\right) - g\cos\Theta_{rs}\theta + \left(f_{A_X} + f_{T_X}\right)/m \\
\dot{v} &= \left(P_{rs}w + W_{rs}p\right) - \left(R_{rs}u + U_{rs}r\right) + g\left(\cos\Theta_{rs}\cos\Phi_{rs}\phi - \sin\Theta_{rs}\sin\Phi_{rs}\theta\right) + \left(f_{A_Y} + f_{T_Y}\right)/m \\
\dot{w} &= \left(Q_{rs}u + U_{rs}q\right) - \left(P_{rs}v + V_{rs}p\right) - g\left(\cos\Theta_{rs}\sin\Phi_{rs}\phi + \sin\Theta_{rs}\cos\Phi_{rs}\theta\right) + \left(f_{A_Z} + f_{T_Z}\right)/m
\end{aligned} \tag{2.22}
$$

With the same condition as in Eq. (2.22), the aircraft also assumes symmetricity about the XZ plane for Eq. (2.17). Therefore, the products of inertia are zero. Then Eq. (2.17) can be rewritten as the differential equations of q, p, and r as follows.

$$
\begin{aligned}
\dot{p} &= \mathrm{I}'\left(\frac{1}{I_{xx}}\left(I_{xz}\left(Q_{rs}p + P_{rs}q\right) + \left(I_{yy} - I_{zz}\right)\left(R_{rs}q + Q_{rs}r\right) + \left(l_A + l_T\right)\right)\right) \\
\dot{q} &= \frac{1}{I_{yy}}\left(\left(I_{zz} - I_{xx}\right)\left(R_{rs}p + P_{rs}r\right) + 2I_{xz}\left(R_{rs}r - P_{rs}p\right) + \left(m_A + m_T\right)\right) \\
\dot{r} &= \mathrm{I}'\left(\frac{1}{I_{zz}}\left(-I_{xz}\left(R_{rs}q + Q_{rs}r\right) + \left(I_{xx} - I_{yy}\right)\left(Q_{rs}p + P_{rs}q\right) + \left(n_A + n_T\right)\right)\right)
\end{aligned} \tag{2.23}
$$

where

$$
\mathrm{I}' = \frac{1}{1 - \left(\dfrac{I_{xz}^2}{I_{xx}I_{zz}}\right)}\begin{bmatrix} 1 & \dfrac{I_{xz}}{I_{xx}} \\ \dfrac{I_{xz}}{I_{zz}} & 1 \end{bmatrix}
$$

In this thesis, the flight condition of interest is the straight-and-level flight with zero bank and sideslip angles. Applying these flight conditions to Eq. (2.21) to (2.23), the linear equations governing translational and rotational motion can be shown as

$$
\begin{aligned}
\dot{u} &= -g\theta + \left(f_{A_X} + f_{T_X}\right)/m \\
\dot{v} &= -U_{rs}r + g\phi + \left(f_{A_Y} + f_{T_Y}\right)/m \\
\dot{w} &= U_{rs}q + \left(f_{A_Z} + f_{T_Z}\right)/m
\end{aligned} \tag{2.24}
$$

$$\begin{aligned}\dot{p} &= \mathrm{I}'\left(l_A + l_T\right)/I_{xx} \\ \dot{q} &= \left(m_A + m_T\right)/I_{yy} \\ \dot{r} &= \mathrm{I}'\left(n_A + n_T\right)/I_{zz}\end{aligned} \tag{2.25}$$

and the angular kinematic equations become

$$\dot{\phi} = p, \quad \dot{\theta} = q \quad \dot{\psi} = r \tag{2.26}$$

2.4.2 Linear equations of the forces and moments

In order to obtain the desired aircraft flight dynamics models, the external forces and moments on the right-hand side of Eq. (2.24) and (2.25) need to be explained. The external forces and moments that apply to the aircraft in this thesis are considered only from the viewpoint of aerodynamics and thrusts. The modeling based on the aircraft is a single-engine aircraft with only primary flight control surfaces. Appling the small perturbation theory as in the aircraft dynamics modeling, the specific small perturbation set of forces and moments can be expressed. The aerodynamic and thrust forces in perturbation set are

$$\begin{aligned}f_{A_X} + f_{T_X} = q_\infty S\Bigg\{&-\left(c_{D_u} + 2c_{D_s}\right)\left(\frac{u}{V_{P_s}}\right) + \left(c_{T_{X\_\mathrm{U}}} + 2c_{T_{X\_s}}\right)\left(\frac{u}{V_{P_s}}\right) + \left(-c_{D_\alpha} + c_{L_s}\right)\alpha - c_{D\_\delta_E}\delta_E\Bigg\} \\ &+\delta T\cos\left(\phi_T + \alpha_s\right)\end{aligned} \tag{2.27 a}$$

$$f_{A_Y} + f_{T_Y} = q_\infty S\left\{\left(c_{Y_\beta} + c_{Y_{T\_\beta}}\right)\beta + c_{Y_p}\left(\frac{pb}{2V_{P_s}}\right) + c_{Y_r}\left(\frac{rb}{2V_{P_s}}\right) + c_{Y\_\delta_A}\delta_A + c_{Y\_\delta_R}\delta_R\right\} \tag{2.27 b}$$

$$\begin{aligned}f_{A_Z} + f_{T_Z} = q_\infty S\Bigg\{&-\left(c_{L_u} + 2c_{L_s}\right)\left(\frac{u}{V_{P_s}}\right) + \left(-c_{L_\alpha} - c_{D_s}\right)\alpha - c_{L_{\dot{\alpha}}}\left(\frac{\dot{\alpha}\bar{c}}{2V_{P_s}}\right) - c_{L_q}\left(\frac{q\bar{c}}{2V_{P_s}}\right) - c_{L\_\delta_E}\delta_E\Bigg\} \\ &-\delta T\sin\left(\phi_T + \alpha_s\right)\end{aligned} \tag{2.27 c}$$

The aerodynamic and thrust moments in perturbation set are

$$l_A + l_T = q_\infty Sb\left\{\left(c_{l_\beta} + c_{l_{T\_\beta}}\right)\beta + c_{l_p}\left(\frac{p}{2V_{P_s}}\right) + c_{l_r}\left(\frac{r}{2V_{P_s}}\right) + c_{l\_\delta_A}\delta_A + c_{l\_\delta_R}\delta_R\right\} \tag{2.28 a}$$

$$\begin{aligned} m_A + m_T = q_\infty S\Bigg\{ & \left(c_{m_u} + 2c_{m_s}\right)\left(\frac{u}{V_{P_s}}\right) + \left(c_{m\_T_u} + 2c_{m\_T_s}\right)\left(\frac{u}{V_{P_s}}\right) + \left(c_{m_\alpha} + c_{m\_T_\alpha}\right)\alpha \\ & -c_{m_{\dot{\alpha}}}\left(\frac{\dot{\alpha}\,\bar{c}}{2V_{P_s}}\right) + c_{m_q}\left(\frac{q\bar{c}}{2V_{P_s}}\right) - c_{m\_\delta_E}\delta_E \Bigg\} \\ & + \delta T\left(d_T\cos\phi_T - X_T\sin\phi_T\right) \end{aligned} \tag{2.28 b}$$

$$n_A + n_T = q_\infty Sb\left\{\left(c_{n_\beta} + c_{n\_T_\beta}\right)\beta + c_{n_p}\left(\frac{p}{2V_{P_s}}\right) + c_{n_r}\left(\frac{r}{2V_{P_s}}\right) + c_{n\_\delta_A}\delta_A + c_{n\_\delta_R}\delta_R\right\} \tag{2.28 c}$$

2.4.3 Decoupled state-space models

To obtain the complete aircraft dynamics model, Eq. (2.27) and (2.28) are substituted into Eq. (2.24) and (2.25) with simplification applied according to the standard shorthand notation.

$$\begin{aligned} \dot{u} &= -g\theta + \left(X_u + X_{T_u}\right)u + X_\alpha\alpha + X_{\delta_E}\delta_E + X_T\delta_T \\ \dot{v} &= g\phi + Y_\beta\beta + Y_p p + Y_r r + Y_{\delta_A}\delta_A + Y_{\delta_R}\delta_R \\ \dot{w} &= Z_u u + Z_\alpha\alpha + Z_{\dot{\alpha}}\dot{\alpha} + \left(Z_q + U_{rs}\right)q + Z_{\delta_E}\delta_E + Z_T\delta_T \end{aligned} \tag{2.29}$$

$$\begin{aligned} \dot{p} &= L_\beta\beta + L_p p + L_r r + L_{\delta_A}\delta_A + L_{\delta_R}\delta_R \\ \dot{q} &= \left(M_u + M_{T_u}\right)u + \left(M_\alpha + M_{T_\alpha}\right)\alpha + M_{\dot{\alpha}}\dot{\alpha} + M_q q + M_{\delta_E}\delta_E + M_{\delta_T}\delta_T \\ \dot{r} &= N_\beta\beta + N_p p + N_r r + N_{\delta_A}\delta_A + N_{\delta_R}\delta_R \end{aligned} \tag{2.30}$$

Table 2.2. The standard shorthand notation for decoupled models.

$X_u = -\left(c_{D_u} + 2c_{D_s}\right) q_\infty S / V_{P_s}$	$Y_\beta = \left(c_{Y_\beta} + c_{Y_{T_\beta}}\right) q_\infty S$	$Z_u = -\left(c_{L_u} + 2c_{L_s}\right) q_\infty S / V_{P_s}$
$X_{T_u} = \left(c_{T_{X_U}} + 2c_{T_{X_s}}\right) q_\infty S / V_{P_s}$	$Y_p = c_{Y_p}\, q_\infty Sb / 2V_{P_s}$	$Z_\alpha = \left(-c_{L_\alpha} - c_{D_s}\right) q_\infty S$
$X_\alpha = \left(-c_{D_\alpha} + c_{L_s}\right) q_\infty S$	$Y_r = c_{Y_r}\, q_\infty Sb / 2V_{P_s}$	$Z_{\dot{\alpha}} = c_{L_{\dot{\alpha}}}\, q_\infty S\bar{c} / 2V_{P_s}$
$X_{\delta_E} = -c_{D_{\delta_E}} q_\infty S$	$Y_{\delta_A} = c_{Y_{\delta_A}} q_\infty S$	$Z_q = -\left(c_{L_q} q_\infty S\bar{c} / 2V_{P_s}\right)$
$X_T = \cos\left(\phi_T + \alpha_s\right)$	$Y_{\delta_R} = c_{Y_{\delta_R}} q_\infty S$	$Z_{\delta_E} = -c_{L_{\delta_E}}$
		$Z_T = \sin\left(\phi_T + \alpha_s\right) q_\infty S$
$L_\beta = \left(c_{l_\beta} + c_{l_{T_\beta}}\right) q_\infty Sb$	$M_u = \left(c_{m_u} + 2c_{m_s}\right) q_\infty S / V_{P_s}$	$N_\beta = \left(c_{n_\beta} + c_{n_{T_\beta}}\right) q_\infty Sb$
$L_p = c_{l_p} q_\infty Sb / 2V_{P_s}$	$M_{T_u} = \left(c_{m_{T_u}} + 2c_{m_{T_s}}\right) q_\infty S / V_{P_s}$	$N_p = c_{n_p}\, q_\infty Sb / 2V_{P_s}$
$L_r = c_{l_r}\, q_\infty Sb / 2V_{P_s}$	$M_\alpha = c_{m_\alpha} q_\infty S$	$N_r = c_{n_r}\, q_\infty Sb / 2V_{P_s}$
$L_{\delta_A} = c_{l_{\delta_A}} q_\infty Sb$	$M_{T_\alpha} = c_{m_{T_\alpha}} q_\infty S$	$N_{\delta_A} = c_{n_{\delta_A}} q_\infty Sb$
$L_{\delta_R} = c_{l_{\delta_R}} q_\infty Sb$	$M_{\dot{\alpha}} = -c_{m_{\dot{\alpha}}}\, q_\infty S\bar{c} / 2V_{P_s}$	$N_{\delta_R} = c_{n_{\delta_R}} q_\infty Sb$
	$M_q = c_{m_q}\, q_\infty S\bar{c} / 2V_{P_s}$	
	$M_{\delta_E} = -c_{m_{\delta_E}} q_\infty S$	
	$M_{\delta_T} = \left(d_T \cos\phi_T - X_T \sin\phi_T\right)$	

Eq. (2.29) and (2.30) with Eq. (2.26) can be regrouped into two significant groups; aircraft longitudinal dynamics and lateral-directional dynamics. With an additional notation that $\alpha = w/U_{rs}$ and $\beta = v/U_{rs}$, the regrouped equations can be expressed in the following equations:

$$
\left.
\begin{aligned}
\dot{u} &= \left(X_u + X_{T_u}\right)u + X_\alpha \alpha - g\theta + X_{\delta_E}\delta_E + X_T\delta_T \\
\dot{\alpha} &= \frac{1}{U_{rs} - Z_{\dot{\alpha}}}\left(Z_u u + Z_\alpha \alpha + \left(Z_q + U_{rs}\right)q + Z_{\delta_E}\delta_E + Z_T\delta_T\right) \\
\dot{q} &= \left(\left(M_u + M_{T_u}\right) + \frac{M_{\dot{\alpha}} Z_u}{U_{rs} - Z_{\dot{\alpha}}}\right)u + \left(\left(M_\alpha + M_{T_\alpha}\right) + \frac{M_{\dot{\alpha}} Z_\alpha}{U_{rs} - Z_{\dot{\alpha}}}\right)\alpha + \left(M_q + \frac{M_{\dot{\alpha}}\left(Z_q + U_{rs}\right)}{U_{rs} - Z_{\dot{\alpha}}}\right)q \\
&\quad + \left(M_{\delta_E} + \frac{M_{\dot{\alpha}} Z_{\delta_E}}{U_{rs} - Z_{\dot{\alpha}}}\right)\delta_E + + \left(M_{\delta_T} + \frac{M_{\dot{\alpha}} Z_{\delta_T}}{U_{rs} - Z_{\dot{\alpha}}}\right)\delta_T \\
\dot{\theta} &= q
\end{aligned}
\right\} \quad (2.31)
$$

$$
\left.
\begin{aligned}
\dot{\beta} &= \frac{1}{U_{rs}}\left(Y_\beta \beta + Y_p p + Y_r r + g\phi + Y_{\delta_A}\delta_A + Y_{\delta_R}\delta_R\right) \\
\dot{p} &= L_\beta \beta + L_p p + L_r r + L_{\delta_A}\delta_A + L_{\delta_R}\delta_R \\
\dot{r} &= N_\beta \beta + N_p p + N_r r + N_{\delta_A}\delta_A + N_{\delta_R}\delta_R \\
\dot{\phi} &= p
\end{aligned}
\right\} \quad (2.32)
$$

The first equation, Eq. (2.31), is called the linear aircraft longitudinal dynamics equation of motion, while the second, Eq. (2.32), is called the aircraft lateral-directional equation of motion. To obtain a suitable format for the design theory, these two groups of equations will be summarized and expressed in the space-state format in the next section.

2.5 Summary of the Aircraft Flight Dynamics Models

The aircraft longitudinal dynamics model in the state-space format is shown in Eq. (2.33), where $\mathbf{x}(t)_{Long}$ is the state vector, $\mathbf{x}(t)_{Long} = \begin{bmatrix} u & \alpha & q & \theta \end{bmatrix}^T$, and $\mathbf{u}(t)_{Long}$ is the input, which consists of elevator defection and thrust, $\mathbf{u}(t)_{Long} = \begin{bmatrix} \delta_E & \delta_T \end{bmatrix}^T$.

$$\frac{d}{dt}\mathbf{x}(t)_{Long} = \mathbf{A}_{Long}\mathbf{x}(t)_{Long} + \mathbf{B}_{Long}\mathbf{u}(t)_{Long}$$
$$= \begin{bmatrix} X'_u & X'_\alpha & X'_q & X'_\theta \\ Z'_u & Z'_\alpha & Z'_q & Z'_\theta \\ M'_u & M'_\alpha & M'_q & M'_\theta \\ 0 & 0 & 1 & 0 \end{bmatrix}\mathbf{x}(t)_{Long} + \begin{bmatrix} X'_{\delta_E} & X'_{\delta_T} \\ Z'_{\delta_E} & Z'_{\delta_T} \\ M'_{\delta_E} & M'_{\delta_T} \\ 0 & 0 \end{bmatrix}\mathbf{u}(t)_{Long} \tag{2.33}$$

$$\mathbf{y}(t)_{Long} = \mathbf{C}_{Long}\mathbf{x}(t)_{Long} = \mathbf{I}_4\mathbf{x}(t)_{Long}$$

The aircraft lateral-directional dynamics model in the state-space format is shown in Eq. (2.34), where $\mathbf{x}(t)_{LatDir}$ is the state vector, $\mathbf{x}(t)_{LatDir} = \begin{bmatrix}\beta & p & r & \phi\end{bmatrix}^T$, and $\mathbf{u}(t)_{LatDir}$ is the input, which consists of aileron and rudder defection, $\mathbf{u}(t)_{LatDir} = \begin{bmatrix}\delta_A & \delta_R\end{bmatrix}^T$.

$$\frac{d}{dt}\mathbf{x}(t)_{LatDir} = \mathbf{A}_{LatDir}\mathbf{x}(t)_{LatDir} + \mathbf{B}_{LatDir}\mathbf{u}(t)_{LatDir}$$
$$= \begin{bmatrix} Y'_\beta & Y'_p & Y'_r & Y'_\phi \\ L'_\beta & L'_p & L'_r & L'_\phi \\ N'_\beta & N'_p & N'_r & N'_\phi \\ 0 & 1 & 0 & 0 \end{bmatrix}\mathbf{x}(t)_{LatDir} + \begin{bmatrix} Y'_{\delta_A} & Y'_{\delta_R} \\ L'_{\delta_A} & L'_{\delta_R} \\ N'_{\delta_A} & N'_{\delta_R} \\ 0 & 0 \end{bmatrix}\mathbf{u}(t)_{LatDir} \tag{2.34}$$

$$\mathbf{y}(t)_{LatDir} = \mathbf{C}_{LatDir}\mathbf{x}(t)_{LatDir} = \mathbf{I}_4\mathbf{x}(t)_{LatDir}$$

Table 2.3. The standard shorthand notation for aircraft flight dynamics models.

$X'_u = \left(X_u + X_{T_u}\right)$	$Z'_u = Z_u \Big/ \left(U_{rs} - Z_{\underset{\alpha}{.}}\right)$	$M'_u = \left(M_u + M_{T_u}\right) + \left(M_{\underset{\alpha}{.}} Z_u \Big/ U_{rs} - Z_{\underset{\alpha}{.}}\right)$
$X'_\alpha = X_\alpha$	$Z'_\alpha = Z_\alpha \Big/ \left(U_{rs} - Z_{\underset{\alpha}{.}}\right)$	$M'_\alpha = \left(M_\alpha + M_{T_\alpha}\right) + \left(M_{\underset{\alpha}{.}} Z_\alpha \Big/ U_{rs} - Z_{\underset{\alpha}{.}}\right)$
$X'_q = 0$	$Z'_q = \left(Z_q + U_{rs}\right) \Big/ \left(U_{rs} - Z_{\underset{\alpha}{.}}\right)$	$M'_q = M_q + \left(M_{\underset{\alpha}{.}} \left(Z_q + U_{rs}\right) \Big/ U_{rs} - Z_{\underset{\alpha}{.}}\right)$
$X'_\theta = -g$	$Z'_\theta = 0$	$M'_\theta = 0$
$X'_{\delta_E} = X_{\delta_E}$	$Z'_{\delta_E} = Z_{\delta_E} \Big/ \left(U_{rs} - Z_{\underset{\alpha}{.}}\right)$	$M'_{\delta_E} = M_{\delta_E} + \left(M_{\underset{\alpha}{.}} Z_{\delta_E} \Big/ U_{rs} - Z_{\underset{\alpha}{.}}\right)$
$X'_{\delta_T} = X_T$	$Z'_{\delta_T} = Z_T \Big/ \left(U_{rs} - Z_{\underset{\alpha}{.}}\right)$	$M'_{\delta_T} = M_{\delta_T} + \left(M_{\underset{\alpha}{.}} Z_{\delta_T} \Big/ U_{rs} - Z_{\underset{\alpha}{.}}\right)$
$Y'_\beta = Y_\beta / U_{rs}$	$L'_\beta = L_\beta$	$N'_\beta = N_\beta$
$Y'_p = Y_p / U_{rs}$	$L'_p = L_p$	$N'_p = N_p$
$Y'_r = Y_r / U_{rs}$	$L'_r = L_r$	$N'_r = N_r$
$Y'_\phi = g / U_{rs}$	$L'_\phi = 0$	$N'_\phi = 0$
$Y'_{\delta_A} = Y_{\delta_A} / U_{rs}$	$L'_{\delta_A} = L_{\delta_A}$	$N'_{\delta_A} = N_{\delta_A}$
$Y'_{\delta_R} = Y_{\delta_R} / U_{rs}$	$L'_{\delta_R} = L_{\delta_R}$	$N'_{\delta_R} = N_{\delta_R}$

Chapter 3

Controller Design Theory

3.1 Overview

This chapter provides fundamental theory for designing a controller. The controller design method used throughout this thesis is Coefficient Diagram Method or CDM. CDM is an algebraic approach for a controller design and has a special diagram called "Coefficient Diagram" as the design tool. The necessary information needed for the controller design is provided by the coefficient diagram. There are only three design parameters in CDM namely the stability index, γ_i, the equivalent time constant, τ, and the stability limit, γ_i^*, makes design processes of CDM is straightforward and has a good design criterion. By using CDM as the design method, the characteristic polynomial and the controller can be designed simultaneously and guaranteed to achieve a good balance between the system stability, response, and robustness. CDM is used to design the servo state-feedback system for the “Aircraft flight control by CDM-designed Servo State-feedback system” or ACDM-SS and details will be given in Chapter 4.

3.2 Coefficient Diagram Method

The Coefficient Diagram Method [88] – [89], or CDM, is one of the controller design theories and was first proposed in 1991 by Shunji Manabe [90]. CDM is an algebraic controller design theory which uses polynomials of the closed-loop controlled system in design processes. CDM uses a specific diagram called the coefficient diagram as a powerful tool to demonstrate the efficiency and performance of a closed-loop controlled system. CDM considers the numerator polynomial and the denominator polynomial

equation of the closed-loop controlled system's transfer function separately for system performance analysis. CDM initially defines the type and order for both the controller polynomial equation and the closed-loop system's characteristic polynomial equation at the beginning of design processes. Both these polynomial equations are designed by considering the system performance requirements. There are three major parameters to determine the closed-loop system's performance: the stability index, γ_i, the equivalent time constant, τ, and the stability limit, γ_i^*.

3.2.1 The CDM standard structure and mathematical relations

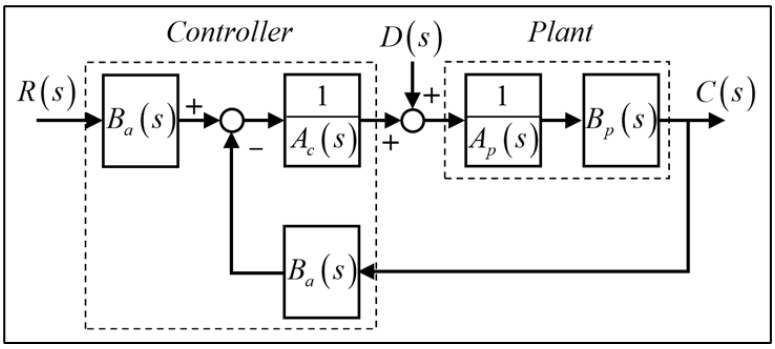

Figure 3.1. The CDM standard structure of the Single-Input Single-Output system. (Permitted reuse reproduction for doctor thesis from the author).

The standard structure of the Single-Input Single-Output (SISO) system to be designed by CDM, is illustrated in Figure 3.1. This SISO system comprises the controller and the plant, where the former is described by the polynomials $A_c(s)$, $B_a(s)$, and $B_c(s)$ while the plant is described by the polynomials $A_p(s)$ and $B_p(s)$. From the standard structure of this SISO system, the $C(s)$ is the output of a closed-loop control system and can be calculated as shown in Eq. (3.1).

$$C(s)=\frac{B_a(s)B_p(s)R(s)+A_c(s)B_p(s)D(s)}{A_c(s)A_p(s)+B_c(s)B_p(s)} \tag{3.1}$$

According to CDM, the characteristic polynomial of Eq. (3.1) can be defined as follows:

$$\begin{aligned} P(s) &= A_c(s)A_p(s)+B_c(s)B_p(s) \\ &= a_n s^n + a_{n-1}s^{n-1} + \ldots + a_1 s + a_0 \\ &= \sum_{i=0}^{n} a_i s^i \end{aligned} \tag{3.2}$$

where a_0, a_1,…, a_n are the coefficients of the characteristic polynomial. These coefficients contain known parameters of plant and unknown parameters of the controller. In this thesis the CDM method is used to design these unknown parameters of the controller. The controller design process will be discussed in detail later in Chapter 4.

The CDM control design method includes vital parameters used in controller design, and these parameters are the stability index, γ_i, which determines the stability of the system; the equivalent time constant, τ, which determines the speed of the system response; and the stability limit, γ_i^*, which indicates the robustness of the control system parameter change. These three parameters are mathematically related to the coefficients of the characteristic polynomial, a_0, a_1,…, a_n, as follows:

$$\gamma_i = \frac{a_i^2}{a_{i+1}a_{i-1}} \tag{3.3}$$

$$\tau = \frac{a_1}{a_0} \tag{3.4}$$

$$\gamma_i^* = \frac{1}{\gamma_{i+1}} + \frac{1}{\gamma_{i-1}}; \quad \gamma_0,\ \gamma_n = \infty \tag{3.5}$$

where $i = 1, \cdots, n-1$. The coefficients of the characteristic polynomial, a_i, can be expressed in the term of the stability index, γ_i, and the equivalent time constant, τ, by using Eq. (3.3) – (3.5) as shown in Eq. (3.6)

$$\begin{aligned} a_i &= a_0 \tau^i \frac{1}{\gamma_{i-1} \cdots \gamma_2^{i-2} \gamma_1^{i-1}} \\ &= a_0 \tau^i \prod_{j=1}^{i-1} \frac{1}{\gamma_{i-j}^j} \end{aligned} \tag{3.6}$$

From Eq. (3.2) and (3.6), the characteristic polynomial, $P(s)$, in term of the stability index, γ_i, and the equivalent time constant, τ, can be explained as follows:

$$P(s) = a_0 \left[\left\{ \sum_{i=2}^{n} \left(\prod_{j=1}^{i-1} 1 \Big/ \gamma_{i-j}^j \right) (\tau s)^i \right\} + \tau s + 1 \right] \tag{3.7}$$

The monic characteristic polynomial, $P_m(s)$, is also obtained by dividing Eq. (3.7) with coefficient, a_n. The coefficient, a_n, can be obtained by using Eq. (3.6).

$$a_n = a_0 \tau^n \prod_{j=1}^{n-1} \frac{1}{\gamma_{n-j}^j} \tag{3.8}$$

From both Eq. (3.7) and (3.8), the monic characteristic polynomial, $P_m(s)$, is shown in Eq. (3.9) and will be used to design the controller by CDM later.

$$P_m(s) = \frac{\prod_{j=1}^{n-1} \left(\gamma_{n-j} \right)^j}{\tau^n} \left[\left\{ \sum_{i=2}^{n} \left(\prod_{j=1}^{i-1} 1 \Big/ \gamma_{i-j}^j \right) (\tau s)^i \right\} + \tau s + 1 \right] \tag{3.9}$$

3.2.2 Coefficient diagram

The controller design principle by CDM has the coefficient diagram as a handy and essential tool in controller design. This coefficient diagram shows the system's stability, response time, and robustness within a single diagram. This style makes it useful for designing high-order polynomials. Besides considering the overall system performance simultaneously, the coefficient diagram is also highly accurate and allows the designer to implement it in the actual design efficiently. As mentioned above, the coefficient diagram's uniqueness gives control system designers the tools to make design decisions that are not available in any other method. The coefficient diagrams are presented with a semi-logarithmic graph. The left vertical axis shows the polynomial coefficient, a_i, while the right vertical axis shows the stability index, γ_i, the equivalent time value, τ, and the stability limit, γ_i^*. The equivalent time constant, τ, is represented by a straight line between 1 and τ, and the horizontal axis represents the order "*i*" of each coefficient of the polynomial.

For an illustration purpose of the coefficient diagram construction, an example is introduced for easier understanding. A characteristic polynomial equation of the closed-loop control system is assumed to be defined as:

$$P(s) = 0.25s^5 + s^4 + 2s^3 + 2s^2 + s + 0.2 \tag{3.10}$$

From Eq. (3.10), the coefficient, a_i, of the characteristic polynomial $P(s)$, and the parameter of CDM can be obtained as:

$$a_i = \begin{bmatrix} 0.25 & 1 & 2 & 2 & 1 & 0.2 \end{bmatrix} \tag{3.11}$$

$$\gamma_i = \begin{bmatrix} 2 & 2 & 2 & 2.5 \end{bmatrix} \tag{3.12}$$

$$\tau = 5 \tag{3.13}$$

$$\gamma_i^* = \begin{bmatrix} 0.5 & 1 & 0.9 & 0.5 \end{bmatrix} \tag{3.14}$$

Using Eq. (3.11) through (3.14), the coefficient diagram shown in Figure 3.2 displays the coefficient, a_i, the stability index, γ_i, the equivalent time constant, τ, and the stability limit, γ_i^*.

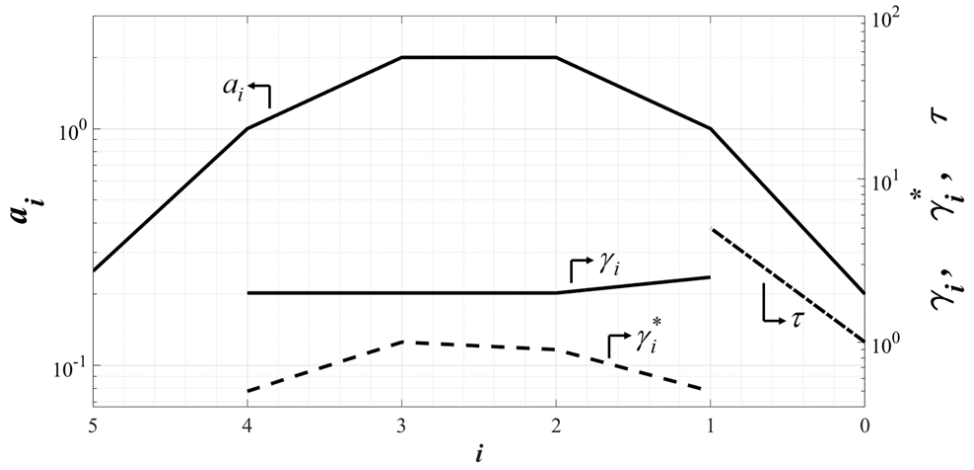

Figure 3.2. Coefficient diagram.

(Permitted reuse reproduction for doctor thesis from the author).

In this diagram, the curve's curvature represents the stability of the system, the slope of the curve represents the speed of the system response, and the deformation of the curve due to the change in system parameters indicates the robustness of the system.

Figure 3.3 (a) indicates the larger the curve of the coefficient, ai, becomes, the more stable the control system will be. It corresponds to the stability index, γ_i, that are greater. In contrast, the smaller the curve of the coefficient, a_i, is the less stable the control system becomes, and this corresponds to the low stability index, γ_i. Figure 3.3 (b) illustrates that

the more left and down the curve of the coefficient, ai, is shifted, the smaller the equivalent time constant, τ , becomes. The response of the control system will be faster.

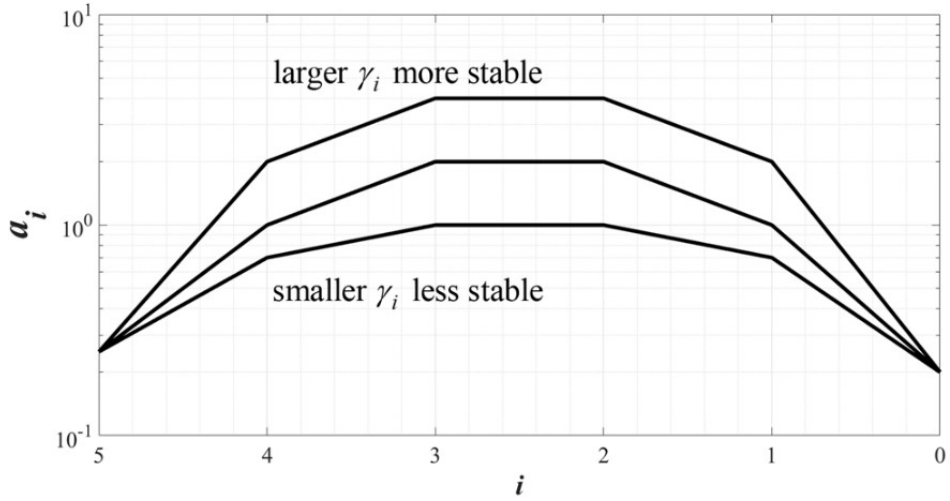

(a) Due to change of the stability index

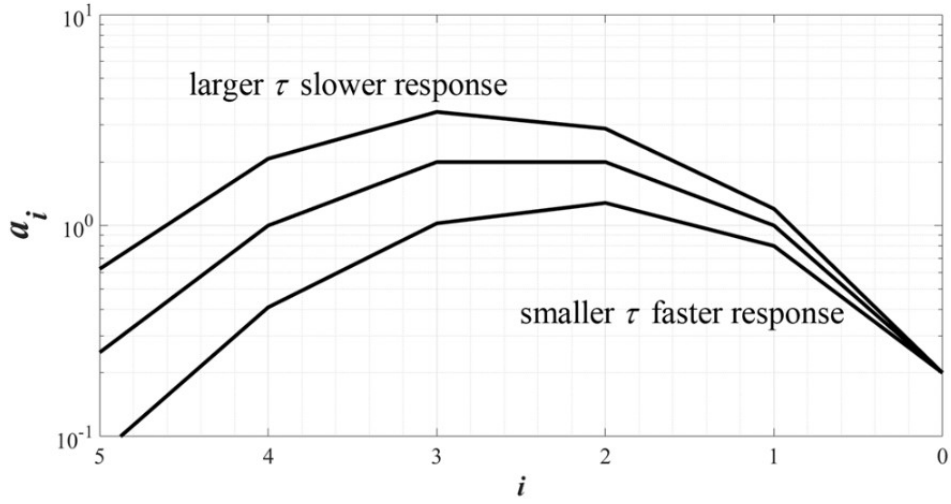

(b) Due to change of the equivalent time constant

Figure 3.3. The shape of coefficient diagram.

(Permitted reuse reproduction for doctor thesis from the author).

3.2.3 The stability condition of CDM

Stability of the control system obtained by means of CDM is analyzed from the viewpoint of the sufficient conditions for Lipatov stability theory [91].

The Routh-Hurwitz stability criterion has a system stability condition for the third-order and can be expressed as follows:

$$a_2 a_1 > a_3 a_0 \tag{3.15}$$

Furthermore, it can be expressed in term of the stability index, γ_i, as follows:

$$\gamma_2 \gamma_1 > 1 \tag{3.16}$$

The stability conditions of the fourth-order system are given as:

$$a_2 > \left(a_1 / a_3\right) a_4 + \left(a_3 / a_1\right) a_0 \tag{3.17}$$

$$\gamma_2 > \gamma_2^* \tag{3.18}$$

By the Routh-Hurwitz stability criterion, Lipatov said this was appropriate to consider a third or fourth-order system's stability. However, this is not enough to take into account the stability of a higher-ordered system. Lipatov offers sufficient system stability and instability conditions for a system of fifth-order or higher in many forms. The sufficient stability and instability of the system suitable for the controller design by CDM is given below.

The sufficient condition for investigating the stability of the system is

$$a_i > 1.2\left[\frac{a_{i-1}}{a_{i+1}} a_{i+2} + \frac{a_{i+1}}{a_{i-1}} a_{i-2}\right] \tag{3.19}$$

$$\gamma_i > 1.12\gamma_i^* \text{ for every value of } i = 2 \sim n-2 \tag{3.20}$$

The sufficient condition for investigating the instability of the system is

$$a_{i+1}a_i \le a_{i+2}a_{i-1} \tag{3.21}$$

$$\gamma_{i+1}\gamma_i \le 1 \text{ for some values of } i = 2 \sim n-2 \tag{3.22}$$

3.2.4 The standard form of CDM

Graham studied the relationship between the characteristic polynomial coefficient and the transient response using the Integral Time Absolute Error or ITAE standard form, presented for the first time in 1953. In 1960, Kessler developed a new standard form by which every stability index is assigned a value of 2 to reduce the oscillations and overshoot of response in the control system designed with the ITAE.

Later in 1998, Shunji Manabe proposed assigning the 1st stability index, γ_1, to be equal to 2.5 and the remaining stability index to 2, by which the obtained response from the control system has no overshoot and the rise time decrease. He assigned this stability index as the standard stability index of CDM, shown as follow:

$$\gamma_{n-1}=...=\gamma_3=\gamma_2=2 \text{ and } \gamma_1 = 2.5 \tag{3.23}$$

He also assigned the equivalent time constant, τ, which relates to the settling time as follow:

$$t_s = 2.5\tau \sim 3\tau \tag{3.24}$$

From Eq. (3.7), it is found that the characteristic polynomial $P(s)$ consists of the stability index, γ_i, and the equivalence time constant, τ. Therefore, the shape of the control system's response is determined by the stability index, γ_i, and the speed of the

response is determined by the equivalent time constant, τ . The properties of the standard form of CDM are summarized as follows.

For a type-1 system, there is no overshoot, and a type-2 system has an overshoot of approximately 40%. The control system's rise time can be designed to assign the equivalent time constant, τ .

The shape of a CDM-designed control system's response is independent of the system's order. However, it depends on the stability index, γ_i, and the equivalent time constant, τ .

The pole locations of the low-rank system are arranged in a straight line, and the pole location of the high-rank system is within 49.5 degrees from the negative real axis with the value of the damping ratio, ζ , greater than 0.65, as shown in Figure 3.4.

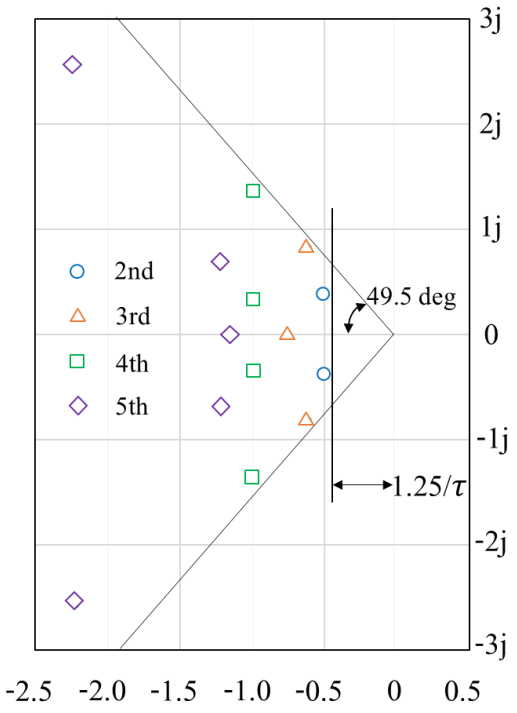

Figure 3.4. The pole location of the various systems.

(Permitted reuse reproduction for doctor thesis from the author).

3.2.5 The stability index criterion

In general, the CDM's standard stability index, γ_i, is a prerequisite for the control system to achieve the stability and response required. However, the designer can modify this stability index, γ_i, to obtain a control system with the desired performance under the condition below.

$$\gamma_i > 1.5\gamma_i^* \tag{3.25}$$

If the control system is required to have robustness, it should be chosen with a high stability index. From sufficient conditions for stability, Lipatov stated that the system is stable if all the stability indices are more than 1.5, which was demonstrated in his research. Furthermore, if all the stability indexes are more than 4, then the system's roots are all negative real numbers. Therefore, typically CDM state that the stability index value generally should be chosen between 1.5 and 4.

Chapter 4

Aircraft Flight Control System and Design

4.1 Overview

This chapter provides the concepts for designing and understanding the aircraft flight control system. The structures of the servo state-feedback systems for aircraft longitudinal and lateral-directional dynamics are first introduced. After describing the decoupled servo systems, the structure of the Aircraft flight control by CDM-designed Servo State-feedback system or ACDM-SS is introduced. ACDM-SS is comprised of the aircraft's longitudinal and lateral-directional servo state-feedback system. Then, the servo system design procedures based on CDM are explained. The final section of the chapter describes the concept and design of Aircraft flight control by CDM-designed Model-Reference Adaptive System or ACDM-RAS. ACDM-RAS uses ACDM-SS as its reference model to specified behavior of the system.

4.2 The Structure of Servo State-Feedback System

Before designing the ACDM-SS and ACDM-RAS, the aircraft flight dynamics models [81] [82] [86] [87], which are detailed in Chapter 2, need to be modified to achieve the required controlled parameters and restructured to suit the controller design. Therefore, the aircraft dynamics models developed in Chapter 2 require further modifications to obtain the desired equation form.

4.2.1 Aircraft longitudinal dynamics servo state-feedback system

The desired aircraft longitudinal dynamics model in this research needs two parameters to be controlled: altitude, *h*, and speed, *u*. Nevertheless, the aircraft longitudinal dynamics model from Chapter 2, Eq. (2.33), does not yet contain an altitude as a state variable. Therefore, it is necessary to customize this equation based on the relationship of heights as

$$\dot{h} = -V_{p_1}\alpha + V_{p_1}\theta \tag{4.1}$$

The modified aircraft longitudinal dynamics model thus can be rewritten as follows:

$$\begin{aligned}\frac{d}{dt}\mathbf{x}_L(t) &= \mathbf{A}_L\mathbf{x}_L(t) + \mathbf{B}_L\mathbf{u}_L(t) \\ &= \begin{bmatrix} X'_u & X'_\alpha & X'_q & X'_\theta & 0 \\ Z'_u & Z'_\alpha & Z'_q & Z'_\theta & 0 \\ M'_u & M'_\alpha & M'_q & M'_\theta & 0 \\ 0 & 0 & 1 & 0 & 0 \\ 0 & -V_{p_1} & 0 & V_{P_1} & 0 \end{bmatrix}\mathbf{x}_L(t) + \begin{bmatrix} X'_{\delta_E} & X'_{\delta_T} \\ Z'_{\delta_E} & Z'_{\delta_T} \\ M'_{\delta_E} & M'_{\delta_T} \\ 0 & 0 \\ 0 & 0 \end{bmatrix}\mathbf{u}_L(t) \\ \mathbf{y}_L(t) &= \mathbf{C}_L\mathbf{x}_L(t) = \mathbf{I}_5\mathbf{x}_L(t)\end{aligned} \tag{4.2}$$

The modified state variable for Eq. (4.2) is $\mathbf{x}_L(t) = \begin{bmatrix} u & \alpha & q & \theta & h \end{bmatrix}^T$, and the input is $\mathbf{u}_L(t) = \begin{bmatrix} \delta_E & \delta_T \end{bmatrix}^T$. When the aircraft longitudinal dynamics model has complete state variables as required, this model will refine the structure to obtain the suitable structure used for designing the controller further.

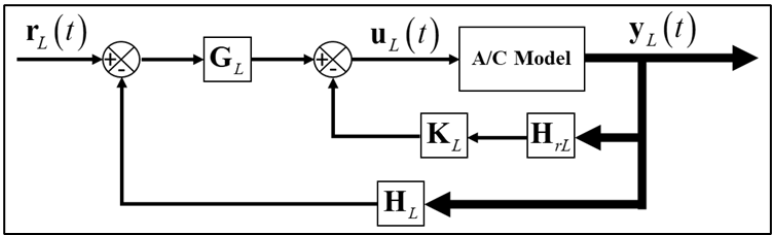

Figure 4.1. Aircraft longitudinal dynamics servo state-feedback system.

(Cited and partially modified from ref. 80).

The structure of the servo state-feedback system [48] [92] shown in Figure 4.1 involves the following matrices, being introduced to complete this servo system.

- The reduced matrices $\mathbf{H}_{rL}$ and $\mathbf{H}_L$

$$\mathbf{H}_{rL} = \begin{bmatrix} 0 & 1 & 0 & 0 & 0 \\ 0 & 0 & 1 & 0 & 0 \\ 0 & 0 & 0 & 1 & 0 \end{bmatrix} \text{ and } \mathbf{H}_L = \begin{bmatrix} 1 & 0 & 0 & 0 & 0 \\ 0 & 0 & 0 & 0 & 1 \end{bmatrix} \tag{4.3}$$

- The feedback loop gain matrix, $\mathbf{K}_L$, and the servo loop gain matrix, $\mathbf{G}_L$

$$\mathbf{K}_L = \begin{bmatrix} k_{l2} & k_{l3} & k_{l4} \end{bmatrix} \text{ and } \mathbf{G}_L = \begin{bmatrix} k_{l1} & k_{l5} \end{bmatrix} \tag{4.4}$$

Therefore, the input $\mathbf{u}_L(t)$ for this aircraft longitudinal dynamics servo state-feedback system can be expressed in Eq. (4.5).

$$\begin{aligned} \mathbf{u}_L(t) &= -\mathbf{K}_L\mathbf{H}_{rL}\mathbf{x}_L(t) + \mathbf{G}_L\left(\mathbf{r}_L(t) - \mathbf{H}_L\mathbf{x}_L(t)\right) \\ &= -\left(k_{l2}x_{l2} + k_{l3}x_{l3} + k_{l4}x_{l4}\right) + \left(k_{l1}r_{l1} + k_{l5}r_{l2} - k_{l1}x_{l1} - k_{l5}x_{l5}\right) \\ &= -\begin{bmatrix} k_{l1} & k_{l2} & k_{l3} & k_{l4} & k_{l5} \end{bmatrix}\begin{bmatrix} x_{l1} \\ x_{l2} \\ x_{l3} \\ x_{l4} \\ x_{l5} \end{bmatrix} + \begin{bmatrix} k_{l1} & k_{l5} \end{bmatrix}\begin{bmatrix} r_{l1} \\ r_{l2} \end{bmatrix} \end{aligned} \tag{4.5}$$

$$\mathbf{u}_L(t) = -\mathbf{K}_{sL}\mathbf{x}_L(t) + \mathbf{G}_L\mathbf{r}_L(t)$$

where $\mathbf{K}_{sL}$ is the overall servo state-feedback gain matrix for this aircraft longitudinal dynamics servo state-feedback system and expressed in Eq. (4.6).

$$\mathbf{K}_{sL} = \begin{bmatrix} k_{I1} & k_{I2} & k_{I3} & k_{I4} & k_{I5} \end{bmatrix} \tag{4.6}$$

4.2.2 Aircraft lateral-directional dynamics servo state-feedback system

Similarly, with the aircraft longitudinal dynamics model, two parameters are controlled in the desired aircraft lateral-directional dynamics model: heading angle, ψ , and side angle, β . Therefore, it is necessary to adjust Eq. (2.34) to archive the desired state variables. The angular kinematic equation, Eq. (2.26), is applied to Eq. (2.34). The modified aircraft lateral-directional dynamics model thus can be rewritten as follows:

$$\begin{aligned} \frac{d}{dt}\mathbf{x}_{LD}(t) &= \mathbf{A}_{LD}\mathbf{x}_{LD}(t) + \mathbf{B}_{LD}\mathbf{u}_{LD}(t) \\ &= \begin{bmatrix} Y'_{\beta} & Y'_{p} & Y'_{r} & Y'_{\phi} & 0 \\ L'_{\beta} & L'_{p} & L'_{r} & 0 & 0 \\ N'_{\beta} & N'_{p} & N'_{r} & 0 & 0 \\ 0 & 1 & 0 & 0 & 0 \\ 0 & 0 & 1 & 0 & 0 \end{bmatrix} \mathbf{x}_{LD}(t) + \begin{bmatrix} Y'_{\delta_A} & Y'_{\delta_R} \\ L'_{\delta_A} & L'_{\delta_R} \\ N'_{\delta_A} & L'_{\delta_R} \\ 0 & 0 \\ 0 & 0 \end{bmatrix} \mathbf{u}_{LD}(t) \end{aligned} \tag{4.7}$$

$$\mathbf{y}_{LD}(t) = \mathbf{C}_{LD}\mathbf{x}_{LD}(t) = \mathbf{I}_5\mathbf{x}_{LD}(t)$$

The modified state variable is $\mathbf{x}_{LD}(t) = \begin{bmatrix} \beta & p & r & \phi & \psi \end{bmatrix}^T$, and the input is $\mathbf{u}_{LD}(t)$ $= \begin{bmatrix} \delta_A & \delta_R \end{bmatrix}^T$. Since these two dynamics models, longitudinal and lateral-directional dynamics, are very similar in terms of the number of state variables and their order of the control variables. Therefore, the aircraft lateral-directional dynamics model's reduced matrices are identical to those of the aircraft longitudinal dynamics model. The overall

servo state-feedback gain matrices of both dynamic models are also identical. These matrices can be expressed as the following equation.

- The reduced matrices $\mathbf{H}_{rLD}$ and $\mathbf{H}_{LD}$

$$\mathbf{H}_{rLD} = \begin{bmatrix} 0 & 1 & 0 & 0 & 0 \\ 0 & 0 & 1 & 0 & 0 \\ 0 & 0 & 0 & 1 & 0 \end{bmatrix}, \text{ and } \mathbf{H}_{LD} = \begin{bmatrix} 1 & 0 & 0 & 0 & 0 \\ 0 & 0 & 0 & 0 & 1 \end{bmatrix} \tag{4.8}$$

- The feedback loop gain matrix, $\mathbf{K}_{LD}$, and the servo loop gain matrix, $\mathbf{G}_{LD}$

$$\mathbf{K}_{LD} = \begin{bmatrix} k_{ld2} & k_{ld3} & k_{ld4} \end{bmatrix} \text{ and } \mathbf{G}_{LD} = \begin{bmatrix} k_{ld1} & k_{ld5} \end{bmatrix} \tag{4.9}$$

- The overall servo state-feedback gain matrix for aircraft lateral-directional dynamics servo state-feedback system

$$\mathbf{K}_{sLD} = \begin{bmatrix} k_{ld1} & k_{ld2} & k_{ld3} & k_{ld4} & k_{ld5} \end{bmatrix} \tag{4.10}$$

4.2.3 The integrated aircraft flight dynamics model and ACDM-SS

In the preceding sections, the servo systems designed by the CDM for aircraft longitudinal dynamics and aircraft lateral-directional dynamics have been obtained. The structure of the Aircraft flight control CDM-designed Servo State-feedback system or ACDM-SS, which serves as the reference model in the Aircraft flight control by CDM-designed Model-Reference Adaptive System or ACDM-RAS, is illustrated in Figure 4.2.

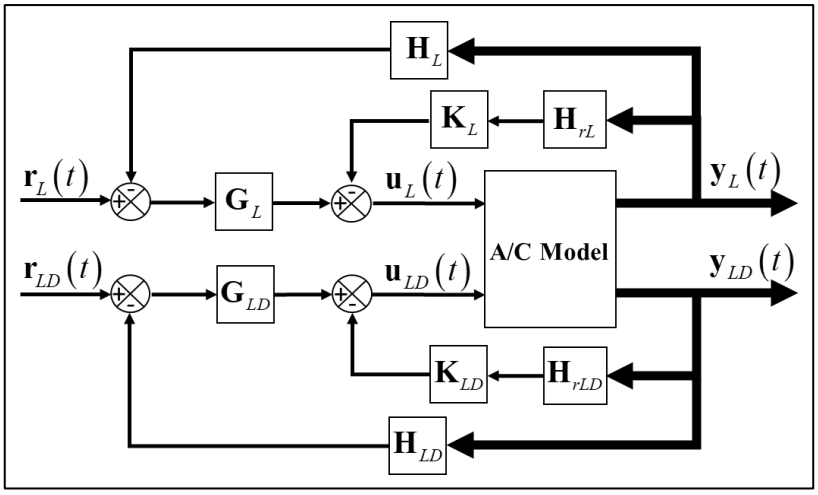

Figure 4.2. The structure of the ACDM-SS.

(Cited and partially modified from ref. 80).

The ACDM-SS consists of three major parts: the aircraft longitudinal dynamics and aircraft lateral-directional dynamics controllers and the integrated aircraft flight dynamics linear model (A/C Model in Figure 4.3). This A/C model combines both the two derived aircraft flight dynamics linear models, Eq. (4.2) and (4.7), as stated in the previous section. This integrated aircraft flight dynamics model will also be used in the simulation to investigate the ACDM-RAS's effectiveness later in Chapter 5. The structure of this integrated aircraft flight dynamics model is expressed by the following equation.

$$\frac{d}{dt}\mathbf{x}(t)=\begin{bmatrix}\mathbf{A}_L & \mathbf{0}\\ \mathbf{0} & \mathbf{A}_{LD}\end{bmatrix}\mathbf{x}(t)+\begin{bmatrix}\mathbf{B}_L & \mathbf{0}\\ \mathbf{0} & \mathbf{B}_{LD}\end{bmatrix}\mathbf{u}(t)$$

$$\mathbf{y}(t)=\begin{bmatrix}\mathbf{C}_L & \mathbf{0}\\ \mathbf{0} & \mathbf{C}_{LD}\end{bmatrix}\mathbf{x}(t) \tag{4.11}$$

where $\mathbf{x}(t)=\begin{bmatrix}\mathbf{x}_L(t)^T & \mathbf{x}_{LD}(t)^T\end{bmatrix}^T$ and $\mathbf{u}(t)=\begin{bmatrix}\mathbf{u}_L(t)^T & \mathbf{u}_{LD}(t)^T\end{bmatrix}^T$.

4.3 ACDM-SS Design Procedures

"Aircraft flight control by CDM-designed Servo State-feedback system" or ACDM-SS in Figure 4.3 uses CDM to design the overall servo state-feedback gain matrices, K_{sL} and K_{sLD} for aircraft longitudinal and lateral-directional dynamics. The summary of the procedures to determine these overall servo state-feedback gain matrices is given as follows.

1) Determine the CDM's characteristic polynomial, Eq. (3.9), using the standard stability index and the equivalent time constant recommended by CDM. The standard stability index values are 2.5 for γ_1 and 2 for γ_2 to γ_{n-1}, and the equivalent time constant, τ, is 5.

$$P_{CDM}(s) = a_n s^n + a_{n-1} s^{n-1} + \ldots + a_1 s + a_0$$

2) Determine the coefficients of CDM's characteristic polynomial, obtained from the first step, which are called CDM's coefficients. These CDM's coefficients will be used to specify the characteristic polynomial of $\mathbf{A}_L - \mathbf{B}_L\mathbf{K}_{sL}$ and $\mathbf{A}_{LD} - \mathbf{B}_{LD}\mathbf{K}_{sLD}$, which are closed-loop system equations of longitudinal and lateral-directional dynamics parts.
3) Determine the characteristic polynomials of $\mathbf{A}_L - \mathbf{B}_L\mathbf{K}_{sL}$ and $\mathbf{A}_{LD} - \mathbf{B}_{LD}\mathbf{K}_{sLD}$. These polynomials are represented with respect to the unknown variables; k_{li} and k_{ldi}, which are the elements of the overall servo state-feedback gain matrix; $\mathbf{K}_{sL}$ and $\mathbf{K}_{sLD}$, respectively. The coefficients are determined from each polynomial.

$$P_L(s) = a_{Ln}\left(A_{Lij}, B_{Lij}, k_{li}\right)s^n + a_{Ln-1}\left(A_{Lij}, B_{Lij}, k_{li}\right)s^{n-1} + \ldots + a_{L1}\left(A_{Lij}, B_{Lij}, k_{li}\right)s + a_{L0}\left(A_{Lij}, B_{Lij}, k_{li}\right)$$

$$P_{LD}(s) = a_{LDn}\left(A_{LDij}, B_{LDij}, k_{ldi}\right)s^n + a_{LDn-1}\left(A_{LDij}, B_{LDij}, k_{ldi}\right)s^{n-1} + \ldots + \\ + a_{LD1}\left(A_{LDij}, B_{LDij}, k_{ldi}\right)s + a_{LD0}\left(A_{LDij}, B_{LDij}, k_{ldi}\right)$$

4) Calculate the values of the overall servo state-feedback gain matrices by matching CDM's coefficients with the polynomial coefficients from step 3. Then the overall servo state-feedback gain matrix's values, $\mathbf{K}_{sL}$ and $\mathbf{K}_{sLD}$, can be obtained.

$$\begin{array}{l|l} a_{Ln}\left(A_{Lij}, B_{Lij}, k_{li}\right) = a_n & a_{LDn}\left(A_{LDij}, B_{LDij}, k_{ldi}\right) = a_n \\ a_{Ln-1}\left(A_{Lij}, B_{Lij}, k_{li}\right) = a_{n-1} & a_{LDn-1}\left(A_{LDij}, B_{LDij}, k_{ldi}\right) = a_{n-1} \\ \vdots & \vdots \\ a_{L1}\left(A_{Lij}, B_{Lij}, k_{li}\right) = a_1 & a_{LD1}\left(A_{LDij}, B_{LDij}, k_{ldi}\right) = a_1 \\ a_{L0}\left(A_{Lij}, B_{Lij}, k_{li}\right) = a_0 & a_{LD0}\left(A_{LDij}, B_{LDij}, k_{ldi}\right) = a_0 \end{array}$$

5) Calculate the values of $\mathbf{K}_L$ and $\mathbf{G}_L$ from $\mathbf{K}_{sL}$ by using Eq. (4.4) and (4.6), and $\mathbf{K}_{LD}$ and $\mathbf{G}_{LD}$ from $\mathbf{K}_{sLD}$ by using Eq. (4.9) and (4.10).

Remark: The adjustments are allowed to meet the system requirement if required. The adjustments can be made through the CDM's parameters, the stability index γ_i, and the equivalent time constant τ. CDM strongly recommends that the values of γ_1, γ_2, and γ_3 be 2.5, 2, and 2, respectively, and the remaining gamma, γ_4 to γ_{n-1} can arbitrarily be adjusted according to Eq. (3.25) but should be chosen between 1.5 and 4. The value of τ can arbitrarily be adjusted according to Eq. (3.24). After adjusting the CDM's parameters, repeat steps 2 to 5, and the coefficient diagrams can be used to investigate system stability and response by considering the shape of the diagram in each parameter adjustment process.

4.4 ACDM-RAS Concept and Design

This section describes the concept of "Aircraft flight control by CDM-designed Model-Reference Adaptive System" or ACDM-RAS. The structure of ACDM-RAS is shown in Figure 4.3. The ACDM-RAS is the Model-reference adaptive system [93] – [96] that adopts the ACDM-SS as the reference model. By the concept of the Model-reference adaptive system, the performance of ACDM-RAS is expressed in the term of ACDM-SS. ACDM-RAS has the reference model and adaptive mechanism as the essential part. These parts make ACDM-RAS different from the ordinary feedback control system. The online adaptive mechanism adjusts the controller parameters according to reducing the error difference between the output of the system and the output of the reference model. Therefore, ACDM-RAS responds to both the input commands and the output of the reference model. Many methods and theories are available for adaptive mechanisms, such as a gradient method or stability theory. ACDM-RAS uses the Lyapunov stability theory to obtain an adaptive mechanism for the system of interest. The following sections show how to prepare ACDM-SS to be the reference model and the processes to obtain the adaptive mechanism.

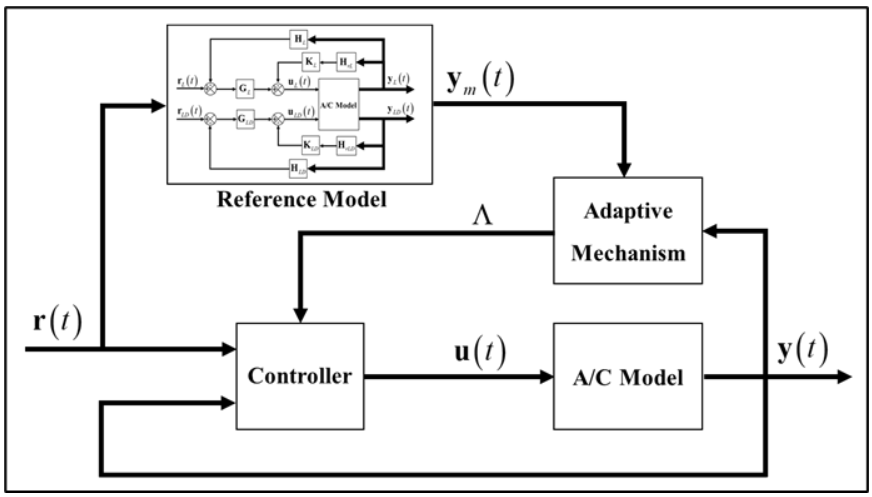

Figure 4.3. The concept of the ACDM-RAS.

4.4.1 The reference model by ACDM-SS

In the reference model preparation, only the aircraft longitudinal dynamics part is used as an example. Find the servo state-feedback system by substituting the input $\mathbf{u}_L(t)$, Eq. (4.5) into the aircraft longitudinal dynamics model, Eq. (4.2). Then the servo state-feedback system can be described as Eq. (4.12).

$$\begin{aligned}\frac{d}{dt}\mathbf{x}_L(t) &= \mathbf{A}_L\mathbf{x}_L(t)+\mathbf{B}_L\left(-\mathbf{K}_{sL}\mathbf{x}_L(t)+\mathbf{G}_L\mathbf{r}_L(t)\right)\\ &= \mathbf{A}_L\mathbf{x}_L(t)-\mathbf{B}_L\mathbf{K}_{sL}\mathbf{x}_L(t)+\mathbf{B}_L\mathbf{G}_L\mathbf{r}_L(t)\\ &= \left(\mathbf{A}_L-\mathbf{B}_L\mathbf{K}_{sL}\right)\mathbf{x}_L(t)+\left(\mathbf{B}_L\mathbf{G}_L\right)\mathbf{r}_L(t)\end{aligned} \tag{4.12}$$

Assign the following parameters for the reference model.

$$\begin{aligned}\mathbf{x}_{mL}(t) &= \mathbf{x}_L(t)\\ \mathbf{A}_{mL} &= \mathbf{A}_L-\mathbf{B}_L\mathbf{K}_{sL}\\ \mathbf{B}_{mL} &= \mathbf{B}_L\mathbf{G}_L\end{aligned} \tag{4.13}$$

$$\begin{aligned}\mathbf{y}_{mL}(t) &= \mathbf{y}_L(t)\\ \mathbf{C}_{mL} &= \mathbf{C}_L\end{aligned}$$

Then, Eq. (4.12) can be rewritten as the reference model, Eq. (4.14).

$$\begin{aligned}\frac{d}{dt}\mathbf{x}_{mL}(t) &= \mathbf{A}_{mL}\mathbf{x}_{mL}(t)+\mathbf{B}_{mL}\mathbf{r}_L(t)\\ \mathbf{y}_{mL}(t) &= \mathbf{C}_{mL}\mathbf{x}_{mL}(t)\end{aligned} \tag{4.14}$$

4.4.2 Adaptive mechanism

In order to obtain the adaptive mechanism based on the concept of ACDM-RAS, Figure 4.3, the error equation is needed. This error equation is the difference between the

output of the actual plant and the output of the reference model. Assuming the general aircraft longitudinal dynamics to be controlled expressed as in Eq. (4.15),

$$\begin{aligned} \frac{d}{dt}\mathbf{x}_{aL}(t) &= \mathbf{A}_{al}\mathbf{x}_{aL}(t) + \mathbf{B}_{aL}\mathbf{u}_{aL}(t) \\ \mathbf{y}_{aL}(t) &= \mathbf{C}_{aL}\mathbf{x}_{aL}(t) \end{aligned} \quad , \tag{4.15}$$

the error equation for the aircraft longitudinal dynamics part can be described in Eq. (4.16), and its time derivative is given in Eq. (4.17).

$$e = \mathbf{x}_{aL}(t) - \mathbf{x}_{mL}(t) \tag{4.16}$$

$$\begin{aligned} \dot{e} &= \frac{d}{dt}\mathbf{x}_{aL}(t) - \frac{d}{dt}\mathbf{x}_{mL}(t) \\ &= \left(\mathbf{A}_{aL}\mathbf{x}_{aL}(t) + \mathbf{B}_{aL}\mathbf{u}_{aL}(t)\right) - \left(\mathbf{A}_{mL}\mathbf{x}_{mL}(t) + \mathbf{B}_{mL}\mathbf{r}_{L}(t)\right) \\ &= \mathbf{A}_{aL}\mathbf{x}_{aL}(t) + \mathbf{B}_{aL}\mathbf{u}_{aL}(t) - \mathbf{A}_{mL}\mathbf{x}_{mL}(t) - \mathbf{B}_{mL}\mathbf{r}_{L}(t) \end{aligned} \tag{4.17}$$

Let the control law $\mathbf{u}_{aL}(t)$ be given by Eq. (4.18).

$$\mathbf{u}_{aL}(t) = -\mathbf{M}\mathbf{x}_{aL}(t) + \mathbf{N}\mathbf{r}_{L}(t) \tag{4.18}$$

where the matrices **M** and **N** will be described later. Substituting the control law $\mathbf{u}_{aL}(t)$ into Eq. (4.17) and adding and subtracting $\mathbf{A}_{mL}\mathbf{x}_{aL}(t)$ from the right-hand side of Eq. (4.17) yields the time derivative of the error equation as in Eq. (4.19),

$$\begin{aligned} \dot{e} &= \mathbf{A}_{aL}\mathbf{x}_{aL}(t) + \mathbf{B}_{aL}\mathbf{u}_{aL}(t) - \mathbf{A}_{mL}\mathbf{x}_{mL}(t) - \mathbf{B}_{mL}\mathbf{r}_{L}(t) \\ &= \mathbf{A}_{mL}e + \left(\mathbf{A}_{aL} - \mathbf{B}_{aL}\mathbf{M} - \mathbf{A}_{mL}\right)\mathbf{x}_{aL}(t) + \left(\mathbf{B}_{aL}\mathbf{N} - \mathbf{B}_{mL}\right)\mathbf{r}_{L}(t) \\ &= \mathbf{A}_{mL}e + \left(\mathbf{A}'(\Omega) - \mathbf{A}'(\Omega_0)\right)\mathbf{x}_{aL}(t) + \left(\mathbf{B}'(\Omega) - \mathbf{B}'(\Omega_0)\right)\mathbf{r}_{L}(t) \end{aligned} \quad , \tag{4.19}$$

where $\mathbf{A}'(\Omega)$ and $\mathbf{B}'(\Omega)$ are the functions that give the sufficient condition for perfect model-following. $\mathbf{A}'(\Omega)$ and $\mathbf{B}'(\Omega)$ are described as in Eq. (4.20), and Ω is the adaptive parameter.

$$\begin{aligned}\mathbf{A}'(\Omega) &= \mathbf{A}_L - \mathbf{B}_L(-\Omega + \mathbf{K}_{sL}) \\ \mathbf{B}'(\Omega) &= \mathbf{B}_L(\Omega + \mathbf{G}_L)\end{aligned} \tag{4.20}$$

Following this condition, Eq. (4.20), it is possible to find the parameter value Ω_0 such that

$$\begin{aligned}\mathbf{A}'(\Omega_0) &= \mathbf{A}_{mL} \\ \mathbf{B}'(\Omega_0) &= \mathbf{B}_{mL}\end{aligned}. \tag{4.21}$$

Therefore, the matrices **M** and **N** are described in term of Ω as in Eq. (4.22).

$$\begin{aligned}\mathbf{M} &= -\Omega + \mathbf{K}_{sL} \\ \mathbf{N} &= \Omega + \mathbf{G}_L\end{aligned} \tag{4.22}$$

Assuming the parameter value Ω_0 equals zero because this value satisfies Eq. (4.21), and substituting Ω_0 into Eq. (4.19), the time derivative of error equation can be rewritten again as in Eq. (4.23).

$$\dot{e} = \mathbf{A}_{mL}e + \mathbf{B}_L\Omega\mathbf{x}_{aL} + \mathbf{B}_L\Omega\mathbf{r}_L \tag{4.23}$$

The Lyapunov function [97] is introduced based on the error equation to derive the adaptive mechanism as shown in Eq. (4.24).

$$V(e,\Omega) = \frac{1}{2}\left(\lambda_L e^T\mathbf{P}e + \mathbf{x}_{aL}^T\Omega^T\Omega\mathbf{x}_{aL} + \mathbf{r}_L{}^T\Omega^T\Omega\mathbf{r}_L\right) \tag{4.24}$$

In this Lyapunov function V, λ_L is the adaptive gain for the aircraft longitudinal dynamics part, and the matrix **P** is a positive definite matrix. Therefore, the function V is also a positive definite. To verify the function V is indeed a Lyapunov function, its total time derivative needs to be examined

$$\frac{dV}{dt} = -\frac{1}{2}\lambda_L e^T \mathbf{Q} e + \left(\mathbf{x}_{aL}^T \Omega^T\right)\left(\lambda_L \mathbf{B}_L^T \mathbf{P} e + \frac{d}{dt}\left(\Omega \mathbf{x}_{aL}\right)\right) + \left(\mathbf{r}_L{}^T \Omega^T\right)\left(\lambda_L \mathbf{B}_L^T \mathbf{P} e + \frac{d}{dt}\left(\Omega \mathbf{r}_L\right)\right) \quad (4.25)$$

where the matrix **Q** is a positive definite matrix and must satisfy the following equation.

$$\mathbf{A}_{mL}^T \mathbf{P} + \mathbf{P}\mathbf{A}_{mL} = -\mathbf{Q} \quad (4.26)$$

The Lyapunov functions theorem for linear systems states that the pair of positive definite matrices **P** and **Q**, which have the relationship as in Eq. (4.26), always exist if $\mathbf{A}_{mL}$ is stable. Since CDM designs $\mathbf{A}_{mL}$, then stable. Therefore, the matrices **P** and **Q** exist. If the adaptive gain λ_L is the positive number and the following equations are chosen to be

$$\begin{aligned} \frac{d}{dt}\left(\Omega \mathbf{x}_{aL}\right) &= -\lambda_L \mathbf{B}_L^T \mathbf{P} e \\ \frac{d}{dt}\left(\Omega \mathbf{r}_L\right) &= -\lambda_L \mathbf{B}_L^T \mathbf{P} e \end{aligned} \quad (4.27)$$

then Eq. (4.28) is obtained as

$$\frac{dV}{dt} = -\frac{1}{2}\lambda_L e^T \mathbf{Q} e \quad (4.28)$$

By observing Eq. (4.28), the total time derivative of function V is negative semidefinite, implying that function V is the Lyapunov function. Using the Barbalat theorem, it can be concluded that the error equation goes to zero when time goes to infinity

under the assumption that all state variables are measurable. That implies that the response of the actual plant is identical to the response of the reference model.

The control law $\mathbf{u}_{aL}(t)$ can be modified by using Eq. (4.18), (4.22), and (4.27), as expressed in Eq. (4.29).

$$\begin{aligned}\mathbf{u}_{aL}(t) &= -\mathbf{M}\mathbf{x}_{aL} + \mathbf{N}\mathbf{r}_L \\ &= \Omega\mathbf{x}_{aL} - \mathbf{K}_{sL}\mathbf{x}_{aL} + \Omega\mathbf{r}_L + \mathbf{G}_L\mathbf{r}_L \\ &= -\lambda_L\int \mathbf{B}_L^T\mathbf{P}e - \mathbf{K}_{sL}\mathbf{x}_{aL} - \lambda_L\int \mathbf{B}_L^T\mathbf{P}e + \mathbf{G}_L\mathbf{r}_L \\ &= -\mathbf{K}_{sL}\mathbf{x}_{aL} + \mathbf{G}_L\mathbf{r}_L + \Lambda_L\end{aligned} \tag{4.29}$$

Λ_L is assigned as the adaptive mechanism for the aircraft longitudinal dynamics part and expressed in Eq. (4.30).

$$\Lambda_L = -2\lambda_L\int \mathbf{B}_L^T\mathbf{P}e \tag{4.30}$$

Due to the similarity between the two aircraft dynamics models, the control law $\mathbf{u}_{aLD}(t)$ and the adaptive mechanism Λ_{LD} for aircraft lateral-directional dynamics are derived in the same way with aircraft longitudinal dynamics part and shown in Eq. (4.31).

$$\begin{aligned}\mathbf{u}_{aLD}(t) &= -\mathbf{K}_{sLD}\mathbf{x}_{aLD} + \mathbf{G}_{LD}\mathbf{r}_{LD} + \Lambda_{LD} \\ \Lambda_{LD} &= -2\lambda_{LD}\int \mathbf{B}_{LD}^T\mathbf{P}e\end{aligned} \tag{4.31}$$

Therefore, the overall control input, $\mathbf{u}(t)$, for the ACDM-RAS in Figure 4.3 can be expressed as Eq. (4.32).

$$\mathbf{u}(t) = \begin{bmatrix}\mathbf{u}_{aL}(t) & \mathbf{u}_{aLD}(t)\end{bmatrix}^T \tag{4.32}$$

Chapter 5

Flight Simulation

5.1 Overview

This chapter describes simulation results in which ACDM-RAS and ACDM-SS are compared in their performance. Both of these control systems are designed base on the CDM method as discussed in Chapter 4. The flight simulations are conducted by means of MATLAB® & Simulink® [98] – [100]. Section 5.2 explains the numerical models which are used to identify controller parameters and execute flight simulation. Section 5.3 investigates the reference model responses to the reference command in tracking command and stabilizing. The final section, Section 5.4, compares ACDM-RAS with ACDM-SS under various flight conditions.

5.2 Numerical Aircraft Dynamics Models

The numerical aircraft flight dynamics models come from the geometric and dimensional stability derivatives of Cessna C182 aircraft. The initial and steady-state conditions are the situation when the aircraft is on the cruise phase. The flight condition data in this cruise phase are shown in Table 5.1 [81] [82].

Recall the aircraft longitudinal dynamics model Eq. (4.2) repeated here as Eq. (5.1). The numerical model of this equation according to Cessna C182 in the flight condition on Table 5.1 is expressed in Eq. (5.2).

Table 5.1. Flight condition for Cessna C182 on cruise phase.

Parameter	Symbol	Value
Altitude (ft)	h	5,000
Mach number	M	0.201
Airspeed (ft/sec)	V_{p_1}	220.1
Dynamic pressure (lbs/ft^2)	$\overline{q}$	49.6
MAC	$\overline{x}_{CG}$	0.264
Angle of attack (deg)	α_1	0

$$\frac{d}{dt}\mathbf{x}_L(t) = \mathbf{A}_L\mathbf{x}_L(t) + \mathbf{B}_L\mathbf{u}_L(t)$$
$$\mathbf{y}_L(t) = \mathbf{C}_L\mathbf{x}_L(t) \tag{5.1}$$

$$\mathbf{A}_L = \begin{bmatrix} -0.0456 & 19.4590 & 0 & -32.2 & 0 \\ -0.0013 & -2.0925 & 0.9706 & 0 & 0 \\ 0.0033 & -13.9387 & -6.8053 & 0 & 0 \\ 0 & 0 & 1 & 0 & 0 \\ 0 & -220.1 & 0 & 220.1 & 0 \end{bmatrix}$$
$$\mathbf{B}_L = \begin{bmatrix} 0 & 0.0117 \\ -0.2026 & 0 \\ -34.7359 & 0 \\ 0 & 0 \\ 0 & 0 \end{bmatrix}, \quad \mathbf{C}_L = \begin{bmatrix} 1 & 0 & 0 & 0 & 0 \\ 0 & 1 & 0 & 0 & 0 \\ 0 & 0 & 1 & 0 & 0 \\ 0 & 0 & 0 & 1 & 0 \\ 0 & 0 & 0 & 0 & 1 \end{bmatrix} \tag{5.2}$$

For the numerical model of the aircraft lateral-directional dynamics, Eq. (4.7) and is shown again in Eq. (5.3). Then the numerical model of this equation according to the same flight condition as previous can be expressed in Eq. (5.4).

$$\frac{d}{dt}\mathbf{x}_{LD}(t) = \mathbf{A}_{LD}\mathbf{x}_{LD}(t) + \mathbf{B}_{LD}\mathbf{u}_{LD}(t)$$
$$\mathbf{y}_{LD}(t) = \mathbf{C}_{LD}\mathbf{x}_{LD}(t) \tag{5.3}$$

$$\mathbf{A}_{LD} = \begin{bmatrix} -0.1868 & -0.0029 & -0.9917 & 0.1463 & 0 \\ -30.25 & -12.97 & 2.14 & 0 & 0 \\ 9.27 & -0.36 & -1.21 & 0 & 0 \\ 0 & 1 & 0 & 0 & 0 \\ 0 & 0 & 1 & 0 & 0 \end{bmatrix}$$
$$\mathbf{B}_{LD} = \begin{bmatrix} 0 & 0.0889 \\ 75.06 & 4.82 \\ -3.41 & -10.19 \\ 0 & 0 \\ 0 & 0 \end{bmatrix}, \quad \mathbf{C}_{LD} = \begin{bmatrix} 1 & 0 & 0 & 0 & 0 \\ 0 & 1 & 0 & 0 & 0 \\ 0 & 0 & 1 & 0 & 0 \\ 0 & 0 & 0 & 1 & 0 \\ 0 & 0 & 0 & 0 & 1 \end{bmatrix} \tag{5.4}$$

These equations, Eq. (5.1) and (5.3), are used to design ACDM-SS and will be described in the following section.

5.3 The Reference Model by ACDM-SS

The reference model in the proposed ACDM-RAS is the Aircraft flight control by CDM-designed Servo State-feedback system or ACDM-SS. The structure of ACDM-SS is shown in Figure 4.2. Procedures to design ACDM-SS by using CDM are the same as those described in Section 4.3. The CDM's parameters, the stability index and the equivalent time constant, have to be identified first. Then the closed-loop poles according to the CDM's monic characteristic polynomial are obtained. Finally, based on these poles, the controller gains are determined by using the conventional technique.

5.3.1 The CDM's parameter

The CDM's parameters comprise the stability index, γ_i, the stability limit, γ_i^*, and the equivalent time constants, τ. The standard stability index values are chosen as the initial value of γ_i following the CDM's recommendation, Eq. (3.23). At the same time, τ are adjusted by following Eq. (3.24), and the γ_i^* relates to γ_i in Eq. (3.5). After tunning until obtained the desired system's response, the CDM's parameters are described as followed.

For the aircraft longitudinal dynamics part, γ_i and τ are expressed in Eq. (5.5), and the coefficient diagram is shown in Figure 5.1.

$$\gamma_1 = 2.5 \text{ and } \gamma_2 = \gamma_3 = \gamma_4 = 2 \tag{5.5 a}$$

$$\tau = 1.1 \tag{5.5 b}$$

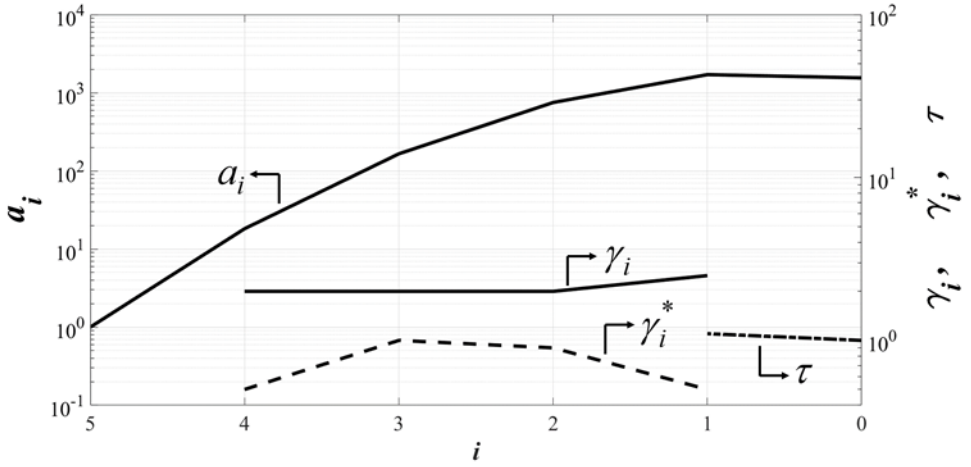

Figure 5.1. The coefficient diagram of the aircraft longitudinal dynamics part.

(Cited and partially modified from ref. 80).

For the aircraft lateral-directional dynamics part, γ_i and τ are expressed in Eq. (5.6), and the coefficient diagram is shown in Figure 5.2.

$$\gamma_1 = 2.5 \text{ and } \gamma_2 = \gamma_3 = \gamma_4 = 2 \tag{5.6 a}$$

$$\tau = 4 \tag{5.6 b}$$

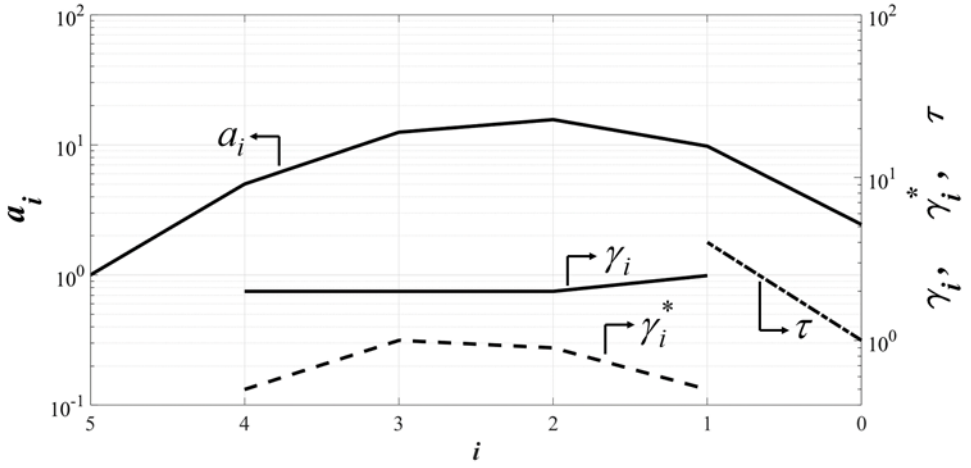

Figure 5.2. The coefficient diagram of the aircraft lateral-directional dynamics part. (Cited and partially modified from ref. 80).

By observing both coefficient diagrams illustrated, found that both aircraft dynamics systems are stable. And both systems have the same values of γ_i. However, the aircraft longitudinal dynamics system has a faster response than the aircraft lateral-directional dynamics system since it has less τ value.

5.3.2 The controller gains of ACDM-SS

The overall servo state-feedback gain matrices, $\mathbf{K}_{sL}$ and $\mathbf{K}_{sLD}$, can be determined after the desired system response is obtained. First, the pole placement technique is used to determine the values of $\mathbf{K}_{sL}$ and $\mathbf{K}_{sLD}$. The feedback loop gain ($\mathbf{K}_L$ and $\mathbf{K}_{LD}$) and the servo loop gain ($\mathbf{G}_L$ and $\mathbf{G}_{LD}$) for both aircraft dynamics systems can be calculated by Eq. (4.4) and (4.9).

The controller gain matrices of the aircraft longitudinal dynamics system are given in Eq. (5.7).

$$\mathbf{K}_{sL} = \begin{bmatrix} 0.0044 & 3.6018 & -0.2123 & -6.0210 & -0.0367 \\ 221.7777 & -4.8475e+3 & 283.3598 & 6.5117e+3 & 66.4017 \end{bmatrix} \tag{5.7 a}$$

$$\mathbf{K}_{L} = \begin{bmatrix} 3.6018 & -0.2123 & -6.0210 \\ -4.8475e+3 & 283.3598 & 6.5117e+3 \end{bmatrix} \tag{5.7 b}$$

$$\mathbf{G}_{L} = \begin{bmatrix} 0.0044 & -0.0367 \\ 221.7777 & 66.4017 \end{bmatrix} \tag{5.7 c}$$

The controller gain matrices of the aircraft lateral-directional dynamics system are given in Eq. (5.8).

$$\mathbf{K}_{sLD} = \begin{bmatrix} -0.2621 & -0.1354 & 0.0275 & 0.0462 & 0.1090 \\ -1.3603 & -0.0705 & -0.1325 & -0.2260 & -0.8185 \end{bmatrix} \tag{5.8 a}$$

$$\mathbf{K}_{LD} = \begin{bmatrix} -0.1354 & 0.0275 & 0.0462 \\ -0.0705 & -0.1325 & -0.2260 \end{bmatrix} \tag{5.8 b}$$

$$\mathbf{G}_{LD} = \begin{bmatrix} -0.2621 & 0.1090 \\ -1.3603 & -0.8185 \end{bmatrix} \tag{5.8 c}$$

5.3.3 ACDM-SS response to tracking command

To investigate the performance of ACDM-SS, the A/C model uses the integrated aircraft flight dynamics model, Eq. (4.11), as the system's plant with the numerical values as stated in the previous sections. The reference commands or input command for investigating tracking command behaviors are the altitude changing command and heading changing command, as shown in Figure 5.3.

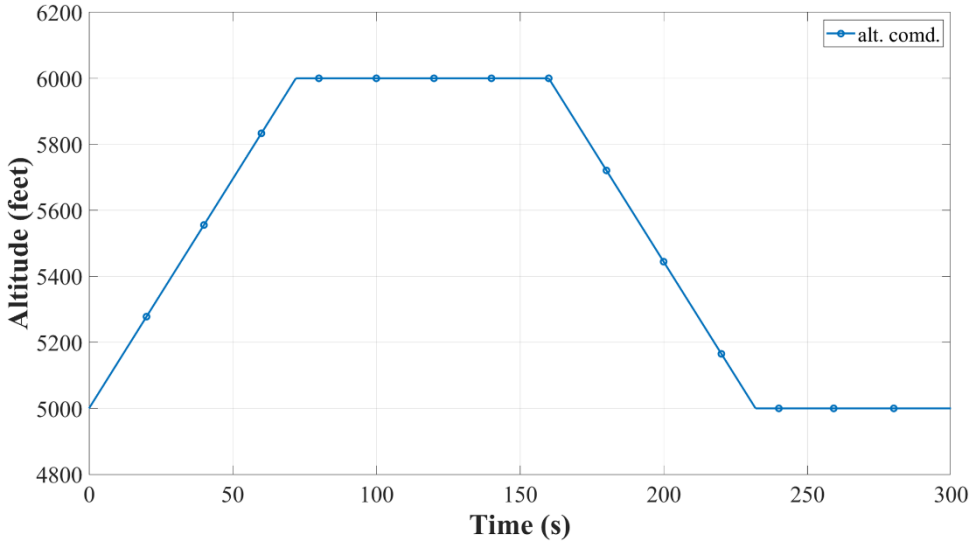

(a) Altitude versus time

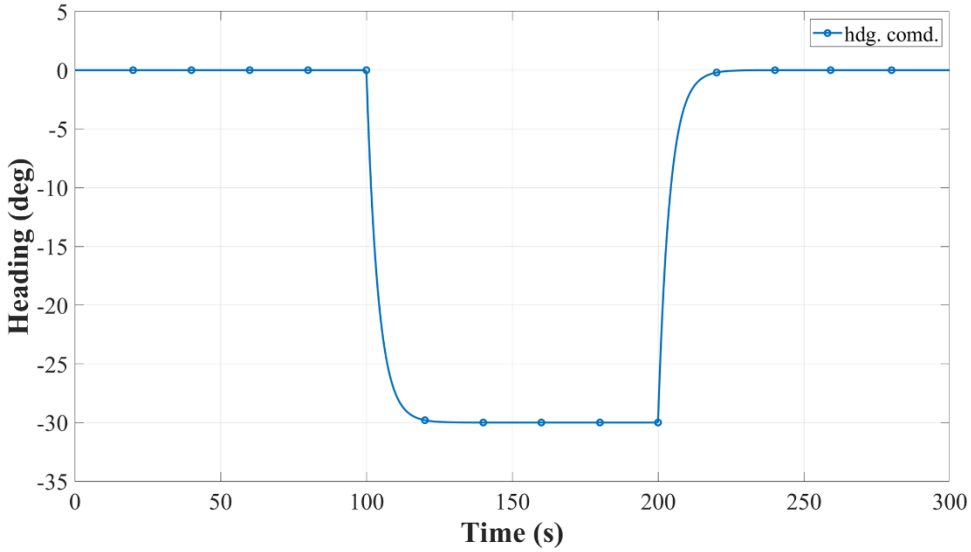

(b) Heading versus time

Figure 5.3. The altitude and heading commands.

When these commands are applied to ACDM-SS, which is the reference model of ACDM-RAS, the altitude and heading responses are shown in Figure 5.4.

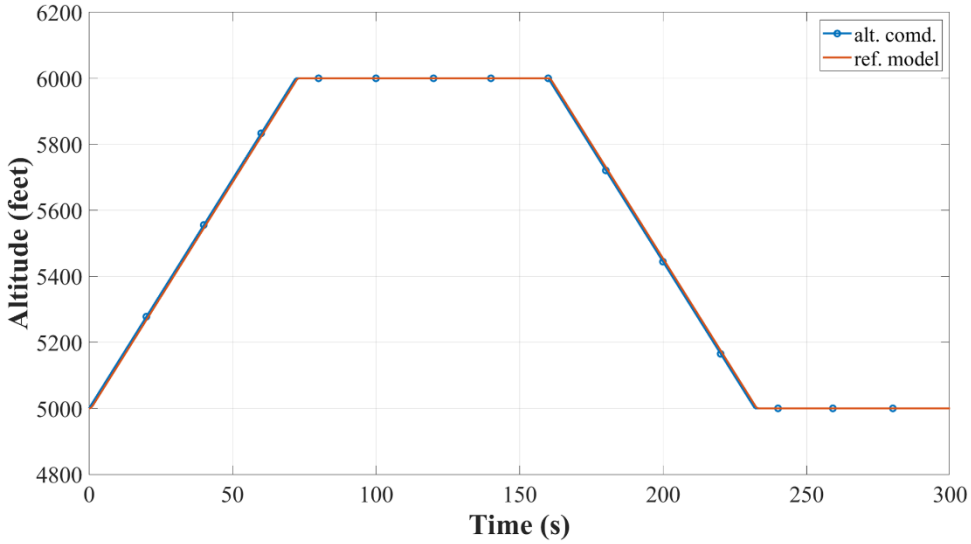

(a) Altitude response versus time

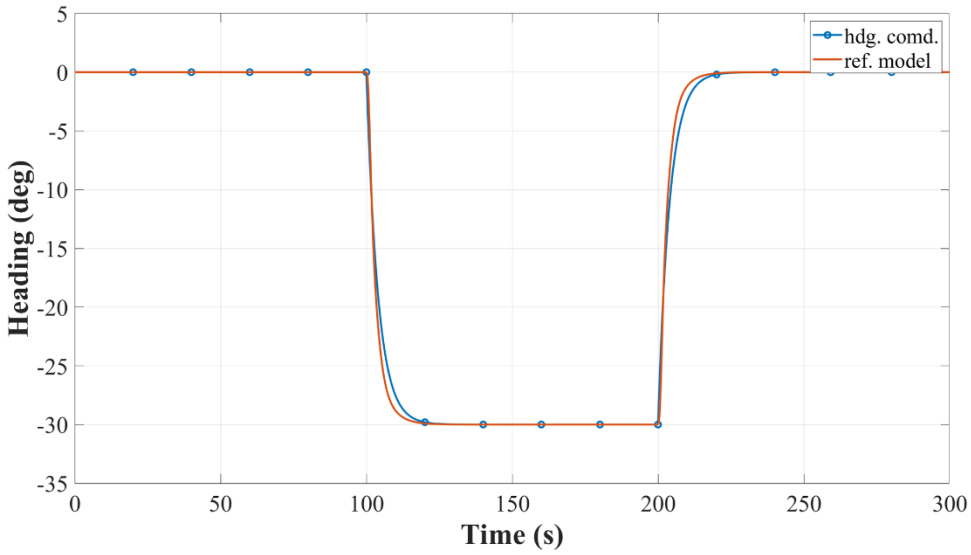

(b) Heading response versus time

Figure 5.4. Responses of the reference model to tracking command.

Observing the reference model response from Figure 5.4 shows that the reference model by ACDM-SS exhibits excellent behavior in tacking the changing commands both in altitude and heading. However, the altitude response is faster than the heading response when the command change occurs due to the difference in the value of τ . The following section will investigate the system's performance in stabilization under the constant conditions.

5.3.4 ACDM-SS in stabilization investigating

In this section, the Altitude Hold and Heading Hold are applied to ACDM-SS for investigating the system stability. The Altitude is held at 5,000 feet, and the Heading is held at 0 degrees. The Altitude Hold and Heading Hold responses are shown in Figure 5.5.

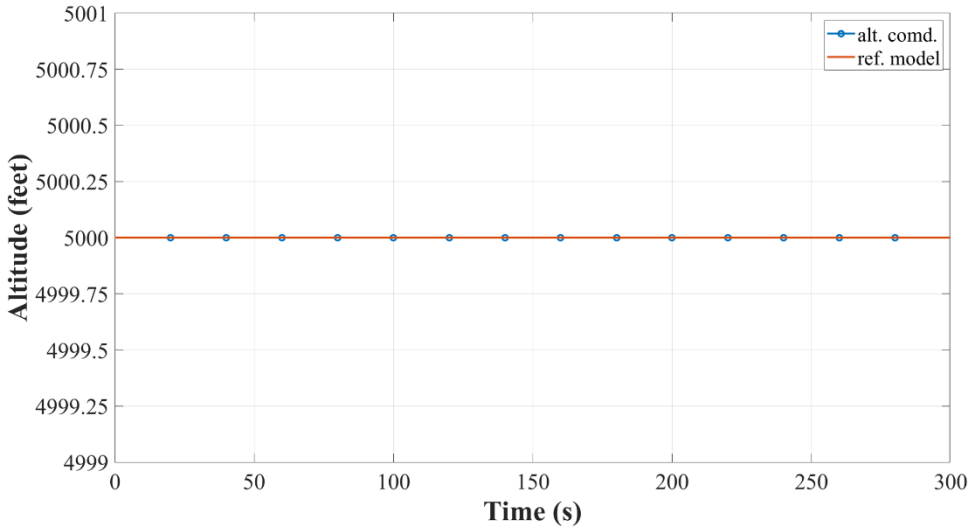

(a) Altitude versus time

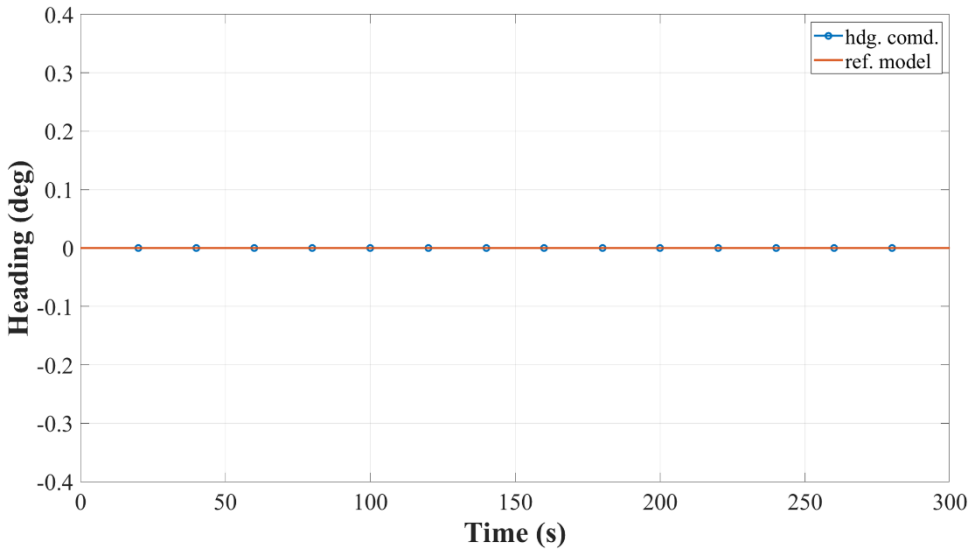

(b) Heading versus time

Figure 5.5. The Altitude Hold and Heading Hold responses of the reference model.

From Figure 5.5, ACDM-SS also exhibits excellent behavior in aircraft stabilizing at the constant altitude and heading without the steady-state error. The altitude disturbance

signal and heading disturbance signals are assumed to occur to the system for investigating the disturbance rejection behavior, as shown in Figure 5.6.

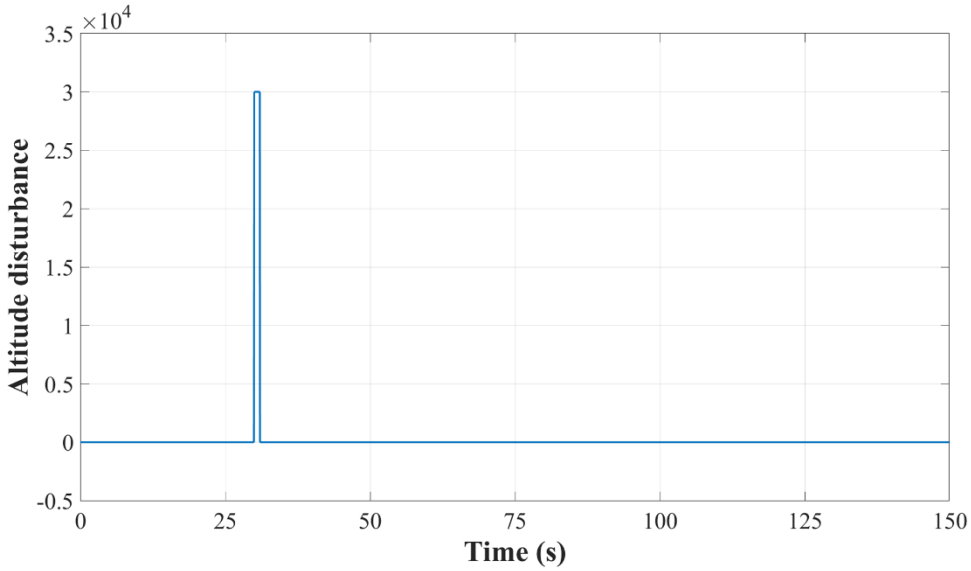

(a) Disturbance signal occurs at 30 seconds

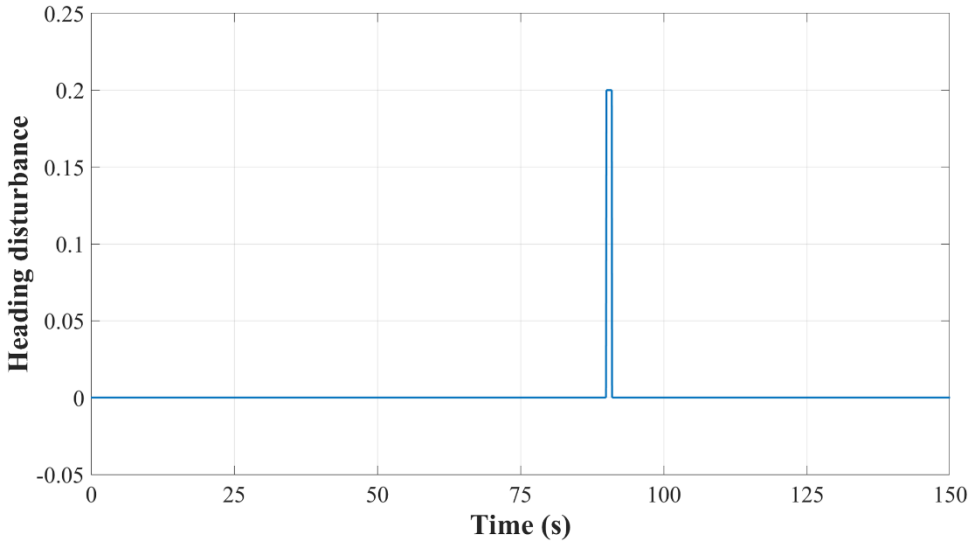

(b) Disturbance signal occurs at 90 seconds

Figure 5.6. The altitude and heading disturbance signals.

The disturbance signals are the impulse signal occur to altitude and heading at 30 and 90 seconds. The responses of ACDM-SS to these disturbances are shown in Figure 5.7. The disturbance rejection responses from both altitude and heading have overshoots

when the disturbance signals occur. However, the overshoots are compensated in a short period. Therefore, the response of the tracking command and the disturbance's rejection leads to a conclusion that ACDM-SS is suitable to be the reference model for ACDM-RAS.

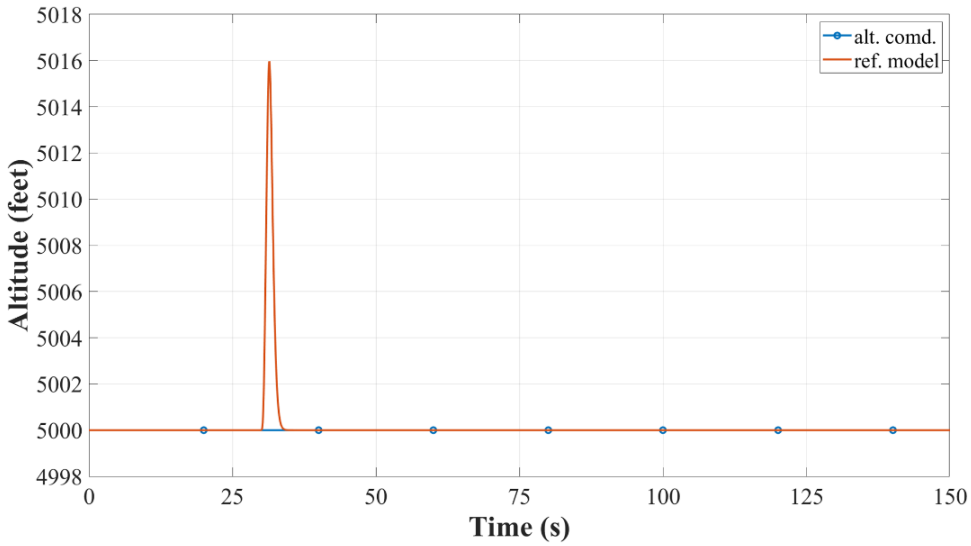

(a) Altitude response versus time

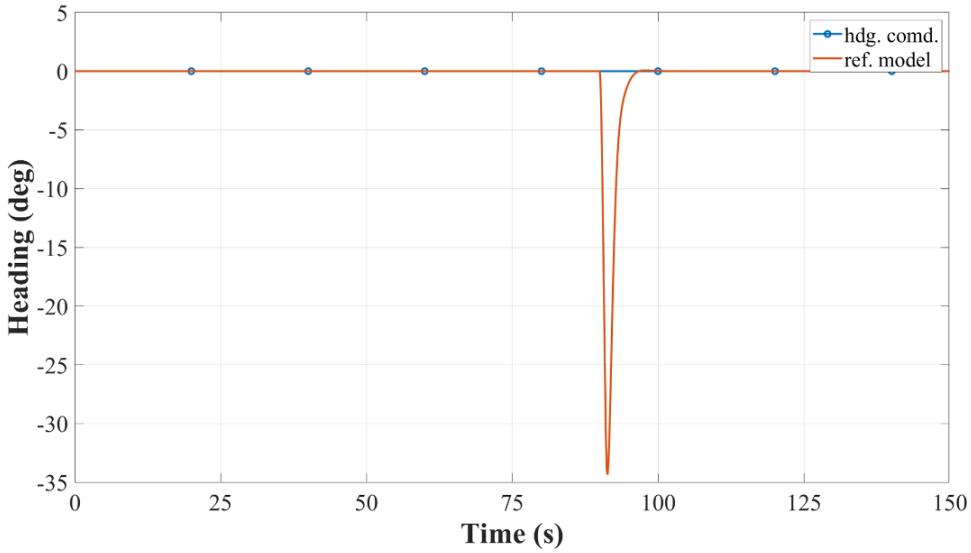

(b) Heading response versus time

Figure 5.7. Responses of the disturbance rejection behavior of ACDM-SS.

5.4 ACDM-RAS Simulation

The proposed Aircraft flight control by CDM-designed Model-Reference Adaptive System or ACDM-RAS has two essential parts. First is the reference model already discussed in the previous section. What is left undiscussed is its adaptive mechanism. Considering the adaptive mechanism from Eq. (4.30) and (4.31), two parameters have to be stated: the adaptive gain λ and the positive definite matrix **P**. The following sections show the numerical value of the matrices **P** and the effect of various values of λ followed by the comparisons between ACDM-RAS and ACDM-SS.

*5.4.1 The numerical values of the matrix **P***

The numerical values of the matrix **P** can be obtained by using Eq. (4.26) and let the positive definite matrix **Q** be as in Eq. (5.9).

$$\mathbf{Q} = \begin{bmatrix} 1 & 0 & 0 & 0 & 0 \\ 0 & 1 & 0 & 0 & 0 \\ 0 & 0 & 1 & 0 & 0 \\ 0 & 0 & 0 & 1 & 0 \\ 0 & 0 & 0 & 0 & 1 \end{bmatrix} \tag{5.9}$$

Although the exact value of the matrix **Q** is used for Eq. (4.26), the values of the matrix **P** are different for each aircraft dynamics part, the system matrices $\mathbf{A}_{mL}$ and $\mathbf{A}_{mLD}$ are different.

The positive definite matrix $\mathbf{P}_L$ for the aircraft longitudinal dynamics part is expressed in Eq. (5.10).

$$\mathbf{P}_L = \begin{bmatrix} 0.1863 & 0.6148 & -0.0500 & -0.9552 & 0.0027 \\ 0.6148 & 1.2925e3 & -32.3412 & -1.6843e3 & -24.1243 \\ -0.0500 & -32.3412 & 0.9490 & 42.7897 & 0.5316 \\ -0.9552 & -1.6843e3 & 42.7897 & 2.2025e3 & 30.8544 \\ 0.0027 & -24.1243 & 0.5316 & 30.8544 & 0.5602 \end{bmatrix} \tag{5.10}$$

The positive definite matrix $\mathbf{P}_{LD}$ for the aircraft lateral-directional dynamics part is expressed in Eq. (5.11).

$$\mathbf{P}_{LD} = \begin{bmatrix} 10.2537 & 0.5650 & -0.4463 & 1.9661 & 9.9438 \\ 0.5650 & 0.4469 & -0.0988 & 0.4491 & 0.3731 \\ -0.4463 & -0.0988 & 0.3333 & -0.1123 & -0.0447 \\ 1.9661 & 0.4491 & -0.1123 & 1.6859 & 1.8824 \\ 9.9438 & 0.3731 & -0.0447 & 1.8824 & 11.6369 \end{bmatrix} \tag{5.11}$$

According to the adaptive mechanism Λ_L, Eq. (4.30), when the positive definite matrices $\mathbf{P}_L$ and $\mathbf{P}_{LD}$ are obtained from the previous section, the remainder essential part is the adaptive gain λ_L and λ_{LD}.

5.4.2 The effect of the adaptive gain λ

In this section, the effect of varying the value of λ is investigated. For this purpose, the Airlib [101] [102] tool block in the Simulink® program is used as the system's plant or the A/C model in Figure 4.3. Airlib is a library of nonlinear general aircraft models. By assigning the specific data of Cessna C182 on the mask of the Airlib model, the desired aircraft model to be the plant of ACDM-RAS is obtained. The investigation of the effect of λ in ACDM-RAS is done similarly with the investigation performance of the reference model in the previous section.

Nevertheless, obtaining the adaptive gain λ is different from the matrix **P**. Because there are no exact criteria for determining the value of λ. However, consideration from

Eq. (4.28) implies that the value of λ must be the positive number. Then, the time derivative of function V is always the negative semidefinite function. Therefore, to illustrate the effect of λ in ACDM-RAS, each simulation compares the response of ACDM-RAS with the reference command by various values of λ. The values of λ are varied in five steps from 10 until 10,000, both in the longitudinal and lateral-direction dynamics. The reference commands or input commands applied to ACDM-RAS have the same pattern as in Figure 5.3. The altitude responses of ACDM-RAS are shown in Figures 5.8 to 5.9, while the heading responses are shown in Figure 5.10.

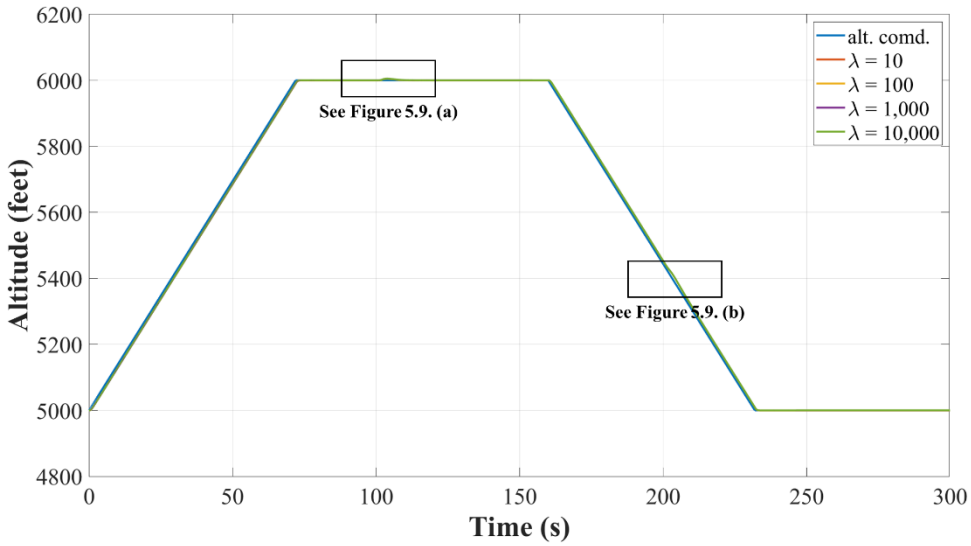

Figure 5.8. The altitude response of ACDM-RAS with the various λ.

From observing Figure 5.8, ACDM-RAS exhibits excellent altitude command tracking in every value of λ. However, there are two periods that altitude response is disturbed. These disturbances come from the effect of heading changing at 100 and 200 seconds. These effects of heading changing on altitude response are shown in Figure 5.9. Although there are disturbances in those two periods, the magnitudes of responses are different as shown in Figure 5.9 (a) and Figure 5.9 (b).

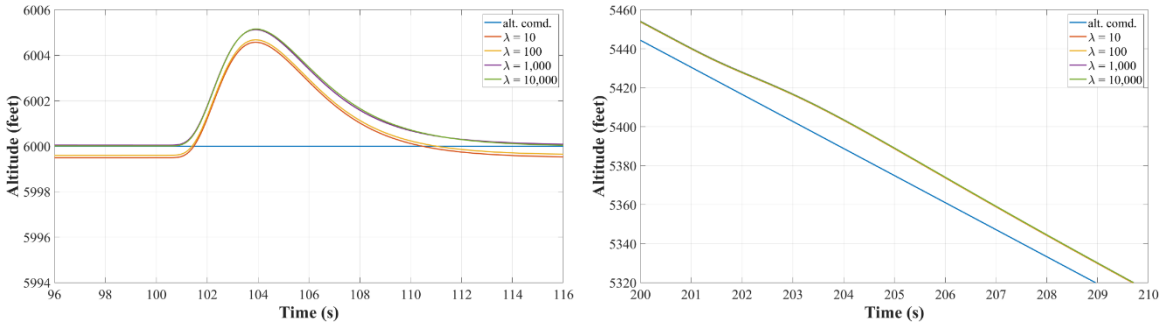

(a) At 100 seconds (b) At 200 seconds

Figure 5.9. The heading changing effect on the altitude response.

Meanwhile, ACDM-RAS exhibits excellent performance in heading response in every value of λ too. Significantly, the changes in altitude do not have any effect on the heading response. However, the heading response seems slower than the altitude response. For illustration, the heading response of ACDM-RAS is shown in Figure 5.10.

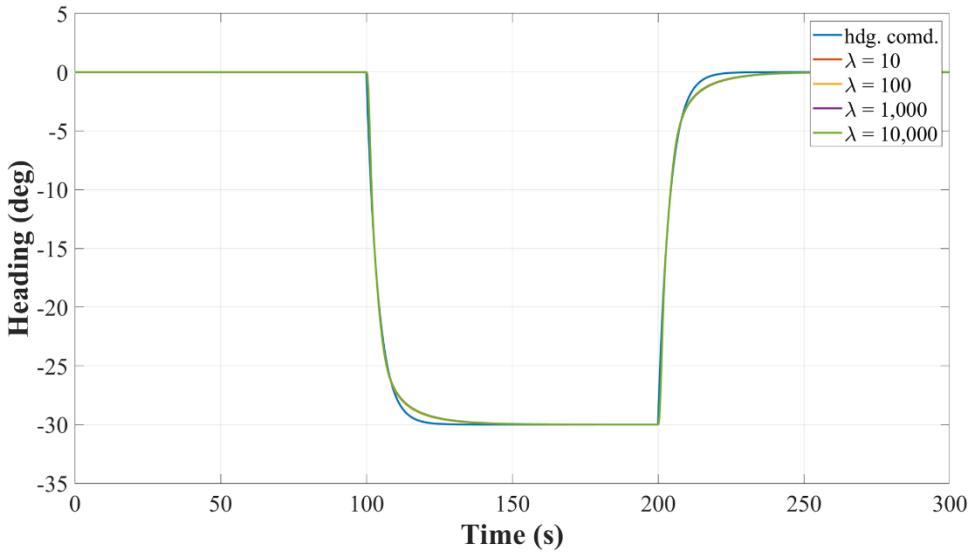

Figure 5.10. The heading response of ACDM-RAS with the various λ.

In the next step, the stabilization performance of ACDM-RAS is investigated. The command is applied to hold the system's altitude constant at 5,000 feet, and the heading is held at 0 degrees. The ACDM-RAS's stabilization responses are shown in Figure 5.11.

Figure 5.11 (a) shows that increasing the value of λ reduces the settling time of the altitude response and reduces the steady-state error. While in Figure 5.11 (b), increasing λ does not affect the Heading Hold response, ACDM-RAS exhibits excellent behavior in the Heading Hold command with every value of λ.

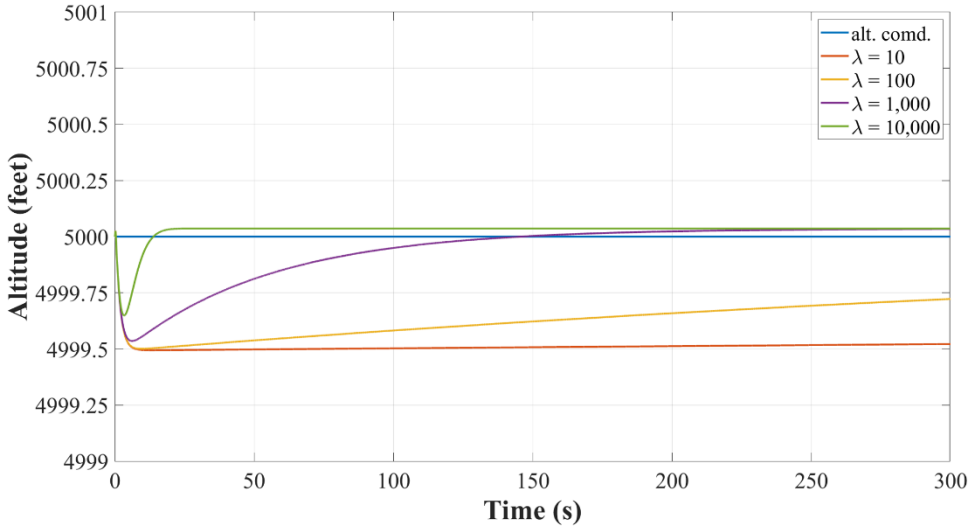

(a) Altitude response with the various λ

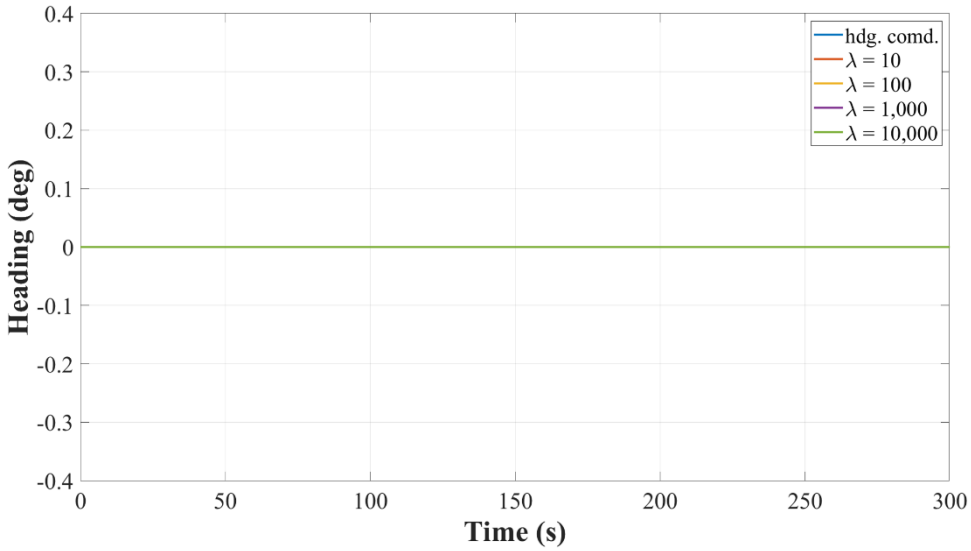

(b) Heading response with the various λ

Figure 5.11. The altitude and heading stabilization response of ACDM-RAS.

The last step is a disturbance rejection investigation. By using the disturbance signal as in Figure 5.6, the disturbance rejection responses are shown in Figure. 5.12.

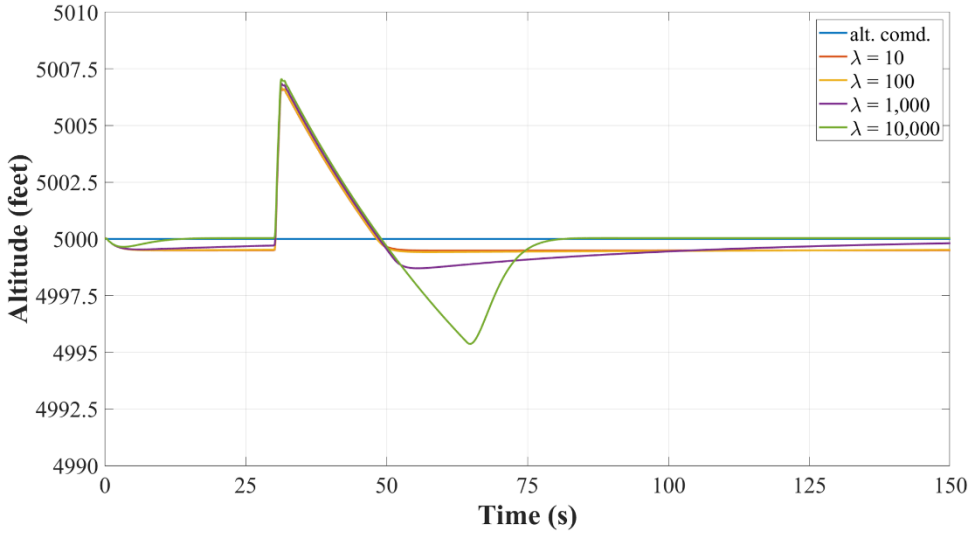

(a) Altitude response with various values of λ

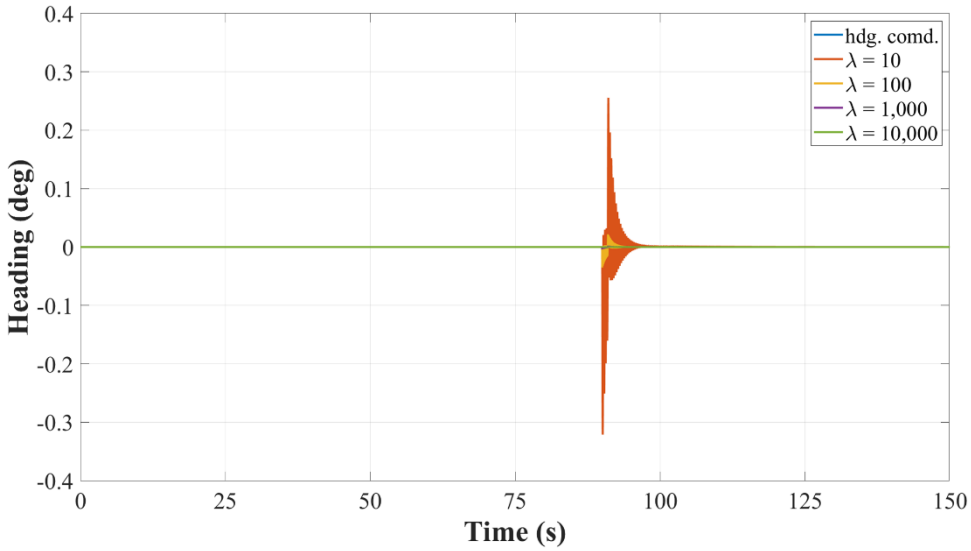

(b) Heading response with various values of λ

Figure 5.12. Responses of the disturbance rejection behavior of ACDM-RAS.

In disturbance rejection, changing the values of λ makes significant differences between the altitude and heading response. In the altitude response, increasing λ yields that the overshoot responses due to the disturbance signal have a similar shape and magnitude of the first-half circle in every λ. Nevertheless, in the second-half circle, the shape and magnitude of the overshoot are considerably different when λ is 10,000 compares with others. However, this value of λ gives the system the fastest settling time

and less steady-state error. While in the heading response, the disturbance signals are compensated quickly and faster than the altitude response. In the meantime, the response's oscillations are smoother, and the magnitudes are reduced when λ increases.

From the previous discussion, the value-changing effect of the adaptive gain lambda on ACDM-RAS influences the aircraft longitudinal dynamics part more than the aircraft lateral-directional dynamics part. Changing in the value of the λ resulted in a significant change in the aircraft longitudinal dynamics part compared to the aircraft lateral-directional dynamics part, for example, as in the system's stabilization.

5.5 ACDM-RAS vs. ACDM-SS

This section illustrates the comparison between ACDM-RAS and ACDM-SS. For reasonable comparison, the Cessna C182 Airlib model is adopted to be the A/C model for both systems. At the same time, the controller parameters of ACDM-SS are the same as in the reference model, Eq. (5.7) and (5.8). ACDM-RAS uses the reference model from Section 5.3, and the adaptive gains are λ_L = 30,000 and λ_{LD} = 30 for longitudinal and lateral-directional dynamics parts, respectively.

5.5.1 ACDM-RAS vs. ACDM-SS in tracking behavior

Apply the altitude and heading command from Figure 5.3 to both ACDM-RAS and ACDM-SS. The responses of these two systems due to these commands are shown in Figures 5.13 to 5.15.

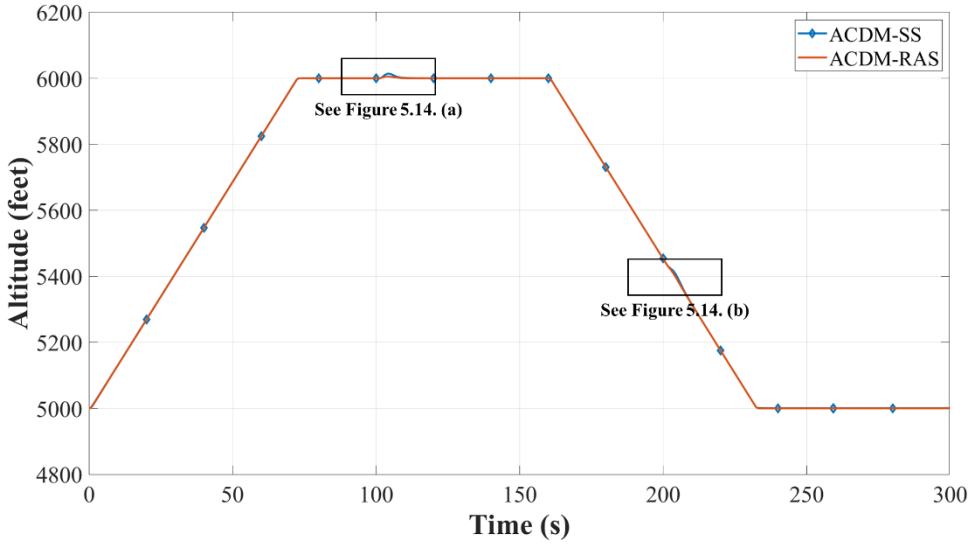

Figure 5.13. The altitude response due to altitude changing command.

From Figure 5.13, both ACDM-RAS and ACDM-SS exhibit excellent command tracking behavior in altitude changing. However, although both systems have similar effects from the heading changing, these effects are more significant differences in magnitude on the ACDM-SS than ACDM-RAS, as shown in Figure 5.14 (a) and (b).

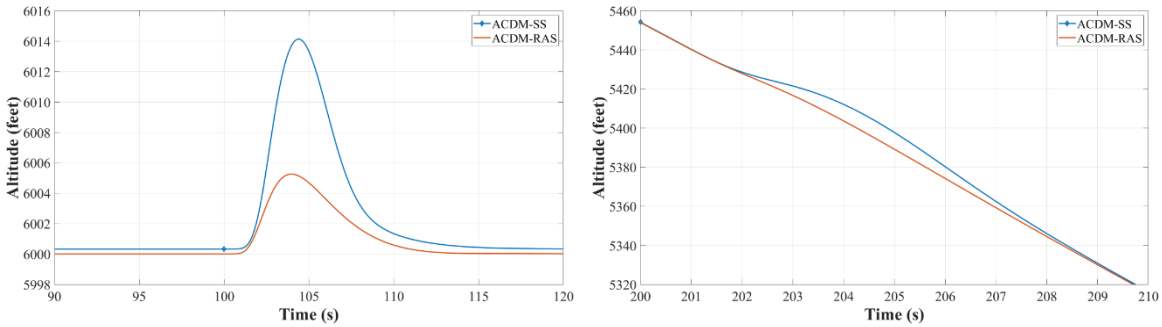

(a) At 100 seconds (b) At 200 seconds

Figure 5.14. The effect of heading changing on the altitude response.

From Figure 5.15, ACDM-RAS and ACDM-SS are still exhibiting good performance in changing heading. However, the response of ACDM-SS is faster, but the response of ACDM-RAS is smoother than ACDM-SS. From the previous discussion, it

can be seen that ACDM-RAS exhibits better performance than ACDM-SS in tracking command. Although in the heading response, ACDM-RAS response is slower than ACDM-SS, this does not compensate for the effect of heading changing on the altitude response.

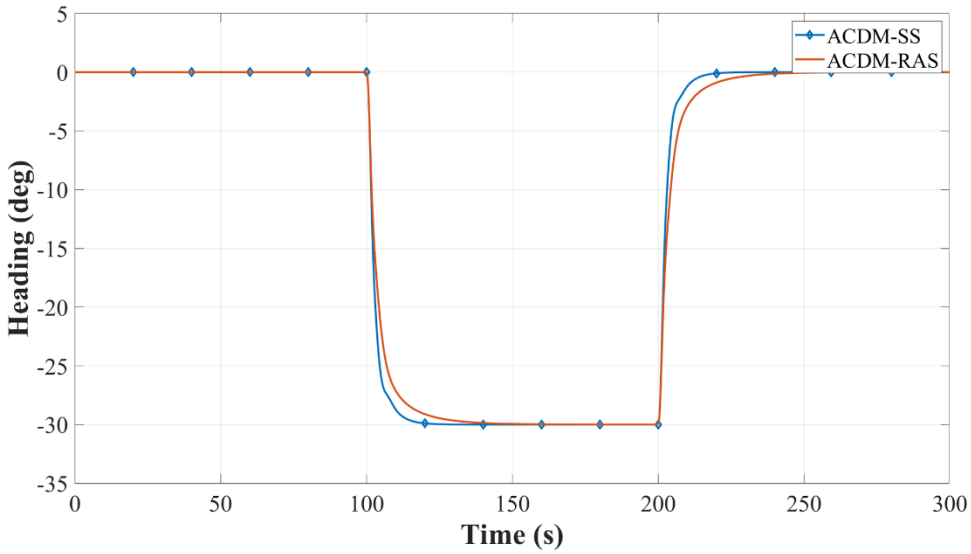

Figure 5.15. The heading response due to the changing heading command.

5.5.2 ACDM-RAS vs. ACDM-SS in the stabilization

In the aircraft stabilization investigation, the aircraft altitude is held at 5,000 feet, and the heading is held at 0 degrees. Figure 5.16 shows the stabilization response compared between ACDM-RAS and ACDM-SS. The altitude response from Figure 5.16 (a) shows that both ACDM-RAS and ACDM-SS have an overshoot at the initial state and have the error at steady-state. However, the magnitude of the overshoot and the steady-state error of ACDM-RAS are smaller than ACDM-SS. There are no significant differences in the heading response between ACDM-RAS and ACDM-SS. Both systems exhibit excellent behavior in holding the heading without any overshoot or error at steady-state. Although both ACDM-RAS and ACDM-SS have an overshoot at the initial state and the steady-state error in altitude response, they have good efficiency in heading response. Therefore, it can

be concluded that both ACDM-RAS and ACDM-SS have an excellent performance to stabilize the aircraft at steady state.

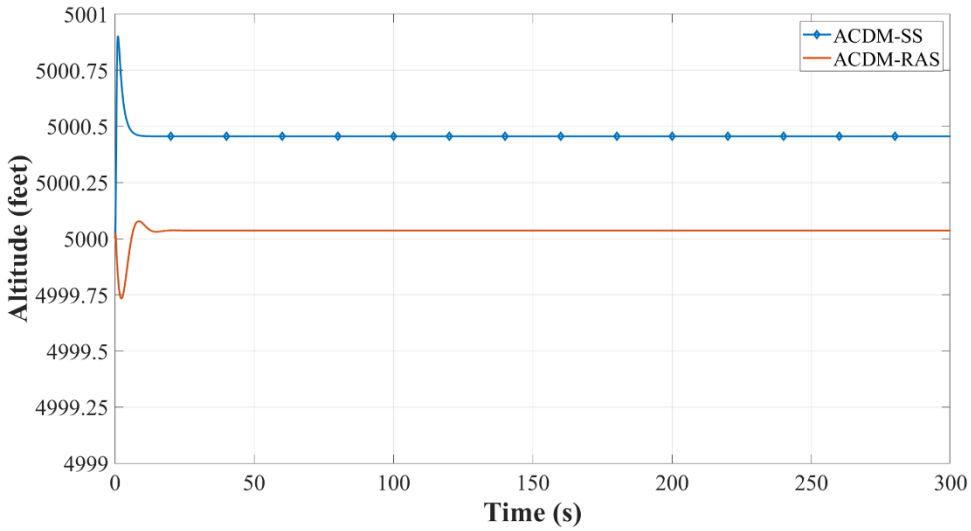

(a) Altitude comparison

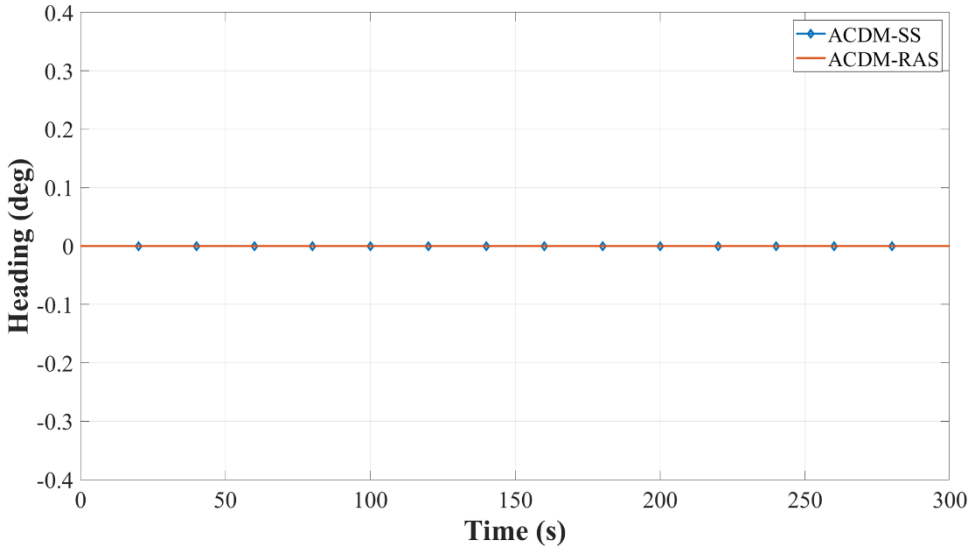

(b) Heading comparison

Figure 5.16. The Altitude Hold and Heading Hold response comparison.

The systems are still commanded to hold the altitude and the heading at 5,000 feet and 0 degrees. Then the disturbance signals as in Figure 5.6 are applied to both ACDM-RAS and ACDM-SS. The results are shown in Figure 5.17.

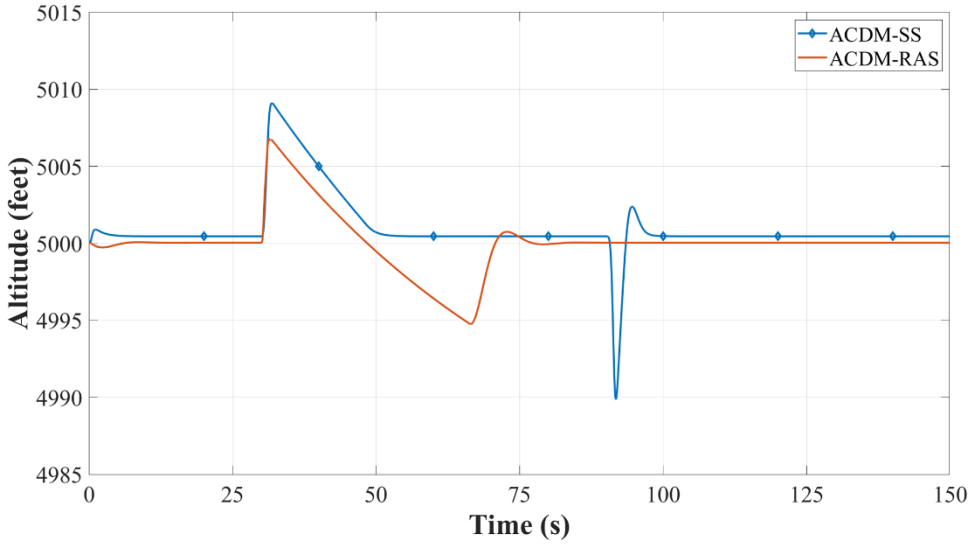

(a) Altitude comparison

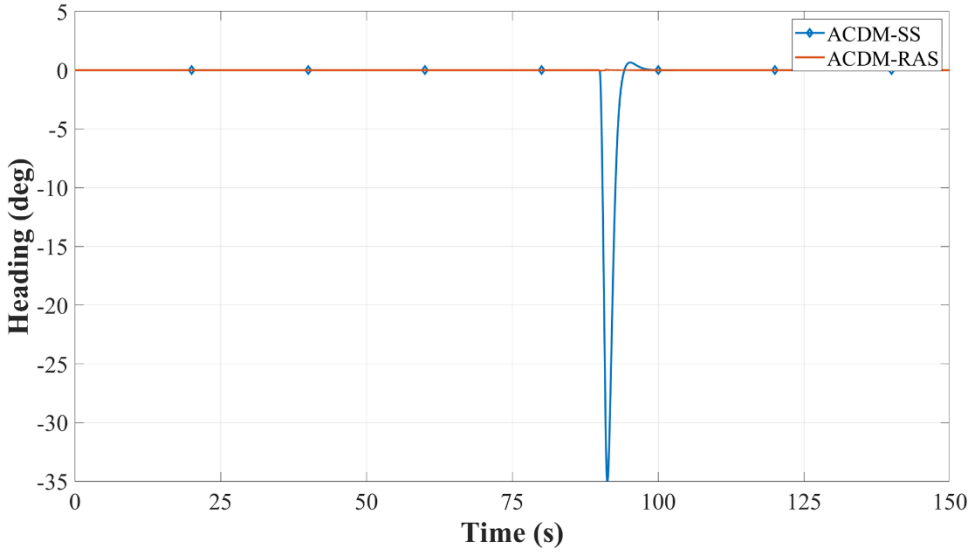

(b) Heading comparison

Figure 5.17. The disturbance rejection comparison.

The results in Figure 5.17 clearly show that ACDM-RAS is more efficient than ACDM-SS regardless of whether the altitude response or heading response is considered. Although in the altitude response, ACDM-RAS has a full circle of the overshoot due to the disturbance, which is directly applied to the altitude, ACDM-RAS does not affect altitude response from the disturbance, which is directly applied to the heading. At the same time,

both systems do not have any effect from the altitude disturbance in the heading response. However, ACDM-SS has a massive overshoot due to the heading disturbance.

5.6 ACDM-RAS Flight Path

For an illustration of the response of ACDM-RAS due to each altitude and heading command, the 3-dimension flight paths are used to express more detail about the aircraft's physical motion. Figure 5.18 shows the flight path I of ACDM-RAS, which is the flight path of the response of ACDM-RAS from Figures 5.13 and 5.15. The flight path in Figure 5.19 is the response of ACDM-RAS when the altitude command is the ramp signal with the slope of 20 feet per second, and the heading command is the ramp signal with the slope of 0.5 degrees per second. The initial point coordinates of both flight paths are [0, 0, 5000] in the [north, west, up] system.

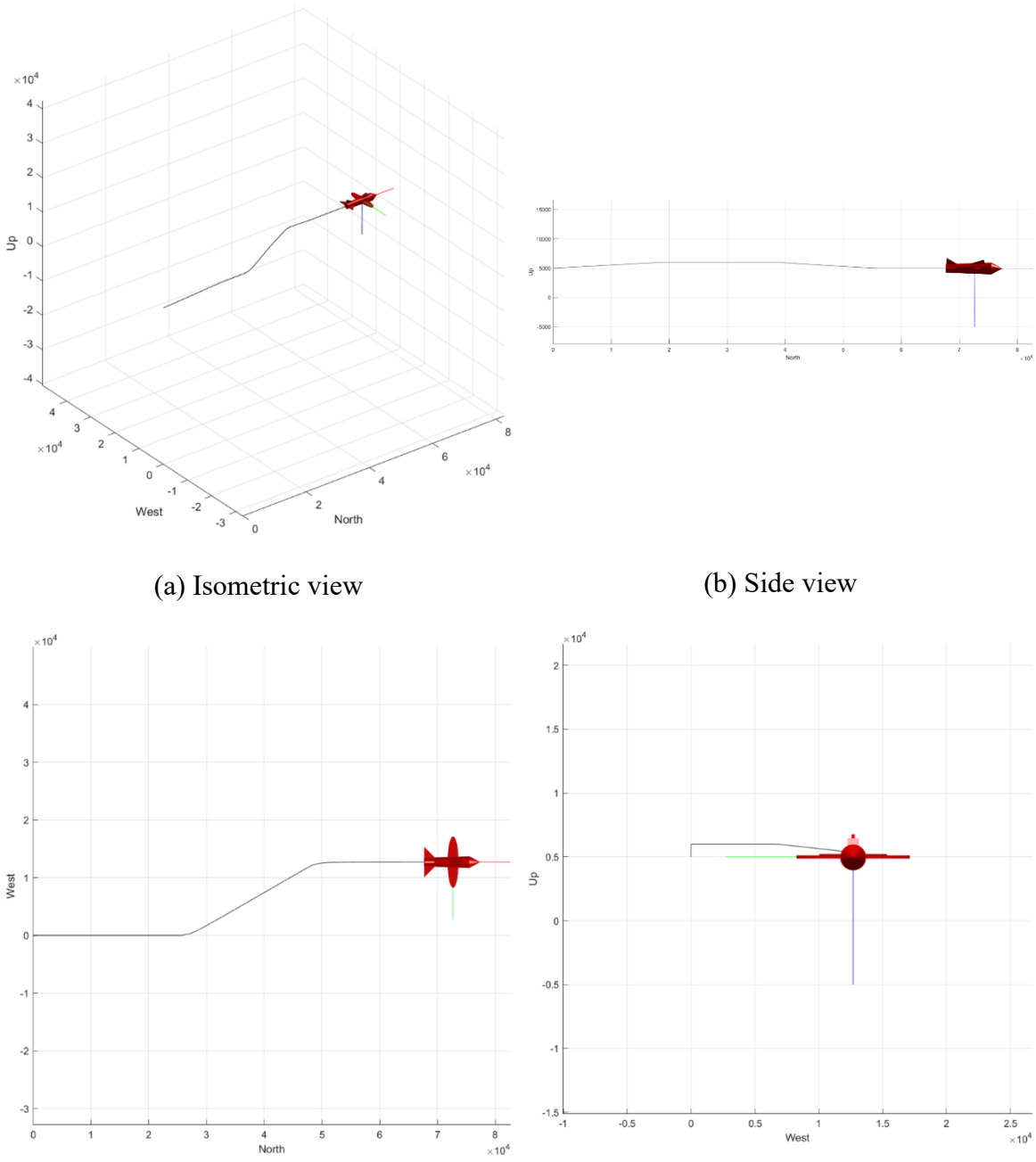

(a) Isometric view

(b) Side view

(c) Top view

(d) Front view

Figure 5.18. ACDM-RAS flight path I.

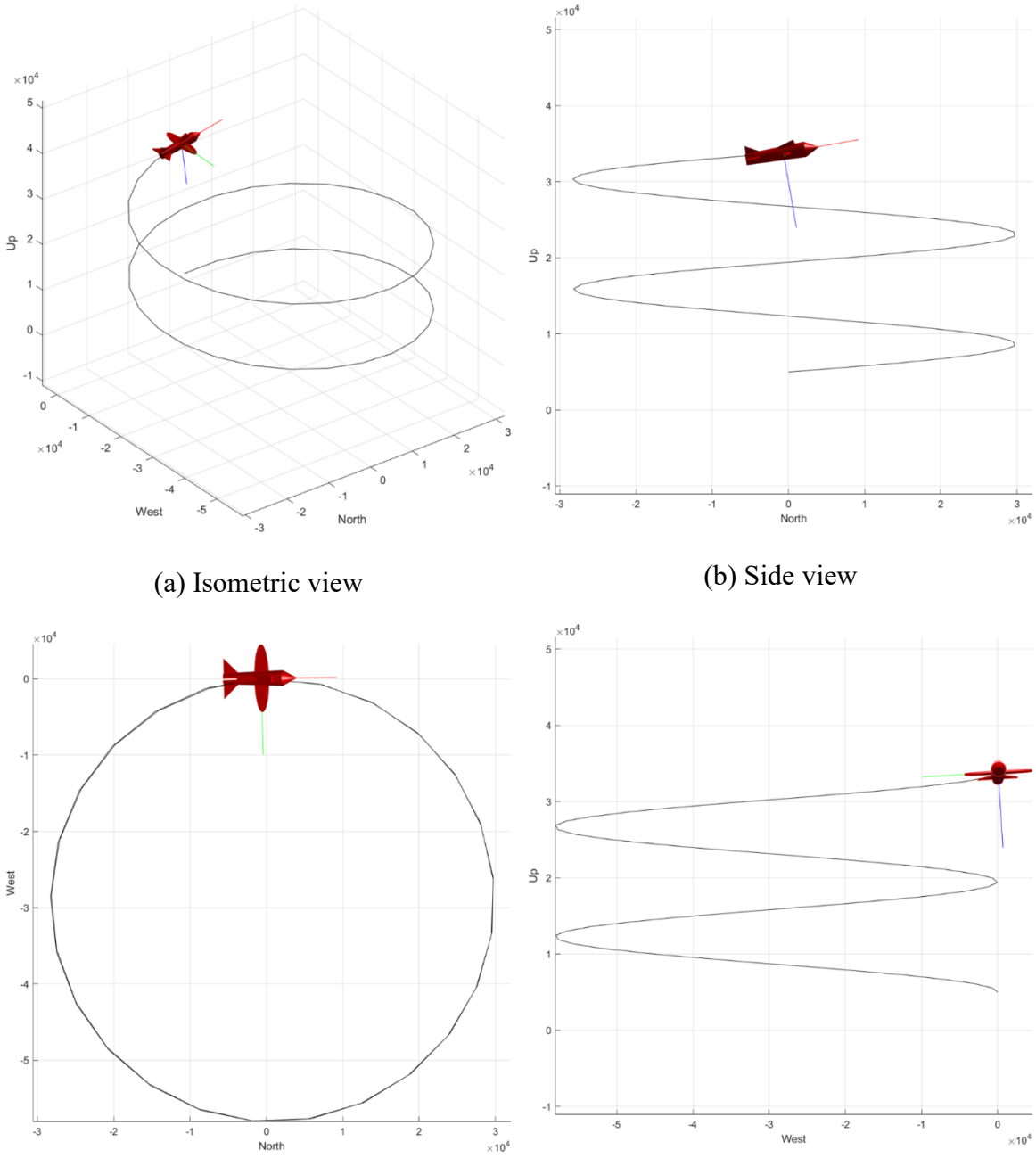

(a) Isometric view

(b) Side view

(c) Top view

(d) Front view

Figure 5.19. ACDM-RAS flight path II.

Chapter 6

Summary

This thesis aims to develop the aircraft flight control system based on the Coefficient Diagram Method or CDM. CDM is used to design the two-servo state-feedback systems for aircraft longitudinal and lateral-directional dynamics control. These servo systems are called the Aircraft flight control by CDM-designed servo state-feedback system or ACDM-SS. After the performance of ACDM-SS was investigated, the concept of the Model-reference adaptive system was implemented for performance improvement of ACDM-SS in case of dealing with a nonlinear aircraft model. Secondly, another type of aircraft flight control system was introduced which is called the Aircraft flight control by CDM-designed Model Reference Adaptive System or abbreviated as ACDM-RAS. ACDM-RAS is the Model Reference Adaptive System, which uses ACDM-SS as the reference model. Performance comparison was made between ACDM-SS and ACDM-RAS through simulation in various situations. The simulation results show that both ACDM-SS and ACDM-RAS exhibited a satisfactory performance as aircraft flight control system, while ACDM-RAS tuned out to perform better than ACDM-SS, especially under the presence of nonlinearity in aircraft model.

6.1 Conclusions

ACDM-RAS and ACDM-SS can control aircraft longitudinal and lateral-direction dynamics motion simultaneously. Satisfactory responses to the reference commands of changing altitude and heading are confirmed for both systems. Both ACDM-RAS and ACDM-SS respond to the Altitude Hold command with small error values at the steady-

state, while the Heading Hold command has no error values. ACDM-RAS and ACDM-SS can also compensate for the disturbance signals which come from the external systems. Using the servo state-feedback system as the central controller in ACDM-SS makes the structure of ACDM-SS straightforward and can be modified easily to meet the designer's requirement. These benefits of using the servo state-feedback system can be verified by comparing ACDM-SS with the previous aircraft flight control systems based on the servo state-feedback system [77] – [80]. Use of CDM as the controller design technique for ACDM-SS can dramatically reduce the complexity in controller design processes. CDM is an algebraic approach in controller design with only three design parameters, the stability index, γ_i, the equivalent time constant, τ, and the stability limit, γ_i^*. These parameters make CDM's concept easy to understand even for ordinary engineers or technicians. CDM recommends the standard stability index values, and the coefficient diagram allows the designer to have excellent criteria or decision-making for design parameter tuning, guaranteeing the balance of system stability, response, and robustness. Although ACDM-SS exhibits excellent performance in the simulation with the linear aircraft model as verified in sections 5.3.3 and 5.3.4, there are some defects in the nonlinear aircraft model.

In order to keep the excellent characteristic of ACDM-SS when applied to the linear aircraft model while eliminating or reducing the defect observed in case of a nonlinear aircraft model, the model reference adaptive system technique is implemented to ACDM-SS. This reason is that the derivation of ACDM-RAS and ACDM-RAS is designed based on the Lyapunov stability theory. There is only one controller gain, adaptive gain λ, in the adaptive part. Although there is no exact rule for tunning the λ, the value of λ is easily obtained. It can be concluded that the value of λ must be only a positive number. Therefore, the value of λ can be obtained by simple trial and error with the positive number.

The comparison between ACDM-RAS and ACDM-SS applied to nonlinear aircraft models is done through the simulation with the same procedure done with ACDM-SS. The results show that ACDM-RAS can eliminate or compensate for the defects of ACDM-SS all in tracking, stabilization, and disturbance rejection. Mainly, ACDM-RAS exhibits excellent behavior in stabilization both with or without the disturbance signals. Both ACDM-SS and ACDM-RAS were found to achieve a good performance as an aircraft flight control system, and the presence of ACDM-RAS helps improve the performance of ACDM-SS even better. The structures of both systems are straightforward, while the design processes are not complex and do not need deep control background and mathematical background.

6.2 Suggestions

Although ACDM-RAS can be considered as an efficient flight control system, there are still guidelines for further development in many ways. An example is the aircraft model development, and it is clear that the aircraft model is of paramount importance in designing the aircraft flight control system. Many essential variables are needed for aircraft modeling, such as the aerodynamic coefficient, static stability, and dynamic derivative characteristics. These variables usually depend on various factors, such as the aircraft type or flight condition. If the vast data of these essential variables can be obtained, the accuracy of the aircraft modeling will be immensely increased and yield more effective aircraft flight control system designing. Solutions to determine these essential data can be explored in many ways, such as physical methods or calculations. An example of the physical method is the use of a wind tunnel. Although a wind tunnel has high accuracy, this method needs high operation costs and maintenance. An example of the calculation method is the use of a computer program or application. Using these programs to determine the essential data

for aircraft modeling may be less accurate than using the wind tunnel, but this method has less operation cost and no maintenance. There are many programs which can be used to determine the essential data for aircraft modeling, such as Digital Datcom [103] [104], Athena Vortex Lattice AVL [105], and OpenVSP [106]. Another method for further development is to use a flight simulator. The main advantages of the flight simulator are safety and sparing costs. A simulator can display the dynamics of test aircraft, which is an advantage before an actual flight test. The use of a flight simulator program also helps to increase the credibility of the aircraft modeling and response. Examples of flight simulators are FlightGear [107] and JSBsim [108].

6.3 Future Work

This thesis focuses on developing the aircraft flight control system, an effective system with powerful design techniques. The following is a list of future works that can be explored based on these proposed systems.

- The loss in flight or the malfunctioning flight control surface: Use ACDM-RAS as the baseline to develop a flexible aircraft flight control system for C182 aircraft. When encountering a situation in which some flight control surfaces are damaged or malfunction during flight, this flexible aircraft flight control system should have the ability to retain the stability of the aircraft to continuously safe flight or landing.
- The flight control system for the new aircraft type: Based on ACDM-RAS, the flight control system for the new aircraft type can be developed. This aircraft may be equipped with the different control surfaces from C182, but it still has the flight quality with the ACDM-RAS.

Appendix A

Cessna 182

The Cessna 182 (called C182) is a light utility aircraft from Cessna Aircraft Company, USA. The Cessna 182 was first introduced in 1956 and is still in production since C182 is the one of most popular aircraft models of Cessna Company. The C182 is a four-seat, single-engine light airplane, tricycle gear, and has various options to meet the objectives such as adding two child seats by installed in the baggage area or modify to be retractable gear type aircraft.

The useful information used in the thesis are described as follows.

General characteristics

- Crew: 1
- Capacity: 3 passengers
- Length: 28 ft 0 in (8.53 m)
- Wingspan: 36 ft 0 in (10.97 m)
- Height: 9 ft 3 in (2.82 m)
- Wing area: 174 sq ft (16.2 m2)
- Empty weight: 1,700 lb (771 kg)
- Max takeoff weight: 2,950 lb (1,338 kg)
- Powerplant: 1 × Lycoming O-470-U 230 hp (170 kW)
- Propellers: 3-bladed constant speed

Performance

- Maximum speed: 148 kn (170 mph, 274 km/h)
- Cruise speed: 144 kn (166 mph, 267 km/h)
- Stall speed: 56 kn (65 mph, 104 km/h)
- Range: 880 nmi (1,013 mi, 1,630 km)
- Service ceiling: 16,500 ft (5,029 m)
- Rate of climb: 1010 ft/min (5.13 m/s)

Dynamics mode approximation

Longitudinal dynamics part

- Short period: $\varsigma_{SP} = 0.8442 \quad \omega_{nSP} = 5.2709$
- Phugoid: $\varsigma_{Ph} = 0.1284 \quad \omega_{nPh} = 0.1713$

Lateral-directional dynamics part

- Dutch roll: $\varsigma_{DR} = 0.2064 \quad \omega_{nDR} = 3.2456$
- Spiral: $T_S = 55.8659$
- Rolling: $T_R = 0.0769$

(a) Side view

(b) Front view

Figure A.1. Cessna C182 from FligthGear Flight Simulator

Appendix B

MATLAB® M-File

An M-files are the text files with an extension '.m' containing MATLAB® commands. When the M-file is run, all MATLAB® commands in the file are executed together. An M-file can be created or modified through the MATLAB® editor. This thesis uses the following M-file to calculate the controller's parameters for both ACDM-RAS and ACDM-SS and cooperates with Simulink® for flight simulation.

```
%******************************************************
% Cessna 182 Model
% Aircraft Dynamics, Marcello N apolitano
% Modern Flight Dynamics, David K. Schmidt
%******************************************************
clear;
clc;
ver = 'acdm_ras';
ver

%******************************************************
% Cessna 182 data
%******************************************************
% Geometric data
S         = 174;    % Wing surface, ft^2
c_bar     = 4.9;    % Mean Aerodynamic Chord (MAC), ft
b         = 36;     % Wing span, ft
% Flight conditions data
H         = 5000;   % Altitude, ft
M         = 0.201;  % Mach number
V_p1      = 220.1;  % True airspeed, ft/sec 220.1
Qbar      = 49.6;   % Dynamic pressure, lbs/ft^2
xbar_CG   = 0.264;  % Location of CG (% of MAC)
alpha_1   = 0;      % Steady state angle of attack, deg
theta_1   = 0;
g         = 32.2;
% Mass and Inertial data
M    = 2650;   % Mass, lbs
I_XX = 948;    % Moment of Inertia x-axis, slug ft^2
I_YY = 1346;   % Moment of Inertia y-axis, slug ft^2
I_ZZ = 1967;   % Moment of Inertia z-axis, slug ft^2
I_XZ = 0;      % Product of Inertia x-axis, slug ft^2
% Longitudinal dimensional stability derivatives
X_u             = -0.0304;
X_Tu            = -0.0152;
X_alpha         = 19.459;
X_deltaE        = 0;
X_deltaT        = 0.0117;

Z_u             = -0.2919;
Z_alpha         = -464.71;
Z_alphaDot      = -1.98;
Z_q             = -4.542;
Z_deltaE        = -44.985;
Z_deltaT        = 0;

M_u             = 0;
```

```
M_Tu            = 0;
M_alpha         = -19.26;
M_Talpha        = 0;
M_alphaDot      = -2.543;
M_q             = -4.337;
M_deltaE        = -35.251;
M_deltaT        = 0;

% Lateral-Directional dimensional stability derivatives
Y_beta          = -41.11;
Y_p             = -0.642;
Y_r             = 1.831;
Y_deltaA        = 0;
Y_deltaR        = 19.56;

L_beta          = -30.25;
L_p             = -12.97;
L_r             = 2.14;
L_deltaA        = 75.06;
L_deltaR        = 4.82;

N_beta          = 9.27;
N_Tbeta         = 0;
N_p             = -0.36;
N_r             = -1.21;
N_deltaA        = -3.41;
N_deltaR        = -10.19;
%*******************************************************

%*******************************************************
% Longitudinal aircraft dynamics equation
%*******************************************************
% x_Long = [u; alpha; q; theta; h]
% y_Long = [u; alpha; q; theta; h]
% u_Long = [deltaE; deltaT]
% u      = velocity (along the X axis), fps
% alpha  = longitudinal angle of attack, rad
% q      = pitch angular rate (around the Y axis),
rad/sec
% theta  = Euler pitch angle, rad
% h  = altitude in an earth-fixed reference frame, ft
% deltaE = elevator deflection, rad
% deltaT = Thrust, lbf

Xprime_u        = X_u + X_Tu;
Xprime_alpha    = X_alpha;
Xprime_q        = 0;
```

```
Xprime_theta    = -1*g*cos(theta_1);

Zprime_u        = Z_u/(V_p1 - Z_alphaDot);
Zprime_alpha    = Z_alpha/(V_p1 - Z_alphaDot);
Zprime_q        = (Z_q + V_p1)/(V_p1 - Z_alphaDot);
Zprime_theta  = -1*g*sin(theta_1)/(V_p1 - Z_alphaDot);

Mprime_u        = (M_alphaDot*Zprime_u) + M_u;
Mprime_alpha    = (M_alphaDot*Zprime_alpha) + M_alpha;
Mprime_q        = (M_alphaDot*Zprime_q) + M_q;
Mprime_theta    = M_alphaDot*Zprime_theta;

a_L11           = Xprime_u;
a_L12           = Xprime_alpha;
a_L13           = Xprime_q;
a_L14           = Xprime_theta;
a_L15           = 0;

a_L21           = Zprime_u;
a_L22           = Zprime_alpha;
a_L23           = Zprime_q;
a_L24           = Zprime_theta;
a_L25           = 0;

a_L31           = Mprime_u;
a_L32           = Mprime_alpha;
a_L33           = Mprime_q;
a_L34           = Mprime_theta;
a_L35           = 0;

a_L41           = 0;
a_L42           = 0;
a_L43           = 1;
a_L44           = 0;
a_L45           = 0;

a_L51           = 0;
a_L52           = -1*V_p1;
a_L53           = 0;
a_L54           = V_p1;
a_L55           = 0;

Xprime_deltaE   = X_deltaE;
Zprime_deltaE   = Z_deltaE/(V_p1 - Z_alphaDot);
Mprime_deltaE   = (M_alphaDot*Zprime_deltaE) +
M_deltaE;
Xprime_deltaT   = X_deltaT;
Zprime_deltaT   = Z_deltaT;
```

```
Mprime_deltaT   = M_deltaT;

b_L11           = Xprime_deltaE;
b_L12           = Xprime_deltaT;

b_L21           = Zprime_deltaE;
b_L22           = Zprime_deltaT;

b_L31           = Mprime_deltaE;
b_L32           = Mprime_deltaT;

b_L41           = 0;
b_L42           = 0;

b_L51           = 0;
b_L52           = 0;

A_Long = [a_L11 a_L12 a_L13 a_L14 a_L15;
          a_L21 a_L22 a_L23 a_L24 a_L25;
          a_L31 a_L32 a_L33 a_L34 a_L35;
          a_L41 a_L42 a_L43 a_L44 a_L45;
          a_L51 a_L52 a_L53 a_L54 a_L55];

B_Long = [b_L11  b_L12;
          b_L21  b_L22;
          b_L31  b_L32;
          b_L41  b_L42;
          b_L51  b_L52];

C_Long = eye(5);

D_Long = zeros(5,2);
%*******************************************************

%*******************************************************
% Servo system for Longitudinal aircraft dynamics
%*******************************************************
% Servo output u and h
H_L          = [1 0 0 0 0;
                0 0 0 0 1];
H_rL         = [0 1 0 0 0;
                0 0 1 0 0;
                0 0 0 1 0];
% Characteristic polynomial of servo system (Open Loop)
P_A_sL          = poly(A_Long);
R_P_A_sL        = roots(P_A_sL);
%*******************************************************
```

```
%*******************************************************
% Longitudinal servo state feedback system by CDM
%*******************************************************
% Longitudinal stability index
g_sL1           = 2.5;
g_sL2           = 2;
g_sL3           = 2;
g_sL4           = 2;
tau_sL          = 1.1; % 1.1

% Longitudinal CDM coefficient
a_sL0           = 0.2;
a_sL1           = a_sL0*tau_sL;
a_sL2           = (a_sL1*tau_sL)/g_sL1;
a_sL3           = (a_sL2*tau_sL)/(g_sL1*g_sL2);
a_sL4           = (a_sL3*tau_sL)/(g_sL1*g_sL2*g_sL3);
a_sL5           =
(a_sL4*tau_sL)/(g_sL1*g_sL2*g_sL3*g_sL4);

% Longitudinal CDM monic polynomial & poles
% P_cdm_sL    = [a_sL5 a_sL4 a_sL3 a_sL2 a_sL1 a_sL0];
P_cdm_sL      = [a_sL5/a_sL5 a_sL4/a_sL5 a_sL3/a_sL5
               a_sL2/a_sL5 a_sL1/a_sL5 a_sL0/a_sL5];
R_cdm_sL      = roots(P_cdm_sL);

% Longitudinal CDM gains
Ks_L            = place(A_Long,B_Long,R_cdm_sL);
K_L             = [Ks_L(:,2) Ks_L(:,3) Ks_L(:,4)];
G_L             = [Ks_L(:,1) Ks_L(:,5)];

pLfb = poly(A_Long - B_Long*Ks_L);
%*******************************************************

%*******************************************************
% Lateral-Directional aircraft dynamics equation
%*******************************************************
% x_LatDir      = [beta; p; r; phi; psi]
% y_LatDir      = [beta; p; r; phi; psi]
% u_LatDir      = [deltaA; deltaR]
% beta          = sidesplip angle, rad
% p             = roll rate, rad/sec
% r             = yaw rate, rad/sec
% phi           = bank angle, rad
% psi           = heading angle, rad
% deltaA        = aileron deflection, rad
% deltaR        = rudder deflection, rad
```

```
Yprime_beta     = Y_beta/V_p1;
Yprime_p        = Y_p/V_p1;
Yprime_r        = (Y_r - V_p1)/V_p1;
Yprime_phi      = g*cos(theta_1)/V_p1;

I_1             = I_XZ/I_XX;
I_2             = I_XZ/I_ZZ;
Lprime_beta     = (L_beta + I_1*N_beta)/(1 - I_1*I_2);
Lprime_p        = (L_p + I_1*N_p)/(1 - I_1*I_2);
Lprime_r        = (L_r + I_1*N_r)/(1 - I_1*I_2);

Nprime_beta     = (I_2*L_beta + N_beta)/(1 - I_1*I_2);
Nprime_p        = (I_2*L_p + N_p)/(1 - I_1*I_2);
Nprime_r        = (I_2*L_r + N_r)/(1 - I_1*I_2);

a_LD11          = Yprime_beta;
a_LD12          = Yprime_p;
a_LD13          = Yprime_r;
a_LD14          = Yprime_phi;
a_LD15          = 0;

a_LD21          = Lprime_beta;
a_LD22          = Lprime_p;
a_LD23          = Lprime_r;
a_LD24          = 0;
a_LD25          = 0;

a_LD31          = Nprime_beta;
a_LD32          = Nprime_p;
a_LD33          = Nprime_r;
a_LD34          = 0;
a_LD35          = 0;

a_LD41          = 0;
a_LD42          = 1;
a_LD43          = 0; %tan(theta_1) or 0(IREASE)
a_LD44          = 0;
a_LD45          = 0;

a_LD51          = 0;
a_LD52          = 0;
a_LD53          = 1; % 0 or 1(IREASE);
a_LD54          = 0; % g/V_p1 or 0(IREASE);
a_LD55          = 0;

Yprime_deltaA   = Y_deltaA/V_p1;
Yprime_deltaR   = Y_deltaR/V_p1;
Lprime_deltaA = (L_deltaA+I_1*N_deltaA)/(1-I_1*I_2);
```

```
Lprime_deltaR = (L_deltaR+I_1*N_deltaR)/(1-I_1*I_2);
Nprime_deltaA = (I_2*L_deltaA+N_deltaA)/(1-I_1*I_2);
Nprime_deltaR = (I_2*L_deltaR+N_deltaR)/(1-I_1*I_2);

b_LD11          = Yprime_deltaA;
b_LD12          = Yprime_deltaR;

b_LD21          = Lprime_deltaA;
b_LD22          = Lprime_deltaR;

b_LD31          = Nprime_deltaA;
b_LD32          = Nprime_deltaR;

b_LD41          = 0;
b_LD42          = 0;

b_LD51          = 0;
b_LD52          = 0;

A_LatDir = [a_LD11 a_LD12 a_LD13 a_LD14 a_LD15;
            a_LD21 a_LD22 a_LD23 a_LD24 a_LD25;
            a_LD31 a_LD32 a_LD33 a_LD34 a_LD35;
            a_LD41 a_LD42 a_LD43 a_LD44 a_LD45;
            a_LD51 a_LD52 a_LD53 a_LD54 a_LD55];

B_LatDir = [b_LD11 b_LD12;
            1*b_LD21 b_LD22;
            b_LD31 b_LD32;
            1*b_LD41 b_LD42;
            1*b_LD51 b_LD52];

C_LatDir = eye(5);

D_LatDir = zeros(5,2);
%*******************************************************

%*******************************************************
% Servo system for Lateral-Directional aircraft
dynamics
%*******************************************************
% Servo output beta and psi
H_LD        = [1 0 0 0 0;
               0 0 0 0 1];
H_rLD       = [0 1 0 0 0;
               0 0 1 0 0;
               0 0 0 1 0];

% Characteristic polynomial of servo system (Open Loop)
```

```
P_A_sLD          = poly(A_LatDir);
R_P_A_sLD        = roots(P_A_sLD);
%*******************************************************

%*******************************************************
% Lateral-Directional servo state feedback system by
CDM
%*******************************************************
% Lateral-Directional stability index
g_sLD1           = 2.5;
g_sLD2           = 2;
g_sLD3           = 2;
g_sLD4           = 2;
tau_sLD          = 4; % 4(IREASE)

% Lateral-Directional CDM coefficient
a_sLD0 = 0.2;
a_sLD1 = a_sLD0*tau_sLD;
a_sLD2 = (a_sLD1*tau_sLD)/g_sLD1;
a_sLD3 = (a_sLD2*tau_sLD)/(g_sLD1*g_sLD2);
a_sLD4 = (a_sLD3*tau_sLD)/(g_sLD1*g_sLD2*g_sLD3);
a_sLD5 =
(a_sLD4*tau_sLD)/(g_sLD1*g_sLD2*g_sLD3*g_sLD4);

% Lateral-Directional CDM monic polynomial & poles
% P_cdm_sLD   = [a_sLD5 a_sLD4 a_sLD3 a_sLD2 a_sLD1
a_sLD0];
P_cdm_sLD = [a_sLD5/a_sLD5 a_sLD4/a_sLD5 a_sLD3/a_sLD5
              a_sLD2/a_sLD5 a_sLD1/a_sLD5
         a_sLD0/a_sLD5];
R_cdm_sLD     = roots(P_cdm_sLD);

% Lateral-Directional CDM gains
Ks_LD          = place(A_LatDir,B_LatDir,R_cdm_sLD);
K_LD           = [Ks_LD(:,2) Ks_LD(:,3) Ks_LD(:,4)];
G_LD           = [Ks_LD(:,1) Ks_LD(:,5)];

pLDfb = poly(A_LatDir - B_LatDir*Ks_LD);
%*******************************************************

%*******************************************************
% Entrie aircraft dynamics equation
%*******************************************************
% x  = [u; alpha; q; theta; h; beta; p; r; phi; psi]
% y  = [u; alpha; q; theta; h; beta; p; r; phi; psi]
% u  = [deltaE; deltaT; deltaA; deltaR]
```

```
A = [A_Long   zeros(5);
     zeros(5) A_LatDir];

B = [B_Long     zeros(5,2);
     zeros(5,2) B_LatDir];

C = [C_Long     zeros(5,5);
     zeros(5,5) C_LatDir];

D = zeros(10,4);
%*******************************************************

coefplot_2_3;   % CDM diagram plot

%*******************************************************
% Adaptive Control section
%*******************************************************

%*******************************************************
% Longitudinal reference model
%*******************************************************
AmL = A_Long - B_Long*Ks_L;

% Amv's elements from matrix_test.m
AmvL =    [2*AmL(1,1) 0 0 0 0 2*AmL(2,1) 2*AmL(3,1)
          2*AmL(4,1) 2*AmL(5,1) 0 0 0 0 0 0;

          0 2*AmL(2,2) 0 0 0 2*AmL(1,2) 0 0 0 2*AmL(3,2)
          2*AmL(4,2) 2*AmL(5,2) 0 0 0;

          0 0 2*AmL(3,3) 0 0 0 2*AmL(1,3) 0 0 2*AmL(2,3)
          0 0 2*AmL(4,3) 2*AmL(5,3) 0;

          0 0 0 2*AmL(4,4) 0 0 0 2*AmL(1,4) 0 0
          2*AmL(2,4) 0 2*AmL(3,4) 0 2*AmL(5,4);

          0 0 0 0 2*AmL(5,5) 0 0 0 2*AmL(1,5) 0 0
          2*AmL(2,5) 0 2*AmL(3,5) 2*AmL(4,5);

          AmL(1,2) AmL(2,1) 0 0 0 AmL(1,1)+AmL(2,2)
          AmL(3,2) AmL(4,2) AmL(5,2) AmL(3,1)
          AmL(4,1) AmL(5,1) 0 0 0;

          AmL(1,3) 0 AmL(3,1) 0 0 AmL(2,3)
          AmL(1,1)+AmL(3,3) AmL(4,3) AmL(5,3)
          AmL(2,1) 0 0 AmL(4,1) AmL(5,1) 0;
```

```
            AmL(1,4) 0 0 AmL(4,1) 0 AmL(2,4) AmL(3,4)
            AmL(1,1)+AmL(4,4) AmL(5,4) 0 AmL(2,1) 0
            AmL(3,1) 0 AmL(5,1);

            AmL(1,5) 0 0 0 AmL(5,1) AmL(2,5) AmL(3,5)
            AmL(4,5) AmL(1,1)+AmL(5,5) 0 0 AmL(2,1) 0
            AmL(3,1) AmL(4,1);

            0 AmL(2,3) AmL(3,2) 0 0 AmL(1,3) AmL(1,2) 0
            0 AmL(2,2)+AmL(3,3) AmL(4,3) AmL(5,3) AmL(4,2)
            AmL(5,2) 0;
            0 AmL(2,4) 0 AmL(4,2) 0 AmL(1,4) 0 AmL(1,2)
            0 AmL(3,4) AmL(2,2)+AmL(4,4) AmL(5,4)
            AmL(3,2) 0 AmL(5,2);

            0 AmL(2,5) 0 0 AmL(5,2) AmL(1,5) 0 0 AmL(1,2)
            AmL(3,5) AmL(4,5) AmL(2,2)+AmL(5,5) 0 AmL(3,2)
            AmL(4,2);

            0 0 AmL(3,4) AmL(4,3) 0 0 AmL(1,4) AmL(1,3) 0
            AmL(2,4) AmL(2,3) 0 AmL(3,3)+AmL(4,4) AmL(5,4)
            AmL(5,3);

            0 0 AmL(3,5) 0 AmL(5,3) 0 AmL(1,5) 0 AmL(1,3)
            AmL(2,5) 0 AmL(2,3) AmL(4,5) AmL(3,3)+AmL(5,5)
            AmL(4,3);

            0 0 0 AmL(4,5) AmL(5,4) 0 0 AmL(1,5) AmL(1,4)
            0 AmL(2,5) AmL(2,4) AmL(3,5) AmL(3,4)
            AmL(4,4)+AmL(5,5)];

qL1 = 1;
qL2 = qL1;
qL3 = qL2;
qL4 = qL3;
qL5 = qL4;

qL6 = 0;
qL7 = qL6;
qL8 = qL7;
qL9 = qL8;
qL10 = qL9;
qL11 = qL10;
qL12 = qL11;
qL13 = qL12;
qL14 = qL13;
qL15 = qL14;
```

```
QL = [qL1 qL6  qL7  qL8  qL9;
      qL6 qL2  qL10 qL11 qL12;
      qL7 qL10 qL3  qL13 qL14;
      qL8 qL11 qL13 qL4  qL15;
      qL9 qL12 qL14 qL15 qL5];

QvL = -
1*[qL1;qL2;qL3;qL4;qL5;qL6;qL7;qL8;qL9;qL10;qL11;qL12;q
L13;qL14;qL15];

PvL = AmvL\QvL;

PL = [PvL(1,1) PvL(6,1)  PvL(7,1)  PvL(8,1)  PvL(9,1);
      PvL(6,1) PvL(2,1)  PvL(10,1) PvL(11,1) PvL(12,1);
      PvL(7,1) PvL(10,1) PvL(3,1)  PvL(13,1) PvL(14,1);
      PvL(8,1) PvL(11,1) PvL(13,1) PvL(4,1)  PvL(15,1);
      PvL(9,1) PvL(12,1) PvL(14,1) PvL(15,1) PvL(5,1)];

lambdaL = 30000; % 30000(IREASE) 200000 1000000

% Test matrix PL
ePL = eig(PL);
nQL = (AmL.'*PL)+(PL*AmL);

%******************************************************

%******************************************************
% Lateral-directional reference model
%******************************************************
AmLD = A_LatDir - B_LatDir*Ks_LD;

% Amv's elements from matrix_test.m
AmvLD =  [2*AmLD(1,1) 0 0 0 0 2*AmLD(2,1) 2*AmLD(3,1)
          2*AmLD(4,1) 2*AmLD(5,1) 0 0 0 0 0 0;

          0 2*AmLD(2,2) 0 0 0 2*AmLD(1,2) 0 0 0
          2*AmLD(3,2) 2*AmLD(4,2) 2*AmLD(5,2) 0 0 0;

          0 0 2*AmLD(3,3) 0 0 0 2*AmLD(1,3) 0 0
          2*AmLD(2,3) 0 0 2*AmLD(4,3) 2*AmLD(5,3) 0;

          0 0 0 2*AmLD(4,4) 0 0 0 2*AmLD(1,4) 0 0
          AmLD(2,4) 0 2*AmLD(3,4) 0 2*AmLD(5,4);

          0 0 0 0 2*AmLD(5,5) 0 0 0 2*AmLD(1,5) 0 0
          2*AmLD(2,5) 0 2*AmLD(3,5) 2*AmLD(4,5);
```

```
            AmLD(1,2) AmLD(2,1) 0 0 0 AmLD(1,1)+AmLD(2,2)
            AmLD(3,2) AmLD(4,2) AmLD(5,2) AmLD(3,1)
            AmLD(4,1) AmLD(5,1) 0 0 0;

            AmLD(1,3) 0 AmLD(3,1) 0 0 AmLD(2,3)
            AmLD(1,1)+AmLD(3,3) AmLD(4,3) AmLD(5,3)
            AmLD(2,1) 0 0 AmLD(4,1) AmLD(5,1) 0;

            AmLD(1,4) 0 0 AmLD(4,1) 0 AmLD(2,4) AmLD(3,4)
            AmLD(1,1)+AmLD(4,4) AmLD(5,4) 0 AmLD(2,1) 0
            AmLD(3,1) 0 AmLD(5,1);

            AmLD(1,5) 0 0 AmLD(5,1) AmLD(2,5) AmLD(3,5)
            AmLD(4,5) AmLD(1,1)+AmLD(5,5) 0 0 AmLD(2,1)
            0 AmLD(3,1) AmLD(4,1);

            0 AmLD(2,3) AmLD(3,2) 0 0 AmLD(1,3) AmLD(1,2)
            0 0 AmLD(2,2)+AmLD(3,3) AmLD(4,3) AmLD(5,3)
            AmLD(4,2) AmLD(5,2) 0;

            0 AmLD(2,4) 0 AmLD(4,2) 0 AmLD(1,4) 0
            AmLD(1,2)          0 AmLD(3,4)
            AmLD(2,2)+AmLD(4,4) AmLD(5,4)
            AmLD(3,2) 0 AmLD(5,2);

            0 AmLD(2,5) 0 0 AmLD(5,2) AmLD(1,5) 0 0
            AmLD(1,2) AmLD(3,5) AmLD(4,5)
            AmLD(2,2)+AmLD(5,5) 0 AmLD(3,2) AmLD(4,2);

            0 0 AmLD(3,4) AmLD(4,3) 0 0 AmLD(1,4)
            AmLD(1,3)          0 AmLD(2,4) AmLD(2,3) 0
            AmLD(3,3)+AmLD(4,4) AmLD(5,4) AmLD(5,3);

            0 0 AmLD(3,5) 0 AmLD(5,3) 0 AmLD(1,5) 0
            AmLD(1,3) AmLD(2,5) 0 AmLD(2,3) AmLD(4,5)
            AmLD(3,3)+AmLD(5,5) AmLD(4,3);

            0 0 0 AmLD(4,5) AmLD(5,4) 0 0 AmLD(1,5)
            AmLD(1,4) 0 AmLD(2,5) AmLD(2,4) AmLD(3,5)
            AmLD(3,4) AmLD(4,4)+AmLD(5,5)];

qLD1 = 1;
qLD2 = qLD1;
qLD3 = qLD2;
qLD4 = qLD3;
qLD5 = qLD4;

qLD6 = 0;
```

```
qLD7 = qLD6;
qLD8 = qLD7;
qLD9 = qLD8;
qLD10 = qLD9;
qLD11 = qLD10;
qLD12 = qLD11;
qLD13 = qLD12;
qLD14 = qLD13;
qLD15 = qLD14;

QLD = [qLD1 qLD6  qLD7  qLD8  qLD9;
       qLD6 qLD2  qLD10 qLD11 qLD12;
       qLD7 qLD10 qLD3  qLD13 qLD14;
       qLD8 qLD11 qLD13 qLD4  qLD15;
       qLD9 qLD12 qLD14 qLD15 qLD5];

QvLD = -
1*[qLD1;qLD2;qLD3;qLD4;qLD5;qLD6;qLD7;qLD8;qLD9;qLD10;q
LD11;qLD12;qLD13;qLD14;qLD15];

PvLD = AmvLD\QvLD;

PLD =    [PvLD(1,1) PvLD(6,1)  PvLD(7,1)  PvLD(8,1)
         PvLD(9,1);
         PvLD(6,1) PvLD(2,1)  PvLD(10,1) PvLD(11,1)
         PvLD(12,1);
         PvLD(7,1) PvLD(10,1) PvLD(3,1)  PvLD(13,1)
         PvLD(14,1);
         PvLD(8,1) PvLD(11,1) PvLD(13,1) PvLD(4,1)
         PvLD(15,1);
         PvLD(9,1) PvLD(12,1) PvLD(14,1) PvLD(15,1)
         PvLD(5,1)];

lambdaLD = 30; % 30(IREASE) 1000

% Test matrix P
ePLD = eig(PLD);
nQLD = (AmLD.'*PLD)+(PLD*AmLD);
%*****************************************************
% table_to_excel_thesis
% plot_from_excel_thesis
```

Appendix C

Simulink®

The diagrams of ACDM-RAS and ACDM-SS in Simulink® are shown in the following figures. This Simulink® cooperates with the M-file for flight simulation purposes.

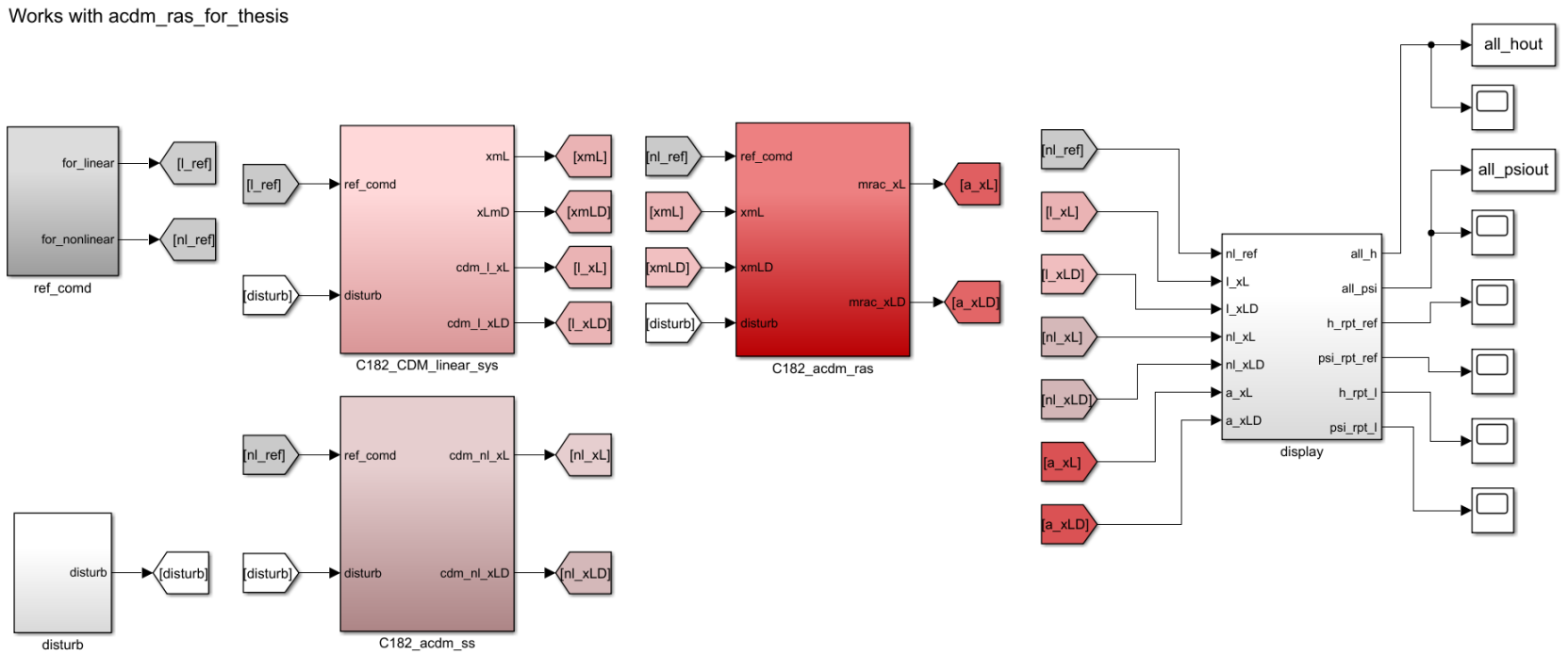

Figure B.1. The Simulink® of ACDM-RAS and ACDM-SS (level 1)

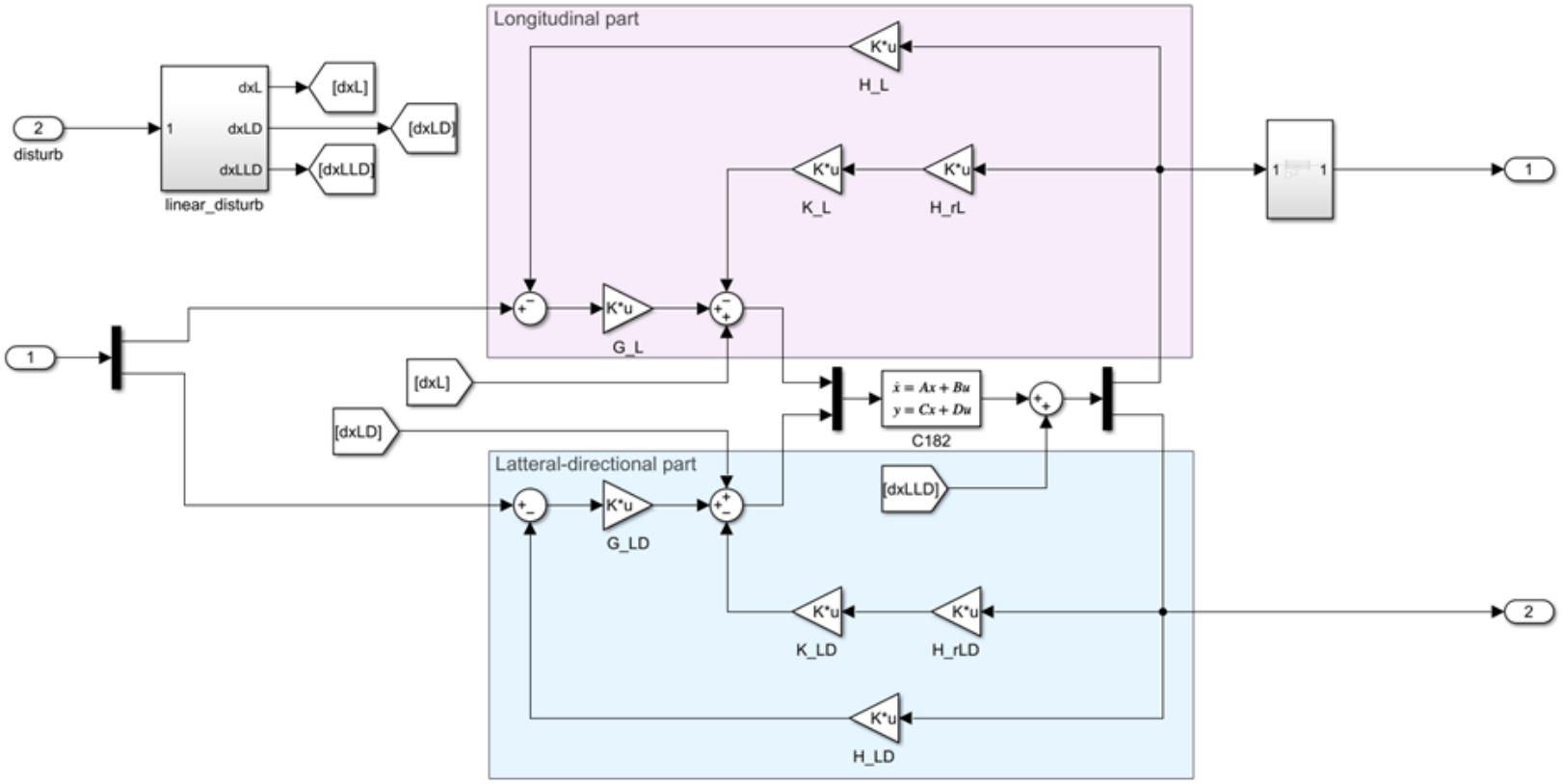

Figure B.2. The Simulink® of the controller part of ACDM-SS

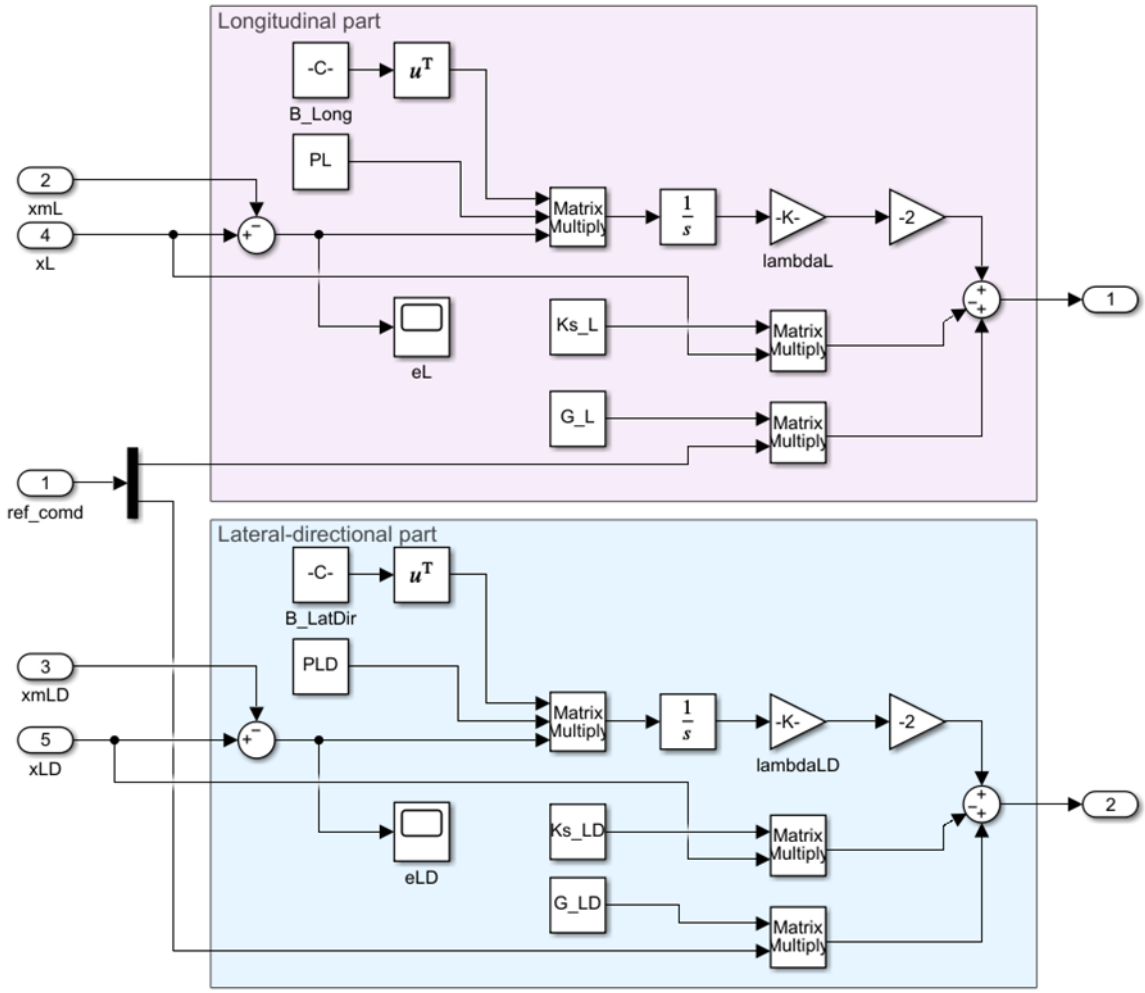

Figure B.3. The Simulink® of the controller part of ACDM-RAS

References

[1] U.S. Department of Transportation, Aviation Maintenance Technician Handbook – Airframe, Volume 1, Federal Aviation Administration, Oklahoma City, USA, (2012).

[2] T. A. Talay, Introduction to the aerodynamics of flight, National Aeronautics and Space Administration, Washington DC., USA, (1975).

[3] A. K. Kundu, M. A. Price and D. Riordan, Theory and practice of aircraft performance, John Wiley & Sons, Inc., (2016).

[4] M. Abbott and L. Kailey, Private pilot handbook, P. Willits (Ed.), Jeppesen Sanderson, Inc., (2004).

[5] U.S. Department of Transportation, Pilot's handbook of aeronautical knowledge, Federal Aviation Administration, Oklahoma City, USA, (2008).

[6] D. McLean, Automatic Fight Control Systems, Prentice Hall International Ltd., Hertfordshire, UK, (1990).

[7] D. T. McRuer, D. Graham and I. Ashkenas, Aircraft Dynamics and Automatic Control, Princeton University Press, Princeton, New Jersey, USA, (1974).

[8] B. L. Stevens, F. Lewis and E. N. Johnson, Aircraft Control and Simulation: Dynamics, Controls Design, and Autonomous Systems, 3rd ed., John Wiley & Sons, Inc., (2015).

[9] E.H.J. Pallett and S. Coyle, Automatic Flight Control, 4th ed., Blackwell Science Ltd., (1993).

[10] D. P. Raymer, Aircraft Design: A Conceptual Approach, American Institute of Aeronautics and Astronautics, Inc., Washington DC., USA, (1992).

[11] D. A. Caughey, Introduction to Aircraft Stability and Control Course Notes for M&AE 5070, Sibley School of Mechanical & Aerospace Engineering, Cornell University, New York, (2011).

[12] F. Gavilan, R. Vazquez and J. Á. Acosta, Adaptive Control for Aircraft Longitudinal Dynamics with Thrust Saturation, Journal of Guidance, Control, and Dynamics, Vol. 38, Issue 4 (2014), pp. 651 – 661.

[13] A. Maqsood and T. H. Go, Multiple time scale analysis of aircraft longitudinal dynamics with aerodynamic vectoring, Nonlinear Dynamics, Vol. 69 (2012), pp. 731 – 742.

[14] Q. Shen, B. Jiang and V. Cocquempot, Adaptive fault-tolerant backstepping control against actuator gain faults and its applications to an aircraft longitudinal motion dynamic, International Journal of Robust and Nonlinear Control, Vol. 23, Issue 15 (2013), pp. 1753 – 1779.

[15] M. E. Argyle and R. W. Beard, Nonlinear Total Energy Control for the Longitudinal dynamics of an aircraft, 2016 American Control Conference (ACC), (2016).

[16] J. Yan, J. B. Hoagg, R. E. Hindman and D. S. Bernstein, Longitudinal Aircraft Dynamics and the Instantaneous Acceleration Center of Rotation, IEEE Control Systems Magazine, Vol. 31, Issue 4 (2011), pp. 68 – 92.

[17] A. M. Wickenheiser and E. Garcia, Longitudinal Dynamics of a Perching Aircraft, Journal of Aircraft, Vol. 43, No. 5 (2006), pp. 1386 – 1392.

[18] A. M. Wickenheiser, E. Garcia and M. Waszak, Longitudinal dynamics of a perching aircraft concept, Smart Structures and Materials 2005: Smart Structures and Integrated Systems, (2005).

[19] Y. Ameho and E. Prempain, Linear parameter varying controllers for the ADMIRE Aircraft longitudinal dynamics, Proceedings of the 2011 American Control Conference, (2011).

[20] H. G. McClelland and C. A. Woolsey, Effects of Two Modeling Assumptions on Wind Reconstruction from Longitudinal Aircraft Motion, Journal of Guidance, Control, and Dynamics, Vol. 43, No. 6 (2020), pp. 1 – 13.

[21] V. H. Nguyen and T. T. Tran, A Novel Hybrid Robust Control Design Method for F-16 Aircraft Longitudinal Dynamics, Mathematical Problems in Engineering, Vol. 2020 (2020), pp. 1 – 10.

[22] S. Swarnkar and M. Kothari, A Simplified Adaptive Backstepping Control of Aircraft Lateral/Directional Dynamics, IFAC-PapersOnLine, Vol. 49, Issue 1 (2016), pp. 579 – 584.

[23] I. K. Ashraf and E.-J. Van Kampen, Adaptive Critic Control for Aircraft Lateral-Directional Dynamics, AIAA Scitech 2020 Forum, (2020).

[24] P. C. Shrivastava and R. F. Stengel, Stability boundaries for aircraft with unstable lateral-directional dynamics and control saturation, Journal of Guidance, Control, and Dynamics, Vol. 12, Issue 1 (1989), pp. 62 – 70.

[25] T. H. Go, Lateral-Directional Aircraft Dynamics Under Static Moment Nonlinearity, Journal of Guidance, Control, and Dynamics, Vol. 32, Issue 1 (2009), pp. 305 – 309.

[26] N. Abramov, M. Goman, M. Demenkov and A. Khrabrov, Lateral-Directional Aircraft Dynamics at High Incidence Flight with Account of Unsteady Aerodynamic Effects, AIAA Atmospheric Flight Mechanics Conference and Exhibit, (2005).

[27] R. Livneh, Improved Literal Approximation for Lateral-Directional Dynamics of Rigid Aircraft, Journal of Guidance, Control, and Dynamics, Vol. 18, No. 4 (1995), pp. 925 – 927.

[28] S. A. Snell, W. L. Garrard Jr. and D. F. Enns, Optimization of lateral-directional dynamics for an aircraft operating at high angle of attack, Navigation and Control Conference, (1991).

[29] A. Snell, Cancellation control law for lateral-directional dynamics of a supermaneuverable aircraft, Guidance, Navigation and Control Conference, (1993).

[30] L. Zhaoxing, F. Jiancheng, G. Xiaolin, L. Jianli, W. Shicheng and W. Yun, Dynamic Lever Arm Error Compensation of POS Used for Airborne Earth Observation, International Journal of Aerospace Engineering, Vol. 2018 (2018), pp. 1 – 13.

[31] C. Tournes and B. Landrum, Adaptive control of aircraft lateral directional axis using subspace stabilization, Proceedings of the 33rd Southeastern Symposium on System Theory (Cat. No.01EX460), (2001), pp. 425 – 429.

[32] X. Xiao, J. J. Zhang and Q. Zhang, Flight control reconfiguration of unmanned tiltrotor aircraft, IOP Conference Series: Materials Science and Engineering, Vol. 439, Issue 3 (2018), 032103.

[33] T. Hongpeng and Weibo, Stability Control of Flight Attitude Angle for Four Rotor Aircraft, 2018 IEEE 9th International Conference on Software Engineering and Service Science (ICSESS), (2018), pp. 332 – 336.

[34] H.-Y. Tian and L. Li, Flight control system for quad-rotor aircraft based on improved integral separation PID, Proceedings of the 2016 4th International Conference on Machinery, Materials and Information Technology Applications, (2016).

[35] B. Porter, A. Manganas and T. Manganas, Design of digital model-following flight-mode control systems for high-performance aircraft, Guidance, Navigation and Control Conference, (1988), 88-4116-CP.

[36] Y. Yu and J. Chen, Research on flight stability performance of rotor aircraft based on visual servo control method, Proceedings of the Chinese Society for Optical Engineering Conferences, (2016), 101411V.

[37] M. Mirzaei, Roll reversal phenomenon control in flight vehicles, Aerospace Science and Technology, Vol. 79 (2018), pp. 413 – 425.

[38] Y. Ochi, H. Kondo and M. Watanabe, Linear Dynamics and PID Flight Control of a Powered Paraglider, AIAA Guidance, Navigation, and Control Conference, (2009).

[39] P. Kumar, S. Narayan and J. Raheja, Optimal design of robust fractional order PID for the flight control system, International Journal of Computer Applications, Vol. 128, No. 14 (2015), 0975-8887.

[40] A. Z. Azfar and D. Hazry, A simple approach on implementing IMU sensor fusion in PID controller for stabilizing quadrotor flight control, 2011 IEEE 7th International Colloquium on Signal Processing and its Applications, (2011), pp. 28 – 32.

[41] D. Luo, W. Xu, S. Wu and Y. Ma, UAV formation flight control and formation switch strategy, 2013 8th International Conference on Computer Science & Education, (2013), pp. 264 – 269.

[42] B. S. Kim and A. J. Calise, Nonlinear Flight Control Using Neural Networks, Journal of Guidance, Control, and Dynamics, Vol. 20, No. 1 (1997), pp. 26 – 33.

[43] A. J. Calise and R. T. Rysdyk, Nonlinear adaptive flight control using neural networks, IEEE Control Systems Magazine, Vol. 18, No. 6 (1998), pp. 14 – 25.

[44] E. N. Johnson and A. J. Calise, Limited Authority Adaptive Flight Control for Reusable Launch Vehicles, Journal of Guidance, Control, and Dynamics, Vol. 26, No. 6 (2003), pp. 906 – 913.

[45] S. Kurnaz, O. Cetin and O. Kaynak, Fuzzy Logic Based Approach to Design of Flight Control and Navigation Tasks for Autonomous Unmanned Aerial Vehicles, Journal of Intelligent and Robotic Systems, Vol. 54 (2009), pp. 229 – 244.

[46] L. Cervantes and O. Castillo, Type-2 fuzzy logic aggregation of multiple fuzzy controllers for airplane flight control, Information Sciences, Vol. 324 (2015), pp. 247 – 256.

[47] F. Santoso, M. A. Garratt and S. G. Anavatti, State-of-the-Art Intelligent Flight Control Systems in Unmanned Aerial Vehicles, IEEE Transactions on Automation Science and Engineering, Vol. 15, No. 2 (2018), pp. 613 – 627.

[48] K. Ogata, Modern Control Engineering, 5th ed., Prentice–Hall International, Inc., New Jersey, (2010).

[49] S. Nundrakwang, T. Benjanarasuth, J. Ngamwiwit and N. Komine, Hybrid PD-Servo State Feedback Control Algorithm for Swing up Inverted Pendulum System, Proceedings of the International Conference on Control, Automation and Systems (ICCAS2005), (2005), pp. 690 – 693.

[50] P. Huantham, V. Kongratana, S. Gulphanich, V. Tipsuwanporn, Controller Design Base on Servo State Feedback for Two-wheeled Balancing Robot, Proceedings of the International MultiCconference of Engineers and Computer Scientists 2012 (IMECS 2012).

[51] A. Ma'arif, A. I. Cahyadi, O. Wahyunggoro and Herianto, Servo state feedback based on Coefficient Diagram Method in magnetic levitation system with feedback linearization, 2017 3rd International Conference on Science and Technology - Computer (ICST), (2017), pp. 22 – 27.

[52] O. Ocal, A. Bir and B. Tibken, Digital design of Coefficient Diagram Method, 2009 American Control Conference, (2009), pp. 2849 – 2854.

[53] J.P. Coelho, T.M. Pinho and J. Boaventura-Cunha, Controller System Design Using the Coefficient Diagram Method, Arabian Journal for Science and Engineering, Vol. 41 (2016), pp. 3663 – 3681.

[54] U. S. Banu, V. Aparna, Yasmin and M. Hussain, Coefficient diagram method based control for two interacting conical tank process, 2017 Trends in Industrial Measurement and Automation (TIMA), (2017).

[55] R. Alib, T. H. Mohameda, Y. S. Qudaihb and Y. Mitanib, A new load frequency control approach in an isolated small power systems using coefficient diagram method, International Journal of Electrical Power & Energy Systems, Vol. 56 (2014), pp. 110 – 116.

[56] H. Ali, G. Magdy, B. Li, G. Shabib, A. A. Elbaset, D. Xu and Y. Mitani, A New Frequency Control Strategy in an Islanded Microgrid Using Virtual Inertia Control-Based Coefficient Diagram Method, IEEE Access, Vol. 7 (2019), pp. 16979 – 16990.

[57] C. Mitsantisuk, M. Nandayapa, K. Ohishi and S. Katsura, Design for Sensorless Force Control of Flexible Robot by Using Resonance Ratio Control Based on Coefficient Diagram Method, Automatika, Vol. 54, Issue 1 (2013), pp. 62 – 73.

[58] M. Z. Bernard, T. H. Mohamed, Y. S. Qudaih and Y. Mitani, Decentralized load frequency control in an interconnected power system using Coefficient Diagram Method, International Journal of Electrical Power & Energy Systems, Vol. 63 (2014), pp. 165 – 172.

[59] B. Meenakshipriya and K. Kalpana, Modelling and Control of Ball and Beam System using Coefficient Diagram Method (CDM) based PID controller, IFAC Proceedings Volumes, Vol. 47, Issue 1 (2014), pp. 620 – 626.

[60] C. Mitsantisuk, M. Nandayapa, K. Ohishi and S. Katsura, Resonance ratio control based on coefficient diagram method for force control of flexible robot system, 2012 12th IEEE International Workshop on Advanced Motion Control (AMC), (2012).

[61] M. Koksal and S. E. Hamamci, A program for the design of linear time invariant control systems: CDMCAD, Computer Applications in Engineering Education, Vol. 12, Issue 3 (2004), pp. 165 – 174.

[62] W. Giernacki, D. Horla, T. Sadalla and J. P. Coelho, Robust CDM and pole placement PID based thrust controllers for multirotor motor-rotor simplified model: The comparison in a context of using anti-windup compensation, 2016 International Siberian Conference on Control and Communications (SIBCON), (2016).

[63] N. Kanagasabai and N. Jaya, Design of Multiloop Controller for Three Tank Process Using Cdm Techniques, International Journal on Soft Computing, Vol. 5, No. 2 (2014), pp. 11 – 20.

[64] S.E. Hamamci and M. Koksal, Robust controller design for TITO processes with coefficient diagram method, Proceedings of 2003 IEEE Conference on Control Applications (CCA 2003).

[65] Z. Fenchouche, M. Chakir, O. Benzineb, M. S. Boucherit and M. Tadjine, Robust controller design for solar plant using extended Coefficient diagram method (CDM) incorporating PID, 2017 6th International Conference on Systems and Control (ICSC), (2017).

[66] K. Erkan, B. C. Yalçın and M. Garip, Three-axis gap clearance I-PD controller design based on coefficient diagram method for 4-pole hybrid electromagnet, Automatika, Vol. 58, Issue 2 (2017), pp. 147 – 167.

[67] H. Ali, G. Magdy and D. Xu, A new optimal robust controller for frequency stability of interconnected hybrid microgrids considering non-inertia sources and uncertainties, International Journal of Electrical Power & Energy Systems, Vol. 128 (2021), 106651.

[68] E. Asa, A. Tantaworrasilp, T. Benjanarasuth, J. Ngamwiwit and N. Komine, Multivariable Control of Overhead Crane System by CDM, the 4th Information and Computer Engineering Postgraduate Workshop 2004, (2004).

[69] E. Asa, T. Benjanarasuth, J. Ngamwiwit and N. Komine, Hybrid controller for swinging up and stabilizing the inverted pendulum on cart, 2008 International Conference on Control, Automation and Systems, (2008).

[70] E. Asa, T. Benjanarasuth, S. Nundrakwang, J. Ngamwiwit and N. Komine, Implementation of Swinging-up and Stabilizing Controllers for Inverted Pendulum on Cart System, 2008 International Symposium on Communications and Information Technologies, (2008), pp. 504 – 507.

[71] E. Asa, T. Benjanarasuth and N. Komine, Swinging-up and Stabilizing Control of Inverted Pendulum on Cart System by Hybrid Controller, Asia Simulation Conference, (2009).

[72] R. Hirokawa, K. Sato and S. Manabe, Autopilot design for a missile with reaction-jet using coefficient diagram method, AIAA Guidance, Navigation, and Control Conference and Exhibit, (2001).

[73] S. Manabe, Coefficient Diagram Method as Applied to the Attitude Control of Controlled-Bias-Momentum Satellite, IFAC Proceedings Volumes, Vol. 27, Issue 13 (1994), pp. 327 – 332.

[74] S. Manabe, Application of Coefficient Diagram Method to MIMO Design in Aerospace, IFAC Proceedings Volumes, Vol. 35, Issue 1 (2002), pp. 43 – 48.

[75] A. Budiyono and H. Rachman, Proportional Guidance and CDM Control Synthesis for a Short-Range Homing Surface-to-Air Missile, Journal of Aerospace Engineering, Vol. 25, Issue 2 (2012), pp. 168 – 177.

[76] J. Zhao, J. Cao, W. Chen, C. Ma and B. Cao, Polynomial Control for Air-to-Air Missiles Based on Coefficient Diagram Methods, IFAC Proceedings Volumes, Vol. 46, Issue 5 (2013), pp. 355 – 361.

[77] E. Asa, Y. Yamamoto and T. Benjanarasuth, Aircraft Altitude Control Based on CDM, 2019 IEEE 2nd International Conference on Information and Computer Technologies (ICICT), (2019), pp. 266 – 269.

[78] E. Asa and Y. Yamamoto, Aircraft Heading Hold Control Based on CDM, 2019 19th International Conference on Control, Automation and Systems (ICCAS), (2019), pp. 247 – 250.

[79] E. Asa and Y. Yamamoto, CDM based Controller design for Stabilizing the Altitude and Heading of an Aircraft, 2019 IEEE International Conference on Cybernetics and Intelligent Systems (CIS) and IEEE Conference on Robotics, Automation and Mechatronics (RAM), (2019), pp. 119 – 123.

[80] E. Asa and Y. Yamamoto, Aircraft Flight Stabilizer System by CDM Designed Servo State-Feedback Controller, Aerospace, Vol. 8, Issue 2 (2021).

[81] R. Marcello, Aircraft Dynamics from Modeling to Simulation, John Wiley & Sons, Inc., New Jersey, (2012).

[82] D. Schmidt, Modern Flight Dynamics, McGraw-Hill, Inc., New York, (2012).

[83] J. Roskam, Airplane Flight Dynamics and Automatic Flight Controls, Part I, Design, Analysis and Research Corporation, Kansas, (2001).

[84] J. Roskam, Airplane Flight Dynamics and Automatic Flight Controls, Part II, Design, Analysis and Research Corporation, Kansas, (1998).

[85] N. Sinha and N. Ananthkrishnan, Advanced Flight Dynamics with Elements of Flight Control, CRC Press, Florida, (2017).

[86] P. Zipfel, Modeling and Simulation of Aerospace Vehicle Dynamics, American Institute of Aeronautics and Astronautics, Inc., Virginia, (2000).

[87] T. Yechout, S. Morris, D. Bossert, and W. Hallgren, Introduction to Aircraft Flight Mechanics: Performance, Static Stability, Dynamic Stability, and Classical Feedback Control, American Institute of Aeronautics and Astronautics, Inc., Virginia, (2003).

[88] S. Manabe, Coefficient Diagram Method, Proceeding of 14th IFAC Symposium in Aerospace, Vol. 31, Issue 21 (1998), pp. 211 – 222.

[89] Y. C. Kim and S. Manabe, Introduction to Coefficient Diagram Method, Proceeding of 1st IFAC Symposium on System Structure and Control, Vol. 34, Issue 13 (2001), pp. 147 – 152.

[90] S. Manabe, URL: http://www.cityfujisawa.ne.jp/~manabes/index.htm

[91] A. Lipatov and N. Sokolov, Some Sufficient Conditions for Stability and Instability of Continuous Linear Stationary Systems, Automation and Remote Control, (1979), pp. 1285 – 1291.

[92] N. Nise, Control Systems Engineering, 6th ed., John Wiley & Sons, Inc., (2011).

[93] K. Åström and B. Wittenmark, Adaptive Control, 2nd ed., Dover Publications, Inc., New York, (2008).

[94] S. Sastry and M. Bodson, Adaptive Control Stability, Convergence, and Robustness, Prentice-Hall, New Jersey, Inc., (1989).

[95] E. Lavretsky and K. Wise, Robust and Adaptive Control with Aerospace Applications, Springer, (2013).

[96] N. Nguyen, Model Reference Adaptive Control A Primer, Springer, (2018).

[97] J. Slotine and W. Li, Applied Nonlinear Control, Prentice-Hall, New Jersey, Inc., (1991).

[98] K. Ogata, MATLAB® for Control Engineers, Prentice–Hall International, Inc., New Jersey, (2008).

[99] D. Frederick and J. Chow, Feedback Control Problems using MATLAB® and the Control System Toolbox, Brooks/Cole Publishing Company, (2000).

[100] R. Colgren, Basic MATLAB®, Simulink®, and Stateflow®, American Institute of Aeronautics and Astronautics, Inc., Virginia, (2007).

[101] G. Campa, Airlib, MATLAB® Central File Exchange,
URL: http://www.mathworks.com/matlabcentral/fileexchange/3019-airlib

[102] Rauw, M.O., FDC 1.2 - A Simulink Toolbox for Flight Dynamics and Control Analysis, Zeist, 2nd ed., Haarlem, Netherlands, (2001),
URL: http://www.dutchroll.sourceforge.net

[103] United States Air Force, The USAF Stability and Control DATCOM, Users Manual, Vol. 1, Public Domain Aeronautical Software, California, (1999).

[104] B. Galbraith, Datcom+ Pro User's Manual, version 3.6, Holy Cows, Inc., Florida, (2016).

[105] M. Drela and H. Youngren, Athena Vortex Lattice AVL, URL: http://web.mit.edu/drela/Public/web/avl/

[106] J.R. Gloudemans, R. McDonald, M. Moore, A. Hahn, B. Fredericks, and A. Gary, OpenVSP, URL: http://openvsp.org/

[107] Curtis L. Olson and FlightGear Projet Members, FlightGear Flight Simulator, URL: https://www.flightgear.org/

[108] Jon S. Berndt and the JSBSim Development Team, JSBSim An open source, platform-independent, flight dynamics model in C++, (2011).